

ScholarWorks@GSU

Carbon Sequestration Potential in Simulated Saline Lake Waters

Authors	Yurman, Scott N
Citation	Yurman, Scott N. Carbon Sequestration Potential in Simulated Saline Lake Waters. May 2012, Georgia State University. https://doi.org/10.57709/2758807 .
DOI	https://doi.org/10.57709/2758807
Download date	2026-03-11 00:53:05
Link to Item	https://hdl.handle.net/20.500.14694/6424

CARBON SEQUESTRATION POTENTIAL IN SIMULATED SALINE LAKE WATERS

by

SCOTT NATHAN YURMAN

Under the Direction of Dr. Daniel M. Deocampo

ABSTRACT

This investigation tested simulated saline lake environments as mineralization sites for sequestering anthropogenic CO₂. Four unique saline lakes were simulated in the laboratory. Two sets of experiments were conducted by diffusing CO_{2(g)} through each simulated lake over 30 days. The first set tested the carbonate system response to elevated CO_{2(g)}. The second set of experiments replicated the same process but used ammonium hydroxide to elevate pH. Water samples were collected daily to test for cation loss via mineralization. Rapid mineralization occurred with the pH enhancer and cation activity was greatly reduced by as much as 38,000 mg/L Ca due to precipitation. This resulted in a mass of 100,000 mg/L of CO₂ being sequestered via Ca and Mg-carbonate mineralization. With proper geochemical conditions, saline lake environments can therefore potentially serve a purpose in sequestering CO_{2(g)}.

INDEX WORDS: Anthropogenic CO₂, Saline lake environments, pH control, Carbonate mineralization, Cation activity, CO₂ sequestration

CARBON SEQUESTRATION POTENTIAL IN SIMULATED SALINE LAKE WATERS

by

SCOTT NATHAN YURMAN

A Thesis Submitted in Partial Fulfillment of the Requirements for the Degree of

Master of Science

in the College of Arts and Sciences

Georgia State University

2012

Copyright by
Scott Nathan Yurman
2012

CARBON SEQUESTRATION POTENTIAL IN SIMULATED SALINE LAKE WATERS

by

SCOTT NATHAN YURMAN

Committee Chair: Dr. Daniel M. Deocampo

Committee: Dr. W. Crawford Elliott

Dr. Seth E. Rose

Electronic Version Approved:

Office of Graduate Studies

College of Arts and Sciences

Georgia State University

May 2012

DEDICATION

To my lovely wife Jessica, thank you for putting up with me through this journey. I can't thank you enough for keeping me on track and pushing me through the tough times I have faced. To my mom and dad, brother Seth, sister-in-law Katy, and, the newest and tiniest member of the Yurman family, my niece Tindal. You guys are great.

I would like to dedicate this thesis to Huxley. You stuck with me through everything over the past 10 years and no matter what, you were always there for me. You are greatly missed every single day. This is for you.

ACKNOWLEDGEMENTS

I would like to thank all the students, staff and members of the Geosciences Department at Georgia State University. I would like to thank Georgia State University for their graduate teacher assistantship program and financial support provided while pursuing my master's degree. I want to thank my advisor, Dr. Dan Deocampo for all the help and guidance you gave me along the way. I have learned a whole lot going through this process and I am definitely a stronger person because of it. Thank you very much for everything. I would like to show great appreciation to my committee members, Dr. W. Crawford Elliott and Dr. Seth Rose for all their help with achieving my goal in getting a master's degree in geology. You guys are both great teachers and I have learned a lot. I would like to thank Ms. Basirat Lawal of the Geoscience Department for helping me obtain my master's degree. I always came to you when I had a problem and you always helped me out. Thank you for ordering all the materials I used in conducting my experiments. I would like to thank the USGS for the grant that Dr. Deocampo received which helped support and fund my experiments. I would like to thank Mrs. Kyle Jones for making edits to my thesis. To my fellow geoscience friends I've gained along the way, we've had some fun and stressful times. I will never forget you guys and the times we had with pursuing our goals. Best of luck to all of you!

TABLE OF CONTENTS

ACKNOWLEDGEMENTS	v
LIST OF TABLES.....	viii
LIST OF FIGURES.....	ix
CHAPTER 1 – INTRODUCTION.....	1
CHAPTER 2 – BACKGROUND ON GREEN RIVER FORMATION	4
CHAPTER 3 – METHODS OF GREEN RIVER FORMATION ANALYSIS.....	15
CHAPTER 4 – RESULTS AND DISCUSSION OF GREEN RIVER FORMATION	18
CHAPTER 5 – BACKGROUND ON SALINE LAKES	19
5.1 – Introduction.....	19
5.2 – Regional Occurrence and Physical Conditions Affecting Geochemistry.....	19
5.3 – Hydrochemistry of Brines	23
5.4 – Brine Evolution	25
CHAPTER 6 – THE CARBONATE SYSTEM AND pH CONTROL	30
CHAPTER 7 – METHODS OF SALINE LAKE EXPERIMENTS.....	35
CHAPTER 8 – RESULTS AND DISCUSSION OF SALINE LAKE EXPERIMENTS.....	51
8.1 – The Dead Sea.....	51
<i>8.1.1 – The Dead Sea with NH₄OH Added</i>	<i>55</i>
<i>8.1.2 – Discussion of Dead Sea Experiments</i>	<i>58</i>
8.2 – Great Salt Lake	59
<i>8.2.1 – Great Salt Lake with NH₄OH Added</i>	<i>62</i>
<i>8.2.2 – Discussion of Great Salt Lake Experiments</i>	<i>65</i>

8.3 – Dabusun Lake	66
8.3.1 – Dabusun Lake with NH_4OH Added	69
8.3.2 – Discussion of Dabusun Lake Experiments	72
8.4 – Donglin Lake	73
8.4.1 – Donglin Lake with NH_4OH Added	76
8.4.2 – Discussion of Donglin Lake Experiments	79
CHAPTER 9 – OVERALL DISCUSSION OF SALINE LAKE EXPERIMENTS	81
CHAPTER 10 – CONCLUSIONS	87
REFERENCES	89
APPENDIX A – ANALYTICAL DATA FROM THE DEAD SEA EXPERIMENTS	92
APPENDIX B – ANALYTICAL DATA FROM THE GREAT SALT LAKE EXPERIMENTS	95
APPENDIX C – ANALYTICAL DATA FROM THE DABUSUN LAKE EXPERIMENTS	97
APPENDIX D – ANALYTICAL DATA FROM THE DONGLIN LAKE EXPERIMENTS	99

LIST OF TABLES

Table 1	Classification of the Green River Formation Lake Type (Smith et al., 2008).	7
Table 2	Saline minerals produced from brines (Eugster, 1980).....	26
Table 3	Major ion concentrations for each lake expressed in mg L ⁻¹	36
Table 4	Major ion concentrations for each lake expressed as molarity (mol L ⁻¹).....	36
Table 5	Lake recipes expressed as molarity.....	37
Table 6	Lake recipes expressed in mg L ⁻¹	37
Table 7	Minerals precipitated that showed a clear indication of effervescence.....	85
Table 8	Analytical data from the Dead Sea experiment.....	92
Table 9	Analytical data from the Dead Sea experiment with the addition of NH ₄ OH.....	94
Table 10	Analytical data from the Great Salt Lake experiment.....	95
Table 11	Analytical data from the Great Salt Lake experiment with the addition of NH ₄ OH.....	96
Table 12	Analytical data from the Dabusun Lake experiment.....	97
Table 13	Analytical data from the Dabusun Lake experiment with the addition of NH ₄ OH.....	98
Table 14	Analytical data from the Donglin Lake experiment.....	99
Table 15	Analytical data from the Donglin Lake experiment with the addition of NH ₄ OH.....	100

LIST OF FIGURES

Figure 1	Map showing the locations of basins and basin-bounding uplifts within the Green River Formation.....	5
Figure 2	Cross section of strata in the.....	9
Figure 3	Sodium carbonate phase as a function of CO ₂ content in the gas phase and temperature.....	13
Figure 4	Flowchart for idealized evaporitic evolution in a closed basin.....	27
Figure 5	Activities of different species in the carbonate system as a function of pH.	33
Figure 6	Ca concentrations from the AA with samples diluted to 0.5%.....	43
Figure 7	Mg Concentrations from the AA calibration curves with samples diluted to 0.5%.	43
Figure 8	Ca concentrations from the AA calibration curve with samples diluted to 0.5%.....	44
Figure 9	Mg concentrations from the AA calibration curve with samples diluted to 0.5%.....	44
Figure 10	Ca concentrations from the AA calibration curve with samples not diluted.	45
Figure 11	Mg Concentrations from the AA calibration curve with samples diluted to 0.5%.....	45
Figure 12	Ca concentrations from the AA calibration curve with samples diluted to 0.5%.....	46
Figure 13	Mg concentrations from the AA calibration curve with samples diluted to 0.5%.....	46
Figure 14	Ca concentrations from the AA calibration curve with samples diluted to 0.5%.....	47
Figure 15	Mg concentrations from the AA calibration curve with samples diluted to 0.5%.....	47
Figure 16	Ca concentrations from the AA with samples diluted to 0.5%.....	48
Figure 17	Ca concentrations by day with non-diluted concentrations.....	48
Figure 18	Ca concentrations from the AA calibration curve with samples diluted to 0.25%.....	49
Figure 19	Ca concentrations from the AA calibration curve with samples diluted to 0.25%.....	49
Figure 20	Ca concentrations from the AA calibration curve with samples diluted to 0.25%.....	50
Figure 21	Mg concentrations from the AA calibration curve with samples diluted to 0.25%.....	50
Figure 22	Ca concentrations by day with non-diluted concentrations.	52
Figure 23	Ca concentrations by sample with non-diluted concentrations.....	52

Figure 24	Mg concentrations by day with non-diluted concentrations.....	53
Figure 25	Mg concentrations by sample with non-diluted concentrations	53
Figure 26	pH values per day.	54
Figure 27	pH values by sample.....	54
Figure 28	Ca concentrations by day with non-diluted concentrations.....	55
Figure 29	Ca concentrations by sample with non-diluted concentrations.....	55
Figure 30	Mg concentrations by day with non-diluted concentrations	56
Figure 31	Mg concentrations by sample with non-diluted concentrations.	56
Figure 32	pH values by day.	57
Figure 33	pH values by sample.....	57
Figure 34	Ca concentrations by day with non-diluted concentrations	59
Figure 35	Ca concentrations by sample with non-diluted concentrations.....	59
Figure 36	Mg concentrations by day with non-diluted concentrations	60
Figure 37	Mg concentrations by sample with non-diluted concentrations	60
Figure 38	pH values by day.	61
Figure 39	pH values by sample.....	61
Figure 40	Ca concentrations by day with non-diluted concentrations	62
Figure 41	Ca concentrations by sample with non-diluted concentrations.....	62
Figure 42	Mg concentrations by day with non-diluted concentrations	63
Figure 43	Mg concentrations by sample with non-diluted concentrations	63
Figure 44	pH values by day.	64
Figure 45	pH values by sample.....	64
Figure 46	Ca concentrations by day with non-diluted concentrations	66
Figure 47	Ca concentrations by sample with non-diluted concentrations.....	66
Figure 48	Mg concentrations by day with non-diluted concentrations	67
Figure 49	Mg concentrations by sample with non-diluted concentrations	67

Figure 50	pH values by day.	68
Figure 51	pH values by sample.	68
Figure 52	Ca concentrations by day with non-diluted concentrations.	69
Figure 53	Ca concentrations by sample with non-diluted concentrations.	69
Figure 54	Mg concentrations by day with non-diluted concentrations.	70
Figure 55	Mg concentrations by sample with non-diluted concentrations	70
Figure 56	pH values by day.	71
Figure 57	pH values by sample.	71
Figure 58	Ca concentrations by day with non-diluted concentrations.	73
Figure 59	Ca concentrations by sample with non-diluted concentrations.	73
Figure 60	Mg concentrations by sample with non-diluted concentrations.	74
Figure 61	Mg concentrations by sample with non-diluted concentrations	74
Figure 62	pH values by day.	75
Figure 63	pH values by day.	75
Figure 64	Ca concentrations by day with non-diluted concentrations.	76
Figure 65	Ca concentrations by sample with non-diluted concentrations.	76
Figure 66	Mg concentrations by day with non-diluted concentrations	77
Figure 67	Mg concentrations by sample with non-diluted concentrations	77
Figure 68	pH values by day.	78
Figure 69	pH values by sample.	78
Figure 70	Total amount of CO ₂ sequestered from lake experiments with the pH enhancer.	83

CHAPTER 1 – INTRODUCTION

Increased emissions of carbon dioxide (CO₂) resulting from anthropogenic (man-made) activities has been on the rise since the industrial revolution (Metz et al., 2005). Environmental concerns involving these inflated levels have begun to grow at an alarming rate in recent years. Due to this dilemma, finding ways to permanently store CO₂ has become an important issue. Established geologic formations have been thought of as a potential solution in sequestering anthropogenic CO₂, also known as carbon sequestration. Geologic reservoirs such as depleted oil and gas reserves, deep sea basalts, oil-bearing shale rock and deep sandstones have all been considered as possible scenarios (Kaldi et al., 2009). This study will introduce a different type of geologic setting as a possible scenario.

This thesis is comprised of two components both related to carbon sequestration. The first component examines the natural carbon sequestration history of the Na-carbonate producing lakes in the Green River Formation located in the western United States (Smith et al., 2008). More specifically, the Na-carbonate mineral trona will be used to determine carbonate flux rates within the sediments of the Wilkins Peak Member located in the Green River Formation. The Wilkins Peak Member housed Lake Gosiute, one of the two major paleo-lakes within the Green River Formation paleo-lake system. Known Na flux rates to the sediments have been calculated in previous paleo-weathering studies (e.g., Smith et al., 2008) and will be exploited during this investigation. Once the carbonate flux rate has been determined, a comparison to the 2009 global CO₂ emission rates will be evaluated. For the first component, the geologic history of the Wilkins Peak Member and the carbonate content of trona will be used to calculate how many of these Wilkins Peak Member formations would be required to sequester the 2009 global

emissions of anthropogenic CO₂. These rates include the total amount of CO₂ emitted from the consumption of energy produced by humans.

The second component and experimental approach of this study is to determine if saline lake environments can sequester CO₂ by carbonate mineralization. Four different saline lakes, from various regions around the world, were simulated in the laboratory by mixing deionized (DI) water and a combination of different salts at room temperature. Evaporation was permitted with no barriers in place to try and resemble a somewhat natural process of lacustrine environments. Weather and biotic activity, two very important factors in saline lake environments, will not be accounted for in the experiments.

The four experimental lakes of study include the Dead Sea located in Israel, Great Salt Lake located in Utah, U.S.A., Dabusun Lake located in the Qaidam Basin, China and Donglin Lake which is also located in the Qaidam Basin, China. These lakes were chosen because they represent a vast difference in ion concentration and overall chemistry. Two rounds of experiments were conducted on each lake. The first round demonstrated the system response to bubbling CO_{2(g)} through a diffuser with no enhancers added to the lakes. The second round replicated the same beginning process as the first round until full saturation of dissolved CO_{2(g)} was achieved. Once saturated, the CO_{2(g)} was stopped and an ammonium hydroxide solution was immediately added to increase the pH. The different variables within these experiments will help decide if carbonate production can occur naturally through the diffusion of CO_{2(g)} or if their needs to be an added enhancer to drive up the pH for carbonate mineralization to occur. This is a feasibility to determine if saline lake environments can sequester CO₂ by carbonate mineralization. Experimental lake samples were collected daily and cation loss of Ca and Mg were tested.

The purpose of this study is to determine if saline lake environments can sequester CO₂ by carbonate mineralization using the experimental approach stated above. Through previous research, saline lake environments have not been studied thus far as being a possible geologic setting for carbon sequestration. The total mass of CO₂ sequestered will be calculated by the loss of Ca and Mg within the experimental lake waters as they precipitate to form Ca and Mg-carbonates. The purpose of the first component creates an image of the size and space needed to sequester the current anthropogenic CO₂ emissions. The well studied Lake Gosiute of the Green River Formation was used to determine this, also providing an idea of the area needed if an analogous modern sedimentary environment were to be constructed.

CHAPTER 2 – BACKGROUND ON GREEN RIVER FORMATION

The Eocene Green River Formation consists of multiple basins that occupy the foreland province just east of the Cordilleran fold and thrust belt in the western United States. The different basins within the Green River Formation are confined by the Seveir orogeny fold and thrust belt and are connected by multiple anticlinal basement-cored uplifts resulting from the Laramide orogeny (Decelles, 2004; Smith et al., 2008). Both the Seveir and Laramide orogenies were active throughout the Cretaceous period. The Seveir orogeny occurred in the earlier part of the Cretaceous followed by the Laramide orogeny which began in the late Cretaceous. Located in Wyoming, Utah and Colorado, as seen in Figure 1, the Green River Formation is comprised of the Greater Green River Basin, Uinta Basin, Piceance Creek Basin and Fossil Basin covering an area of approximately 110,000 km² at maximum extent (Bohacs et al., 2002; Smith et al., 2003).

Different fine-grained sedimentary facies ranging from sandstones, mudstones, claystones and shales are found deposited throughout the shoreward areas of the basins while carbonate deposits make up the center of the basins. Volcanic material derived from the Absaroka and Challis volcanic fields are interlayered between the sedimentary strata deposited within the Green River Formation. Numerous efforts to determine the geochronology of the formation have been conducted on the volcanoclastic sediments preserved in the ash beds and sedimentary structures within the basins. Recent radiometric dating of ⁴⁰Ar/³⁹Ar using biotite and sanadine from different ash beds throughout the Greater Green River Basin, Piceance Creek Basin and Uinta Basin has refined the time span of the Green River Formation to 8 Ma during the Eocene Epoch (Smith et al., 2008). The volcanic material discovered within the formation makes it possible to pinpoint ages, sediment accumulation rates and geologic history of the Green River Formation.

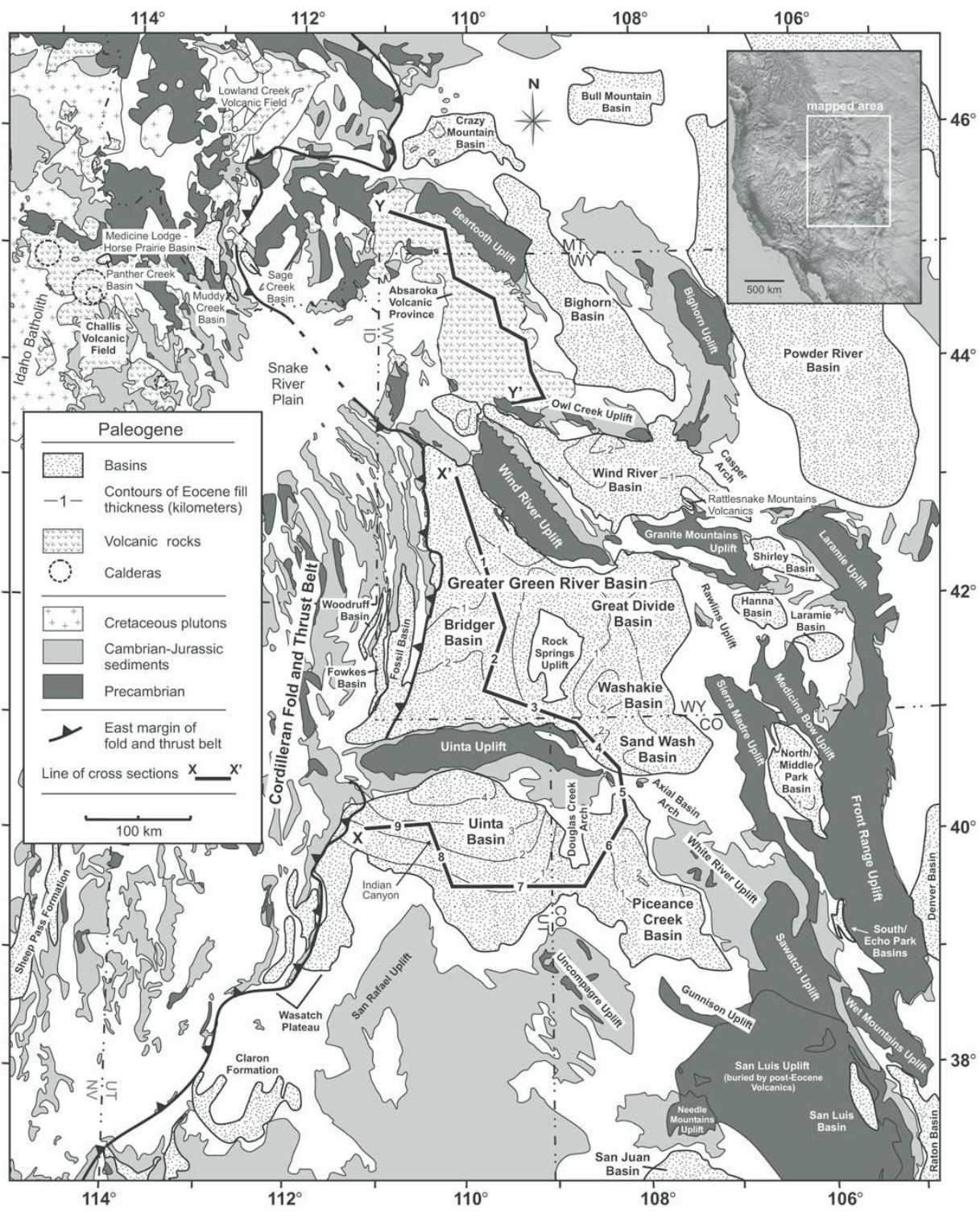


Figure 1 Map showing the locations of basins and basin-bounding uplifts within the Green River Formation (from Smith et al., 2008).

Several thick lacustrine facies within the rock record signify that the Green River Formation had a vast system of paleo-lakes during its 8 Ma span. The two most significant paleo-lakes within this system are Lake Gosiute and Lake Uinta located in the Greater Green River Basin and Uinta Basin respectively. These, and the entire paleo-lake system within the Green River Formation, are some of the most well known and studied ancient lake deposits that help geologists understand lacustrine type environments. Each of these paleo-lakes indicate a wide range of diversity in their chemistries and areal coverage during the course of Green River Formation deposition (Smith et al., 2008).

Tectonic and climatic influences on lacustrine facies associated with the Green River Formation give rise to the complexity of the ancient lake system. Tectonic basin subsidence and uplift altered the drainage patterns within the different basins providing lakes with a cycling type pattern between open and closed hydrological systems. Variations in the rates of accommodation space and water plus sediment supply during the extent of the Green River Formation gave distinct characteristics within the stratigraphy observed in the lacustrine facies (Carroll and Bohacs, 1999). In the Greater Green River Basin and its various members, changes within the facies have been recorded in lake evolution ranging from being overfilled to balance-filled to underfilled and then back through balance-filled to overfilled (Bohacs et al., 2002). The other major basins within the Green River Formation show the same type of distinction in lake-basin evolution as the Greater Green River Basin.

In overfilled lake basins, the influx of sediment plus water generally exceeds the amount of potential accommodation space. Predominantly, the inflow of water equals the outflow of water in overfilled lake basins resulting in minimal fluctuation of the water level in the lake. An increase in water plus sediment may surpass the accommodation space. This can result in the

lake water spilling and draining into different basins or lakes lower in elevation. Freshwater lakes and open lake systems are typical examples of overfilled lake basins. Balance-filled lake basins occur when accommodation space approximately equals water plus sediment supply. Fluctuation in the water level may occur in balance-filled lake basins which can affect the salinity of the water. Brackish or saline lakes are usually associated with balance-filled lake basins. In underfilled lakes basins, accommodation space continuously exceeds the water plus sediment supply resulting in a closed lake system. Hypersaline lakes are common with underfilled lake basins giving rise to bedded evaporites. Marine life is usually absent dealing within underfilled lake basins due to the high salinity and low oxygen levels. Three principle lacustrine facies have been associated with the Green River Formation for interpreting the different lake types: fluvial lacustrine, fluctuating profundal and evaporative (Carrol and Bohacs, 1999; Smith et al., 2008). Theses lacustrine facies and their associations with lake-basin fill can be seen in Table 1.

Table 1 Classification of the Green River Formation Lake Type (Smith et al., 2008).

Basin Type	Facies Association	Typical Facies	Stratigraphy	Fauna	Hydrologic Interpretation
Overfilled	Fluvial Lacustrine	Sandstone, coal, massive to laminated mudstone, coquina limestone	Dominantly progradational	Molluscs common; occasional fish	Freshwater open lake
Balance-filled	Fluctuating profundal	Organic-rich laminated mudstone, stromatolites, oolites	Mixed aggradational and progradational	Fish, ostracodes	Fluctuating salinity, intermittently open and closed lake
Underfilled	Evaporative	Na-rich evaporites, mudcracked mudstones and siltstone, thin organic-rich laminated mudstone beds	Aggradational	Fauna absent	Hypersaline closed lake

Sedimentation rates have varied in location throughout the Green River Formation's duration, resulting in a history of changing basin fill types. Volcaniclastic material from the Absaroka and Challis volcanic fields entered the Green River Formation from the north approximately 51.3 Ma and migrated southward depositing an increased amount of volcanic sediment and water in different basins along the way. The most rapid sediment accumulation occurred between 49 Ma and 47.5 Ma (Smith et al., 2003; Smith et al., 2008). The increased sediment supply and distinct drainage patterns within the basins have played an important role in altering lake-basin characteristics. From 53.5 – 52 Ma, overfilled freshwater lakes appeared to be dominant throughout the Green River Formation. Balance-filled lakes first occurred and became abundant between 52.0 – 51.3 Ma and again between 49.6 to 48.5 Ma. Underfilled evaporative type lakes showed their dominance in various basins between 51.3 and 45.1 Ma. In the Greater Green River Basin, sediment accumulation rates were approximately three times faster in the center of the basin versus the basins' margin during times when its various members, including the popular Wilkins Peak Member, were underfilled. At other times when the Greater Green River Basin's members were balance-filled to overfilled, sediment accumulation rates occurred faster at the margins compared to the center of the basin (Smith et al., 2008). Other basins within the Green River Formation displayed similar characteristics as the Greater Green River Basin.

The Greater Green River Basin consists of four subbasins: Bridger, Great Divide, Washakie, and Sand Wash. These are separated from one another by the Rock Springs Uplift, which is located towards the center of the basin and several smaller tectonic structures creating a diverse drainage system within the basin. These subbasins are further divided into various members each describing a unique set of lacustrine facies that make up the chemical evolution of

Lake Gosiute, one of the two major lakes found in the Green River Formation. The Luman Tongue, Tipton, Wilkins Peak and Laney Members are the four major members which represent the different time periods of evolution and distinct facies changes throughout Lake Gosiute's existence. In the vertical sequence from oldest to youngest, the Luman Tongue, Tipton, Wilkins Peak and Laney Members record a progression of facies changes from fluvial-lacustrine (freshwater) to fluctuating profundal (saline) to evaporative (hypersaline) and then back to fluctuating profundal and eventually fluvial-lacustrine (Carroll and Bohacs, 1999; Smith et al., 2003; Smith et al., 2008).

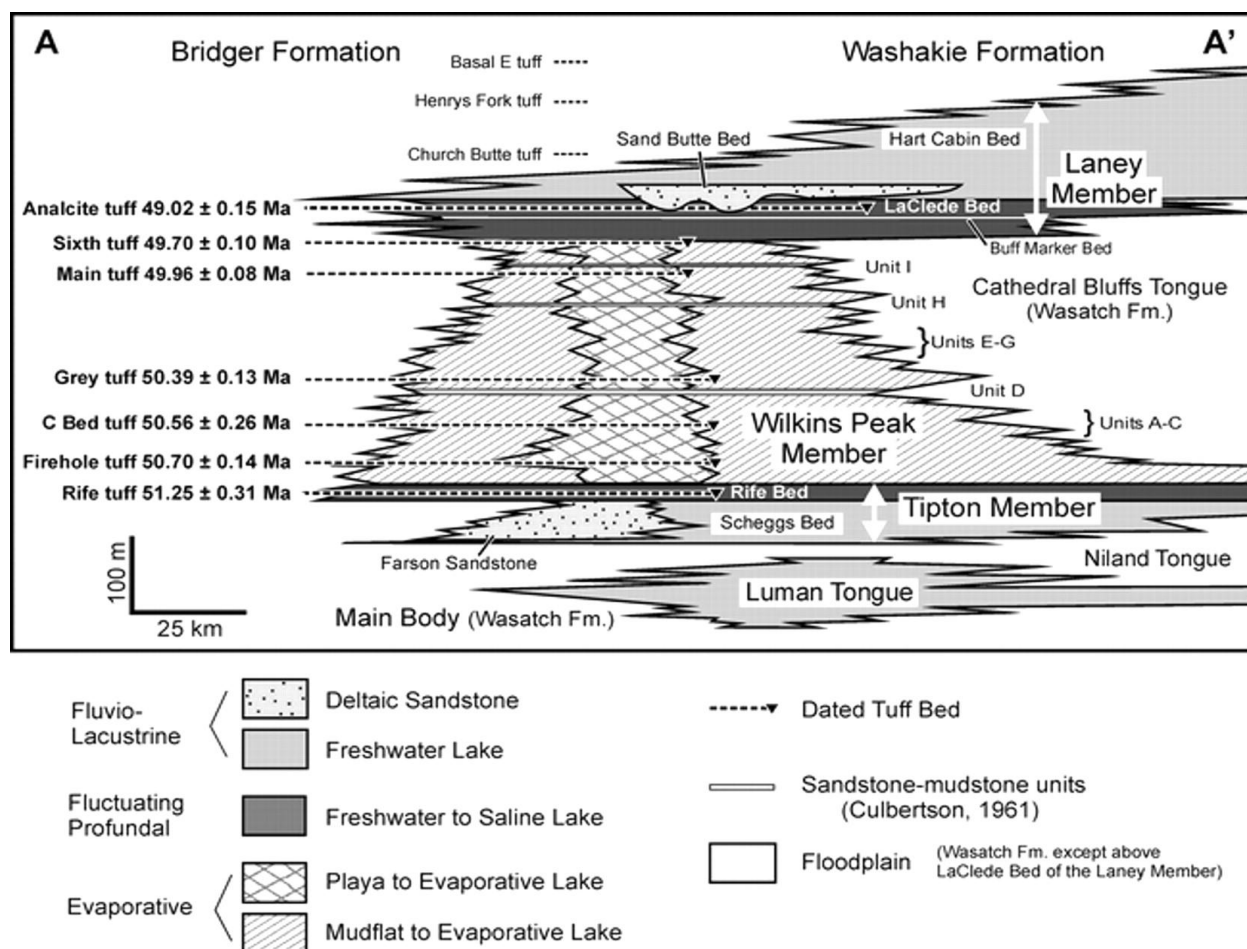


Figure 2 Cross section of strata in the Greater Green River Basin with ages of dated tuff beds to the left (from Smith et al., 2003).

The Wilkins Peak Member, primarily restricted to the Bridger subbasin of the Greater Green River Basin, produced the most exploited section of strata in the Green River Formation. Deposition of the Wilkins Peak Member occurred while sediment production was approximately three times faster in the center of the basin than on its margins, resulting in an underfilled lacustrine environment towards the basins center. Evaporative facies are dominant in the Wilkins Peak Member providing evidence that evaporation rates dominated in Lake Gosiute at the time. Volcaniclastic sediments deposited from the migration of the Absaroka and Challis volcanic fields, as well as inflow waters from drainage within the Greater Green River Basin, resulted in enriched deposits produced by Cl-Na-HCO₃-CO₃ waters in Lake Gosiute. Salts and sodium carbonates such as halite, trona, nahcolite and shortite are found interbedded in mass amounts within the Wilkins Peak Member (Warren, 2010).

Natural trona deposits within the Wilkins Peak Member are beyond any other lithologic formation in the world in relative fashion. Trona, also known as soda-ash, is a sodium carbonate that is used in the manufacturing of glass, chemicals, soap and detergents, pulp and paper, water treatment and flue gas desulfurization. The formation of trona occurs in lake waters that are enriched in HCO₃+CO₃ versus Mg and Ca. Once Mg and Ca are depleted due to carbonate precipitation, the excess HCO₃+CO₃ combines with Na to form trona, chemical formula Na₃(CO₃)(HCO₃)*2H₂O, and other sodium carbonates (Pellant, 1992; Warren, 2010). Evaporite minerals and other salts are also abundant within and surrounding trona formations. A further in-depth look at the evolution of evaporites and carbonates in saline waters will be discussed in Chapter 5.

Approximately 127 billion tons of trona and other soda-ash reserves, such as nacholite, shortite and dawsonite, are present in the Green River Formation with 70 billion tons occurring

in the Wilkins Peak Member. The Piceance Creek Basin also holds vast amounts of trona and soda-ash deposits at approximately 44 billion tons. More than 42 trona beds are deposited in the Wilkins Peak Member with 25 of the beds measuring more than one meter thick (Bradley and Eugster, 1969; Smith et al., 2008; Warren, 2010). Room and pillar mining is the dominant technique used to extract trona and other soda-ash from the Wilkins Peak Member. Solution mining is another technique used in the Green River Formation but on a much smaller scale. Lake Magadi in Kenya and Lake Natron in Tanzania, both located in the East African Rift Valley, are some other areas in the world where vast amounts of trona deposits have been produced but not to the extent found in the Green River Formation (Jones et al., 1977; Warren, 2010).

As discussed, many important factors must be applicable for trona to form. An underfilled hydrologically closed lacustrine basin where evaporation rates exceed inflow must be present. Lake waters within the basin must be enriched and show high ratios of Na/(Ca and Mg) and $(\text{HCO}_3 + \text{CO}_3)/(\text{SO}_4 \text{ and } \text{Cl})$. Along with this, an excess of CO_2 is needed to feed the brine and enhance the carbonate production leading to the formation of trona (Warren, 2010).

According to the National Oceanic and Atmospheric Administration (NOAA), as of December 2011 the level for CO_2 in the Earth's atmosphere was approximately 391 parts per million (ppm). The Eocene showed a wide range in atmospheric CO_2 with concentrations estimating between 100 and 3500 ppm (Lowenstein and Demicco, 2006). Another time in Earth's history where trona was found in mass quantities was during the Archean eon. The Archean eon demonstrated a very rich CO_2 atmosphere where trona and other soda-ash such as nahcolite were the primary marine salts at the time. Nahcolite, chemical formula NaHCO_3 , has the second most abundant deposits in the Green River Formation registering at approximately 27 billion tons (Warren,

2010). Although both sodium carbonates, the difference between trona and nahcolite is that nahcolite precipitates only under elevated CO₂ conditions. The minimum CO₂ levels in which nahcolite precipitates tested under experimental conditions is approximately 1330 ppm. According to Lowenstein and Demicco (2006), with the presence of halite, as seen within the interbedded or surrounding strata in the Green River Formation, a lower minimum level of CO₂ is needed to precipitate nahcolite at approximately 1125 ppm. Along with CO₂ concentration, temperature also plays a factor with the precipitation of trona, nahcolite, and other sodium carbonates as seen in Figure 3 below. At present day CO₂ conditions, trona will crystallize only at temperatures above 25°C. Trona may crystallize in slightly lower temperatures but elevated CO₂ levels must be present. As seen with nahcolite in Figure 3, high amounts of CO₂ must be present and temperatures may be slightly less than what is needed for trona. In either setting, elevated CO₂ conditions must be present in order for trona and nahcolite to form. Magmatic influences and high amounts of organic material, as seen in the oil shales of the Green River Formation, may have been some potential reasons for excess CO₂ throughout the Eocene. The decomposition and respiration of organisms will cause atmospheric CO₂ levels to rise as oxygen and organic matter are being converted to CO₂.

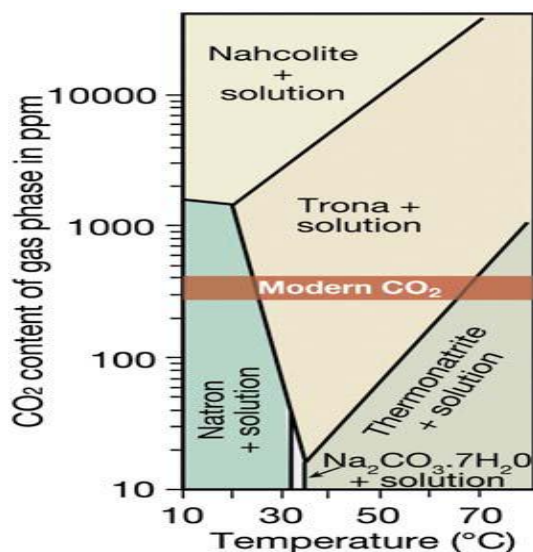


Figure 3 Sodium carbonate phase as a function of CO₂ content in the gas phase and temperature (from Lowenstein and Demicco, 2006).

High amounts of atmospheric $p\text{CO}_2$ will likely lead to increased amounts of $p\text{CO}_2$ found in soils. With increased amounts of $p\text{CO}_2$ present in soils, a carbonic acid forms as CO_2 reacts with water leading to the enhancement of chemical weathering and silicate dissolution. At this point, cations and anions are dissociated from one another and left alone to react with other phases. Major cations such as Ca, Mg and Na can react with CO_2 and water to form carbonates. This process represents an important negative feedback as atmospheric CO_2 is being consumed in carbonate minerals within the soils. The consumption of CO_2 in carbonate minerals causes CO_2 to be trapped, rendering it immobile for an extended period of time. This demonstrates a natural example of how CO_2 becomes sequestered.

With the more recent problem of atmospheric CO_2 increasing somewhat rapidly due to anthropogenic reasons, figuring out ways to sequester CO_2 manually has become an issue. Decreasing the amount of added anthropogenic CO_2 to the atmosphere will hopefully slow down global temperature increases that are ongoing (Metz et al., 2005). Various geologic formations possess the capabilities of storing anthropogenic CO_2 instead of adding it to the Earth's

atmosphere. Studying the geologic history of the Green River Formation has made it possible to develop a real world scenario describing how much CO₂ can potentially fit into a geologic formation. In this study, the geologic history of the Wilkins Peak Member and the carbonate content of trona are used to calculate how many of these formations would be required to sequester current global emissions of anthropogenic CO₂ if an analogous modern sedimentary environment were to be constructed.

CHAPTER 3 – METHODS OF GREEN RIVER FORMATION ANALYSIS

Weathering rates of Na have been calculated throughout the extent of the Wilkins Peak Member in a study conducted by Smith et al (2008). In their study, six ash horizons were age dated using the $^{40}\text{Ar}/^{39}\text{Ar}$ radiometric dating method to Figure the duration of the Wilkins Peak Member to 1.5 Ma. However, the majority of Na, approximately 93%, is found in the lower half of the Wilkins Peak Member and was deposited over a span of approximately 0.7 Ma. Information involving the duration of the Wilkins Peak Member makes it possible to calculate the accumulation rates of lacustrine carbonates and alluvium during the entire period of deposition of the Wilkins Peak Member.

An estimated area of 17,900 km² enclosed the Greater Green River Basin paleocatchment which fed Lake Gosiute and the Wilkins Peak Member. Springs, streams and rivers travelled through this region weathering rocks and transporting minerals that were eventually deposited into Lake Gosiute, producing the Wilkins Peak Member. The majority of the Na deposited came from the Precambrian crystalline basement of the Greater Green River Basin paleocatchment, with lesser amounts coming from the Phanerozoic strata deposited on top of the basement. Approximately 93% of Na was deposited in the lower half of the Wilkins Peak Member while the upper portion contained little amounts of Na. There has not been an exact explanation to why this happened, but it is most likely due to the change of lake-basin hydrology and chemistry (Smith et al., 2008). The lower half of the Wilkins Peak Member is where the majority of the Na-carbonates reside.

Na accumulation rates within the duration of the lower half of the Wilkins Peak Member yielded annual values of approximately 3.5 t/km²/yr. This value includes the Greater Green River Basin paleocatchment area of 17,900 km². Converting tonnes to grams gives an annual

value of 3.5×10^6 g/km². The atomic mass of Na is equal to 22.99 g/mol, which means that 1 mole of Na weighs 22.99 grams. Dividing the annual Na flux of 3.5×10^6 g by 22.99 g/mol of Na results in 1.52×10^5 moles of Na/km². Referring back to the chemical formula of trona, Na₃(CO₃)(HCO₃)*2H₂O, demonstrates a ratio of three moles of Na per two moles of C or a 3:2 ratio. Using the answer of 1.52×10^5 moles of Na/km² and dividing that by 1.5 (the 3:2 ratio) will result in the amount of moles of C which is 1.01×10^5 moles of C/km². These numbers result in the annual amount of moles of Na and C per km². Multiplying both these numbers by the duration of the lower half of the Wilkins Peak Member of 0.7 million years gives values of 1.07×10^{11} moles of Na/km² and 7.1×10^{10} moles of C/km². Multiplying these by the paleocatchment area of 17,900 km² gives values of 1.92×10^{15} moles of Na and 1.27×10^{15} moles of C. These numbers represent the total amount of moles of Na and C throughout the duration of the lower half of the Wilkins Peak Member. Flux rates of Na and C in tonnes/year within the given area show values of 63,000 and 21,790 respectively. This represents a breakdown of the estimated Na flux rates within the 17,900 km² Greater Green River Basin paleocatchment.

As stated in 2008 by Smith et al., mapped trona beds in the Wilkins Peak Member contained approximately 4.1×10^{10} tonnes of Na. This number may be greatly underestimated due to many thin unmapped trona horizons as well as disseminated halite and other Na-carbonates (Smith et al., 2008). Converting the 4.1×10^{10} tonnes to grams and then moles of Na gives values of 4.1×10^{16} g and 1.78×10^{15} moles of Na. Using the 3:2 ratio of Na to C in trona results in 1.19×10^{15} moles of C. This concludes that 1.19×10^{15} moles of C were naturally sequestered within the lower half of the Wilkins Peak Member. This information reveals that the amount of Na present in the mapped trona beds is very close to that of the Na accumulation value

of 1.27×10^{15} moles determined above. The amount of naturally sequestered C within the mapped trona beds will be compared to the current global CO₂ emission rates.

Global CO₂ emissions data was provided by the U.S. Energy Information Administration (EIA) which is a branch of the Department of Energy (DOE). The most recent completed global CO₂ emissions data is from 2009 and includes all CO₂ emissions from the consumption of energy.

CHAPTER 4 – RESULTS AND DISCUSSION OF GREEN RIVER FORMATION

The result of global CO₂ emissions in 2009 was 30,313.25 million tonnes or 3.03×10^{10} tonnes of CO₂. The continent of Asia led the way with 1.32×10^{10} million tonnes of CO₂ emitted. China, the country that produced the most CO₂, accounted for over half of that at 7.7×10^9 tonnes. As a continent, North America came in second with 6.41×10^{10} tonnes. The United States accounted for the second most CO₂ emitted at 5.42×10^9 tonnes (<http://www.eia.gov>).

The 2009 total of 3.03×10^{10} tonnes converts to 3.03×10^{16} grams of CO₂ produced. Dividing that number in grams by the atomic weight of C (12.01 g/mol) gives a total of 2.52×10^{15} moles of C. In this scenario, the amount of CO₂ produced globally in 2009 would be able to be sequestered into the Wilkins Peak Member of the Green River Formation 0.47 times. This shows that approximately half of the worlds CO₂ output from 2009 would equal the size of one Wilkins Peak Member formation. This area included 17,900 km² of the Greater Green River Basin paleocatchment which fed minerals into the Wilkins peak member and Lake Gosiute. This led to the highest production of trona deposits in the world. This area naturally generated 1.19×10^{15} moles of C, which accumulated during the lower half of the Wilkins Peak Member's 0.7 million year duration, and deposition of sediments. If an event like this were to occur, the size and space of approximately two Wilkins Peak Member formations would be needed to sequester the entire 2009 global emissions of anthropogenic CO₂.

CHAPTER 5 – BACKGROUND ON SALINE LAKES

5.1 – Introduction

Saline lakes are important geologic features that provide scientists with a range of information from past environmental settings to valuable economic resources that can be used in the world today. Ancient sediments studied within these intracontinental lake basins offer clues to past climates, tectonics, and hydrologic variations that these lakes encounter throughout their geologic existence. The complexity of saline lakes stems from their diverse geochemistry which involves meteoric precipitation, weathering, groundwater, evaporation, precipitation-dissolution reactions and biotic activity. Today, saline lakes have a significant geochemical impact on ecology, water resources and economic activity around the world (Jones and Deocampo, 2003).

5.2 – Regional Occurrence and Physical Conditions Affecting Geochemistry

Saline lakes are found in every continent all over the world. Dependent upon the region in which they are formed, these lacustrine basins show a unique set of characteristics from one area to the next. Hydrologic closure, among several other important features, is a must for saline lakes to occur. For this reason, past tectonic events play a key role in determining the location of a saline lake. Probably the most favorable location for saline lakes is in the rain-shadows of high mountain ranges, which acts as a barrier against excessive rainfall to the basin floor as well as providing a catchment area for precipitation (Eugster, 1980; Jones and Deocampo, 2003). Several of the world's largest saline lakes were formed in tectonically active regions displaying a wide range in elevation from exceeding 1 km to below sea level. Great Salt Lake in Utah and Lake Van in Turkey are some saline lakes found in regions which exceed 1 km. Other saline lakes such as the Dead Sea in Israel and the Caspian Sea in western Asia, which holds most of the world's saline lake water, exhibit elevations that are below sea level. Deep rift basins, such

as the East African Rift and the Kenyan Rift Valley, also host a series of large saline lakes which include Lake Turkana and Lake Magadi respectively (Jones and Deocampo, 2003). Along with the Caspian Sea, there are many other saline lakes such as the Aral Sea that inhabit the steppes of central Asia.

As mentioned above, tectonics may be the main determinant for the formation and fate of a saline lake. Tectonic basin subsidence along with surrounding uplift is the ideal tectonic setting for a saline lake. Typically, saline lakes form in low flat lying basins surrounded by mountains on every side (Eugster, 1980). The surrounding mountains act as a rain-shadow to the basin floor. If the surrounding mountains were not in place, excessive amounts of rainfall would enter the basin floor and most likely keep the basin overfilled with water. In this scenario, water inflow would nearly always equal outflow and sediments would not have time to accumulate in the water table. For a saline lake to persist, the accommodation space in the basin floor will continuously exceed water inflow plus the sediment supply which typifies an underfilled lake basin (Carrol and Bohacs, 1999). Once the tectonic setting is in place, the physical aspects of the surrounding hydrology, climate and geology will each play a major role in affecting the lakes geochemistry.

Saline lakes are hydrologically closed basins that follow three basic conditions in order to form and survive. First, outflow must be absent or extremely minimal to ensure hydrologic closure within the basin. Second, evaporation must exceed or approximate inflow. Finally, there must be a sufficient amount of inflow to maintain a permanent body of water at or very close to the surface (Jones and Deocampo, 2003). Evaporation must be the main component accounting for the outflow of water in a hydrologically closed basin. Minimal factors such as lake basin leakance into the surrounding soils and groundwater may occur, but this will be extremely

minute compared to the evaporation rate. Most importantly, evaporation rates must closely approximate or exceed the inflow of surface or groundwater entering the basin.

The influential difference between surface runoff and groundwater will have a major affect on the chemistry of a saline lake. If dominated by surface water, lake level fluctuation will occur especially in a monsoonal type season. Heavy rain events will cause an excess of surface water entering the basin causing lake levels to rise. Conversely, drought periods will cause lake levels to fall. Heavy droughts may also affect the amount of solutes entering the lake basin which can result in dropping the lake's salinity. With surface waters being dominant, the surrounding lithology will play a major role in deciding what solutes will be entering the lake. An example of lake fluctuation was evident during the 1.5 million year span of the Wilkins Peak Member, which housed Lake Gosiute in the Green River Formation. Lake Gosiute went through periods of being overfilled to balance-filled to underfilled and then back through balance-filled to overfilled (Bohacs et al., 2002). Lake level fluctuation, such as Lake Gosiute, is apparent when looking at the sedimentological, biological and geochemical evidence left behind in the surrounding stratigraphy. Changes in the hydrologic budget for a basin will also result in lake level fluctuation (Jones and Deocampo, 2003).

Groundwater's impact on lake chemistry will be affected more by Earth's internal processes than what is seen on the surface. Meteoric waters will collect solutes either from aerosols or surrounding sediments below the surface as the water percolates through the soils and into the water table. Interstitial fluids within subsurface sediments will result in an increase of solutes entering groundwater which is eventually fed into the lake basin. Hydrothermal fluids, though usually discharged in small amounts, may cause a big change in lake water chemistry. These fluids are usually extremely rich in metals produced within the mantle and can cause a

major addition of solutes entering a lacustrine environment. Various aquifer characteristics such as residence time and hydraulic conductivity within an aquifer system can also be a determining factor in lake basin chemistry (Jones and Deocampo, 2003).

Climate is another factor that plays a role in deciding the fate of a saline lake. As mentioned above, seasonal variations between monsoonal type events and drought periods will cause changes in water chemistry as well as lake level fluctuation. Heavy rains may bring an influx of metals, such as Ca and Mg, which will increase the amount of solutes entering a lake basin and accumulating in the water column. Conversely, heavy rains may also dilute lake waters if metals are insufficient within the rainwater's chemistry. Precipitation of carbonates and sulfates may occur during these times as the additional Ca and Mg ions are being removed from solution. Regional temperature variations will also affect the physical conditions of a closed-basin lake. Increased temperatures can lead to higher evaporation rates which can drop lake surface levels as well as increase the salinity. Colder arid temperatures surrounding saline lakes may result in a "freeze-out" affect within the minerals and slow down certain reactions that would persist in a normal temperature setting (Jones and Deocampo, 2003).

The geology of the basin and watershed surrounding a saline lake will determine what major solutes are affecting the lake's chemistry. Surface waters, such as rivers and streams entering a lake basin will transport sediments collected from the weathering of rocks within the area. The solutes draining into the lake will be the deciding factor on the rocks and minerals that may precipitate out of the water column. An example of this was seen in the Wilkins Peak Member of the Green River Formation. Inflow waters collected volcanoclastic sediments from the Absaroka and Challis volcanic fields which led to an influx of Na entering the basin. This resulted in one of the biggest trona deposits in the world (Smith et al., 2008). Additional inflow

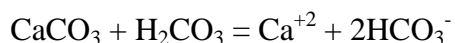
points entering a basin can lead to an even further complex lake chemistry. Two or more chemically different rivers can result in the mixing of solutes once entered into the lake. Lake stratification may occur if this happens as heavier metals may sink to deeper levels.

5.3 – Hydrochemistry of Brines

Evaporite deposits in saline lakes can only form if there is a sufficient amount of solutes being introduced from various inflow sources. Furthermore, the most concentrated saline lake waters result from a closely maintained balance between inflow and evaporation (Eugster, 1980; Jones and Deocampo, 2003). Following these two rules from above, saline lake evaporites will be defined by their inflow sources. The surrounding lithology will be the key indicator in describing this matter. The source of solutes can be extremely different from one area to the next. Neighboring basins, separated only by a watershed, may produce widely different chemistry and mineralogy (Eugster, 1980).

Like in all natural waters, the composition of saline lakes can be represented by less than 10 major solutes. Typically, there are four major cations and three major anions present which include Na^+ , K^+ , Ca^{+2} , Mg^{+2} , Cl^- , SO_4^{-2} and $\text{HCO}_3^- + \text{CO}_3^{-2}$. Other minor solutes such as SiO_2 , B, NO_3 and PO_4 are rarer in appearance but may be of concern. Of all these, Na is the most common cation in solution (Eugster, 1980; Jones and Deocampo, 2003). Rain water and weathering are the main sources providing solutes to saline lakes basins. Besides silica, rainwater can produce all of the solutes listed above but will be most enriched in Na, Cl, SO_4 and HCO_3 (Eugster, 1980). Regional differences may affect the chemistry of rainwater. Sea spray entering the atmosphere will provide an increase of Na and Cl in rainwater water chemistry. Conversely, greater distances from these type sources may vary in amounts of Na and Cl. Pollution may also be a factor when dealing with rainwater chemistry.

There are many different kinds of weathering reactions that supply solutes to inflow sources. The most common aspect of chemical weathering is the dissolution of soluble minerals such as gypsum, halite and calcite. Major solutes produced from these minerals will include Na, Cl, Ca, SO₄ and CO₃. Calcite, which is the dominant mineral in limestone, will dissolve readily in CO₂ charged waters. As water flows through and across limestone aquifers, inflow waters will be enriched in Ca and HCO₃ as the reaction below occurs:



Dolomite will produce the same type waters but be enriched in Mg as well as Ca. Igneous and metamorphic type lithologies, as seen in the Green River Formation, will yield waters containing high amounts of Ca, Na, HCO₃ and SiO₂. Waters flowing across sulfur-rich sediments will produce high amounts of sulfates. Mafic and ultramafic rocks will add Mg and HCO₃ to the mix, as well as SiO₂ and different type feldspars (Warren, 2010).

Accounting for all the major solutes, Eugster (1980) distinguished five major brine types that are applicable for hydrologically closed basins:

1. Ca – Mg – Na – (K) – Cl
2. Na – (Ca) – SO₄ – Cl
3. Mg – Na – (Ca) – SO₄ – Cl
4. Na – CO₃ – Cl
5. Na – CO₃ – SO₄ – Cl

Any of these waters found within a particular evaporitic basin will produce an array of evaporite minerals. Although each of these brines characterizes a difference in chemistry, the most common mineral to precipitate from all five type waters is halite (Eugster, 1980; Warren, 2010).

A list of the more common saline minerals produced from each of these brines can be found in table 2 on the following page.

Brine chemistry, as well as other factors such as biotic activity, will have an effect on the pH of a saline lake. The pH is usually close to neutral for saline waters containing mostly chloride and sulfate salts. Waters that contain Ca – Mg carbonates are mildly alkaline and can range in pH from around 7.5 – 8.5. The higher pH waters, where pH can reach up to 12, are associated with alkali carbonate solutes and relatively high silica content. Acidic saline lake waters, where the pH can reach as low as 2-3, are obtained in the absence of carbonates or with the low silicate buffer capacity (Jones and Deocampo, 2003). A more detailed approach involving the pH of lake waters will be discussed in chapter 6.

5.4 – Brine Evolution

The chemical evolution of lake brines begins with defining the different solutes being introduced from various inflow sources. The surrounding lithology within a lake basin watershed will be the principle factor determining the resulting solute concentrations that enter a lake basin which make up the hydrochemistry of the brines. Atmospheric input that precipitates in rainwater will also bring additional solutes to a lake basin but will be small in comparison to the surrounding lithology. Groundwater flow will work the same way by collecting solutes from the different rock types and soils in the area, eventually entering the lake basin through baseflow.

The chemical interaction between the major cations and anions will control the fate of saline water evolution. Figure 4 is a flowchart of idealized evaporitic evolution of a closed basin that will be used to describe the progression of solute interaction (Jones and Deocampo, 2003). Chloride, although not mentioned in Figure 4, is considered to be ubiquitous in this situation.

Table 2 Saline minerals produced from brines (Eugster, 1980)

Brine Type	Saline Mineral		
Ca – Mg – Na – (K) – Cl	Antarcticite	$\text{CaCl}_2 \cdot 6\text{H}_2\text{O}$	
	Bischofite	$\text{MgCl}_2 \cdot 6\text{H}_2\text{O}$	
	Carnallite	$\text{MgCl}_2 \cdot \text{KCl} \cdot 6\text{H}_2\text{O}$	
	Halite	NaCl	
	Sylvite	KCl	
	Na – (Ca) – SO_4 – Cl	Tachyhydrite	$\text{CaCl}_2 \cdot 2\text{MgCl}_2 \cdot 12\text{H}_2\text{O}$
Glauberite		$\text{CaSO}_4 \cdot \text{Na}_2\text{SO}_4$	
Gypsum		$\text{CaSO}_4 \cdot 2\text{H}_2\text{O}$	
Halite		NaCl	
Mirabilite		$\text{Na}_2\text{SO}_4 \cdot 10\text{H}_2\text{O}$	
Thenardite		Na_2SO_4	
Mg – Na – (Ca) – SO_4 – Cl		Bischofite	$\text{MgCl}_2 \cdot 6\text{H}_2\text{O}$
	Bloedite	$\text{Na}_2\text{SO}_4 \cdot \text{MgSO}_4 \cdot 4\text{H}_2\text{O}$	
	Epsomite	$\text{MgSO}_4 \cdot 7\text{H}_2\text{O}$	
	Glauberite	$\text{CaSO}_4 \cdot \text{Na}_2\text{SO}_4$	
	Gypsum	$\text{CaSO}_4 \cdot 2\text{H}_2\text{O}$	
	Halite	NaCl	
	Hexahydrite	$\text{MgSO}_4 \cdot 6\text{H}_2\text{O}$	
	Kieserite	$\text{MgSO}_4 \cdot \text{H}_2\text{O}$	
	Mirabilite	$\text{Na}_2\text{SO}_4 \cdot 10\text{H}_2\text{O}$	
	Thernadite	Na_2SO_4	
	Na – CO_3 – Cl	Halite	NaCl
		Nahcolite	NaHCO_3
Natron		$\text{Na}_2\text{CO}_3 \cdot 10\text{H}_2\text{O}$	
Thermonatrite		$\text{NaCO}_3 \cdot \text{H}_2\text{O}$	
Trona		$\text{Na}_3(\text{CO}_3)(\text{HCO}_3) \cdot 2\text{H}_2\text{O}$	
Na – CO_3 – SO_4 – Cl	Burkeite	$\text{Na}_2\text{CO}_3 \cdot 2\text{Na}_2\text{SO}_4$	
	Halite	NaCl	
	Mirabilite	$\text{Na}_2\text{SO}_4 \cdot 10\text{H}_2\text{O}$	
	Nahcolite	NaHCO_3	
	Natron	$\text{Na}_2\text{CO}_3 \cdot 10\text{H}_2\text{O}$	
	Thernadite	Na_2SO_4	
Thermonatrite	$\text{NaCO}_3 \cdot \text{H}_2\text{O}$		

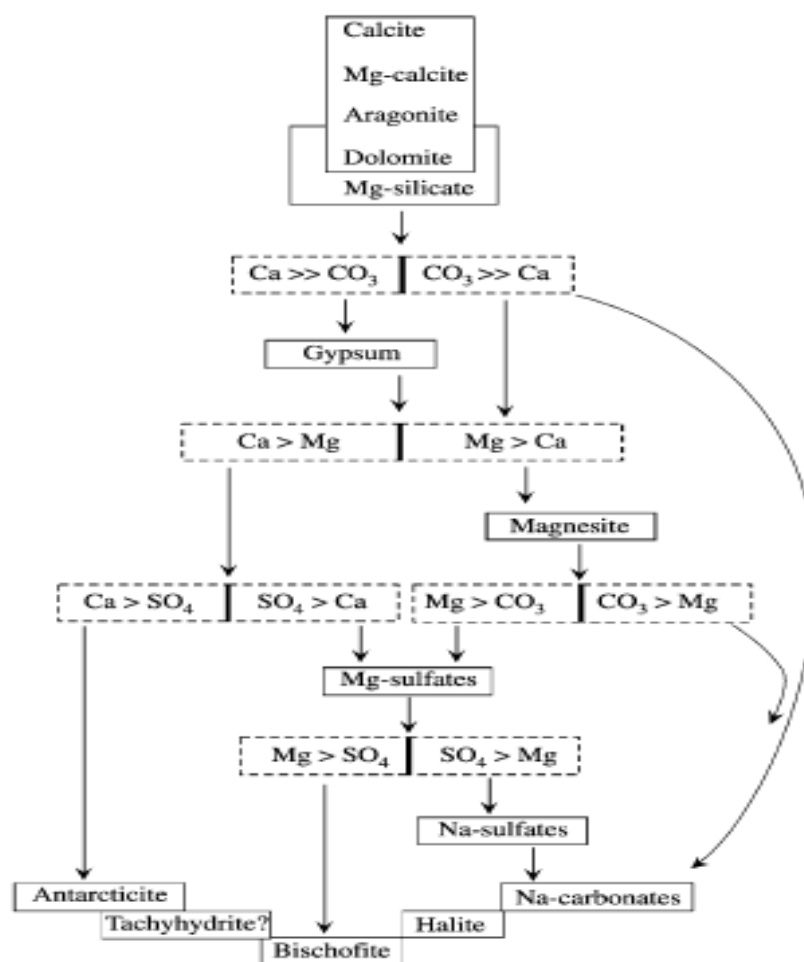


Figure 4 Flowchart for idealized evaporitic evolution in a closed basin. CO_3 will refer to all aqueous CO_2 species (from Jones and Deocampo, 2003).

The first minerals to precipitate from the concentrated brines are the alkaline earth carbonates (Jones and Deocampo, 2003; Warren, 2010). These include the minerals toward the top of the flowchart which will be calcite, low and high-magnesium calcite, aragonite and dolomite. Mineralogy of the initial precipitates will be dependent on the Mg/Ca ratio of the brine (Warren, 2010). At this stage, the initial ratio of $\text{HCO}_3^- / (\text{Ca} + \text{Mg})$ will determine the early stages of the evolution pathway of saline waters (Jones and Deocampo, 2003).

The equilibrium precipitation of pure calcite will result in 1 mole of Ca^{+2} and 1 mole of CO_3^{-2} being lost from solution. As this occurs, the Ca/CO_3 ratio will begin to change unless these two ions were found in equal proportions within the solution, which is virtually impossible. The unequal proportions of these solutes will dictate the dominant constituent on further concentrations. After calcite precipitation begins, the more abundant ion will eventually begin to increase as the less abundant ion decreases until it is depleted. If Ca was the ion to increase, CO_3 will begin to decrease or vice versa (Jones and Deocampo, 2003). In this matter, calcite precipitation marks the first chemical divide in the evolution of lake brines and will determine if the remaining solution becomes carbonate rich or carbonate poor (Eugster, 1980; Jones and Deocampo, 2003).

The next step in Figure 4 will show the division between the brines becoming carbonate rich or carbonate poor. Following the right side of the flow chart demonstrates lake waters being enriched in CO_3 and is denoted as $\text{CO}_3 \gg \text{Ca}$. For the situation, Ca as well as Mg will be in decline. Following this progression, excess CO_3 will be abundant in the brines as Ca and Mg become depleted. As CO_3 is the most abundant ion in the waters, it will combine with Na to form Na-carbonates which is displayed by the arrow on the right side from $\text{CO}_3 \gg \text{Ca}$ to Na-carbonates. Minerals such as trona, natron and nachcolite, which can be seen in table 2, will begin form. These minerals represent the vast deposits found in the Wilkins Peak Member of the Green River Formation which were precipitated from these type waters.

Following the left side of the division, opposite from the waters above, will display Ca and Mg becoming enriched compared to CO_3 . This will be represented by $\text{Ca} \gg \text{CO}_3$ on the flow chart. After the initial carbonates precipitate, the CO_3 anion will begin to decrease as Ca and Mg become the dominant cations in the brine. Carbonate precipitation will cease in this situation and

the abundant cations left in the water will begin to combine with the sulfate, SO_4^{-2} , anion. This marks the second chemical divide with respect to Ca and SO_4 to form gypsum. Large volumes of gypsum and other minerals such as epsomite will begin to precipitate out of solution. Bristol Dry Lake and Cadiz Lake, found in the Mohave Desert in California, represent these type waters and mineral production (Warren, 2010).

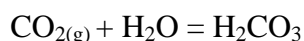
The middle of the flow chart, below $\text{Ca} \gg \text{CO}_3$ precipitation to gypsum, exemplifies when $(\text{Ca} + \text{Mg}) / \text{CO}_3$ are nearly uniform. Large amounts of alkaline earth carbonates will form in this process. As this occurs, Mg will become strongly enriched over Ca as Ca combines with CO_3 and eventually becomes exhausted (Eugster, 1980). The remaining Mg and CO_3 will interact to form the mineral magnesite. High-Mg calcite and dolomite may also form in this situation. Conversely, if Ca is the dominant cation in solution and the CO_3 anion becomes exhausted along with the Mg cation, the remaining Ca will again bond with SO_4 and the brine will become saturated with gypsum.

The bottom part of Figure 4 symbolizes the period when both the CO_3 and SO_4 anions become exhausted and cations such as Ca, Mg Na and K are still in abundance. As mentioned in section 5.3, three major anions can be found in all natural waters. With the CO_3 and SO_4 anions being consumed, chloride, Cl^- , remains as the only anion left in solution. Major cations will interact with Cl to form minerals such as antarcticite, bischofite, halite, carnallite and sylvite. All these minerals can be found in table 2 within the Ca – Mg – Na – (K) – Cl brine type. As the different evolution pathways of brines occur, chloride, as well as sodium, is considered to be ubiquitous (Jones and Deocampo, 2003).

CHAPTER 6 – THE CARBONATE SYSTEM AND pH CONTROL

The pH of most saline lakes, as well as most natural waters, is controlled by reactions involving the carbonate system (Drever, 97). As seen throughout the experiments conducted during this study, the introduction of CO₂ into saline lake environments can quickly change the pH from being alkaline to acidic. The amount of CO₂ within these waters can vary drastically depending on the surrounding conditions. High atmospheric levels of *p*CO₂ can increase the amount of CO₂ entering lake brines as well as the peripheral soils and geology. Increased levels of *p*CO₂ in soils can eventually react with the groundwater that drains into a saline lake basin through baseflow. Biotic activity can play a major role with the production or reduction of CO₂ through respiration and photosynthesis. In areas where microbial respiration is in access, *p*CO₂ levels can reach two to three orders of magnitude higher than atmospheric conditions. In this scenario, microbial respiration would have to exceed the amount of CO₂ that is being degassed into the atmosphere (Jones and Deocampo, 2003).

When CO₂ gas comes in contact with water, the CO₂ will dissolve until equilibrium is reached (Drever, 97). As this occurs, the reaction between the dissolved CO₂ and water generates a carbonic acid, H₂CO₃. The equation for this reaction is as follows:



At equilibrium, the activity of the dissolved CO₂, or H₂CO₃, will be proportional to its pressure. Another way of stating this is that when the activity of the dissolved CO₂ is around 1, or at its full saturation point, the pressure or *p*CO₂ is also close to its full capacity. This concept follows Henry's law constant for a dissolved gas being proportional to its pressure (Drever, 97).

As the activity of H_2CO_3 increases, the pH of the water will become acidic. Acidic waters that contain H_2CO_3 will have a $\text{pH} < 6.4$. Extremely high amounts of $p\text{CO}_2$, where constant pressure is being applied, may drive the pH down to as low as 3-4. This was seen in some of the saline lake experiments conducted during this study and will be discussed in chapter 8. As the carbonate system progresses, the importance of the transition to bicarbonate (HCO_3^-) and carbonate (CO_3^{2-}) will depend on the pH of the solution (Andrews et al., 2004).

At some point, $p\text{CO}_2$ levels may begin to decrease and H_2CO_3 will begin to dissociate as the pH rises. This marks the first dissociation process of the carbonate system. As this occurs, H_2CO_3 will separate into hydrogen and bicarbonate ions. The equation for this reaction is as follows:



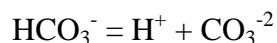
The dissociation constant, denoted as K , for this reaction will be:

$$K_1 = \frac{a\text{H}^+ * a\text{HCO}_3^-}{a\text{H}_2\text{CO}_3} = 10^{-6.4}$$

K_1 stands for the first dissociation constant and 'a' designates the activity of the ions.

Dissociation constants are derived at equilibrium for components that can dissociate to form charged species or ions. These constants are ratios of dissociated species to undissociated species, like the equation above. The dissociation constants for the carbonate system are known values and follow the same equation for each of the carbonate species (Andrews et al., 2004). K_1 being equal to $10^{-6.4}$ states that at a pH of 6.4, the activity of H_2CO_3 will equal that of HCO_3^- (Drever, 97).

The second dissociation of HCO_3^- is:



The dissociation constant for this reaction is as follows:

$$K_2 = \frac{aH^+ * aCO_3^{-2}}{aHCO_3^-} = 10^{-10.3}$$

At a pH of 10.3 from the K_2 equation, the activity of HCO_3^- will be equal to the activity of CO_3^{-2} . Extremely alkaline waters will have a pH >10.3 and the activity of CO_3^{-2} will always be greater than that of HCO_3^- . As the pH of alkaline waters go beyond 10.3, the activity of CO_3^{-2} will increase where as the activity of HCO_3^- will decrease.

The K_1 and K_2 dissociation constants explain the activity of the major species in water as a function of pH. As seen from the equations above, the first dissociation, K_1 , occurs at a pH of 6.4. At this pH, the activity of H_2CO_3 and HCO_3^- are equal. Once the water becomes slightly more acidic, the activity of H_2CO_3 will increase while the activity of HCO_3^- begins to decrease. The more acidic the water becomes denotes the higher the activity of H_2CO_3 . This also states that as the water becomes more acidic, HCO_3^- will become less and less abundant until it is eventually gone or at a zero concentration. This same rule applies for the second dissociation, K_2 . A pH less than 10.3 and greater than 6.4 will lead to the HCO_3^- anion being most abundant, or having a higher activity than both CO_3^{-2} and H_2CO_3 . As mentioned above, CO_3^{-2} will be the dominant specie at a pH greater than 10.3.

The alkalinity in most natural continental waters is dominated by the HCO_3^- anion and ranges in pH between 7 and 9 (Andrews et al., 2004). To demonstrate ionic activity, the dissociation constant equation can be rearranged for a typical pH value of continental waters. For example, many saline waters display a pH value around 8. Rearranging the second dissociation constant equation for HCO_3^- and CO_3^{-2} will be as follows:

$$aHCO_3^- = \frac{aH^+ * aCO_3^{-2}}{K_2}$$

Substituting the pH value of 8 for H^+ ($pH = -\log_{10}aH^+$) and the second dissociation constant of 10.3 for K_2 gives:

$$aHCO_3^- = \frac{10^{-8} * aCO_3^{2-}}{10^{-10.3}} = 200aCO_3^{2-}$$

This states that for a pH value of 8, the HCO_3^- anion is 200 times more abundant than the CO_3^{2-} anion (Andrews et al., 2004). The rearrangement of the dissociation constant equation can be manipulated for any pH value of concern. Once a range of pH values have been chosen and the activities of the individual species have been determined, a graph known as the Bjerrum plot can be displayed (Drever, 97). An example of the Bjerrum plot is shown below in Figure 5.

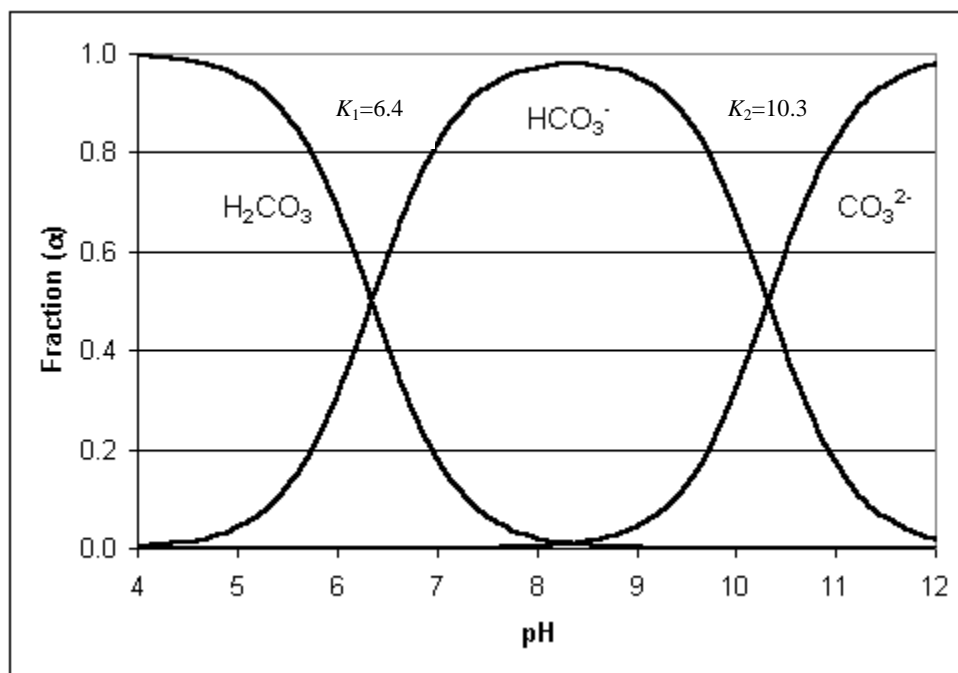


Figure 5 Activities of different species in the carbonate system as a function of pH.

Fraction (α) located on the y-axis can be thought of as the activity of each species. At fraction (α) = 1, the activity of that species is at its highest. The dissociation constants, K_1 and K_2 ,

are in their respectable places to show the dissociation of H_2CO_3 and HCO_3^- . These constants display the equilibrium of the undissociated to newly dissociated specie and therefore, the activity for those species will be equal at that point. As seen in Figure 5, the increase of one carbonate specie will lead to the decrease of another. For example, at a pH of 5.4, the activity of H_2CO_3 will be around 0.91 while the activity of the HCO_3^- will register at 0.09. The activities for these species will be reversed at a pH of 7.4 (Drever, 97). As mentioned above, the dominant carbonate specie at any given time is pH dependent. Below K_1 , H_2CO_3 is the dominant species and its activity increases as the water becomes more acidic. Looking between the dissociation constants of K_1 and K_2 , where most natural waters reside, the HCO_3^- anion is the dominant specie. Finally, above a pH value of 10.3 or K_2 , CO_3^{2-} becomes the dominant species.

CHAPTER 7 – METHODS OF SALINE LAKE EXPERIMENTS

All experiments were conducted in a laboratory facility located in the Department of Geosciences at GSU. Four simulated saline lakes were created by mixing deionized (DI) water and a combination of different salts. All salts used in the experiments were purchased from Fisher Scientific. The four lakes of study included the Dead Sea located in Israel, Great Salt Lake located in Utah, U.S.A., Dabusun Lake located in the Qaidam Basin, China and Donglin Lake which is also located in the Qaidam Basin, China. Two rounds of experiments were conducted on each lake. The first round included a natural process of bubbling $\text{CO}_{2(g)}$ through a diffuser with no pH enhancers added to the lakes. This round was conducted to see if any ion interaction would take place just by diffusing $\text{CO}_{2(g)}$ throughout each of the lakes. The second round replicated the same beginning process as the first round until full saturation of dissolved $\text{CO}_{2(g)}$ was achieved. Full saturation of dissolved CO_2 was determined by following the pH levels in the simulated lakes during the first round of experiments. Once the pH levels dropped to their lowest values in each of the simulated lakes, full saturation of dissolved CO_2 was achieved. Once accomplished, the $\text{CO}_{2(g)}$ was ceased and an ammonium hydroxide solution was immediately added to enhance the pH.

Lake chemistry composition was obtained through previously published literature. The Dead Sea and Great Salt Lake chemistries were acquired through Jones and Deocampo's 2003 *Geochemistry of Saline Lakes, Treatise on Geochemistry*. The chemical composition of Dabusun Lake and Donglin Lake of the Qaidam Basin, China were gathered through Spencer's 1990 publication of the *Origin of potash salts and brines in the Qaidam Basin, China*. Lake chemistry for each lake was provided as individual ion concentrations. The major ions included Na, K, Ca, Mg, SO_4 , Cl and $\text{HCO}_3 + \text{CO}_3$. Tables 3 and 4 state the individual ion concentrations for each

saline lake in mg L^{-1} and molarity respectively. These concentrations were taken directly from the published literature mentioned above and may vary from other published studies.

Table 3 Major ion concentrations for each lake expressed in mg L^{-1}

All Results in mg L^{-1}								
Locality	Na	K	Ca	Mg	SO ₄	Cl	HCO ₃ +CO ₃	Σ
Dead Sea	39,330	6,500	17,750	40,450	760	212,600	290	317,680
Great Salt Lake	85,700	4,550	319	8,050	17,400	147,000	327	263,346
Dabusun Lake	20,300	18,063	882	79,161	5,764	264,869	2,502	391,541
Donglin Lake	1,890	23	60,518	110,101	19	426,145	0	598,696

Table 4 Major ion concentrations for each lake expressed as molarity (mol L^{-1})

All results in mol L^{-1}								
Locality	Na	K	Ca	Mg	SO ₄	Cl	HCO ₃ +CO ₃	Σ
Dead Sea	1.711	0.166	0.443	1.664	0.0079	5.997	0.00239	9.99129
Great Salt Lake	3.73	0.12	0.008	0.33	0.18	4.15	0.003	8.521
Dabusun Lake	0.883	0.462	0.022	3.257	0.06	7.471	0.041	12.196
Donglin Lake	0.0822	0.0006	1.51	4.53	0.0002	12.02	0	18.143

All ion concentrations were converted to molarity, as shown in table 4, in order to create a recipe for each lake. Once determined, the recipe of each lake was produced by using a combination of different salts. The salts used for each experiment included NaCl (rock salt), KCl (crystals, reagent grade), CaCl₂ (anhydrous, granular), MgCl₂*6H₂O (hexahydrate, crystals, lab grade), Na₂SO₄ (anhydrous) and Na₂CO₃ (anhydrous). The final recipe for each lake is shown in table 5 and 6.

Table 5 Lake recipes expressed as molarity

Locality	All results in mol L ⁻¹					
	NaCl	KCl	CaCl ₂	MgCl ₂	Na ₂ SO ₄	Na ₂ CO ₃
Dead Sea	1.7	0.17	0.44	1.66	0.008	0.002
Great Salt Lake	3.37	0.12	0.008	0.33	0.18	0.003
Dabusun Lake*	0.681	0.232	0.022	3.257	0.06	0.041
Donglin Lake	0.082	0.0006	1.51	4.53	0.0002	0

*0.23 mol of KOH was added to Dabusun Lake to avoid excess Cl.

Table 6 Lake recipes expressed in mg L⁻¹

Locality	All results in mg L ⁻¹					
	NaCl	KCl	CaCl ₂	MgCl ₂	Na ₂ SO ₄	Na ₂ CO ₃
Dead Sea	99,350	12,670	48,830	158,140	1,140	210
Great Salt Lake	196,940	8,950	890	31,440	25,570	320
Dabusun Lake*	39,800	17,300	2,440	310,280	8,520	4,350
Donglin Lake	4,790	40	167,590	431,550	28	0

*12,910 mg L⁻¹ of KOH was added to Dabusun Lake to avoid excess Cl.

As mentioned with an asterisk in table 5 and 6, KOH was added to Dabusun Lake's recipe in order to avoid an excessive amount of Cl. This was not performed during the second round of experiments. A determination was made after the first round that KOH, being a hydroxide, may enhance the pH of the lake and tamper with the results. An insufficient amount

of Cl, approximately 0.23 mol or 8,154 mg under the needed amount, would serve better during this study as Cl is not a major ion of concern.

The final recipe of each lake was then converted from molarity, to mg L^{-1} and finally g L^{-1} for weighing purposes. A scientific digital scale, units displayed in grams, was used to weigh out each of the salts. The digital scale read values to the hundredth place and therefore provided very good accuracy when weighing the salts to match their true values. The precision with weighing the salts showed a standard deviation value of 0.02 g. Once the appropriate weights were achieved, the salts were mixed with DI water (room temperature) to equal approximately 1000 mL of solution in a 2000 mL glass beaker. All simulated solutions were placed on a Fisher Scientific Isotemp stir plate for at least 24 hours to hopefully ensure that all salts dissolve properly. For the first round of experiments, a temperature of 40 °C was added to the stir plate to help the salts dissolve.

Unexpectedly, getting the salts to fully dissolve was the hardest part of the experiment. After 24 hours of stirring and sometimes longer, a good portion of the salts were still in there solid state and did not dissolve. This may have been due to the quality of the salts or the minor impurities that they possess. An important factor needed before beginning the experiments is to ensure that all salts are totally dissolved. As this did not go as planned, a decision was made to filter the remaining solids out of the solution. A 0.45 μm filter was used to extract any remaining solids. This changed the chemical composition of each lake and turned out to be the biggest error throughout the experiment. The first samples collected from each simulated lake experiment represented the actual values of Ca and Mg concentrations after the lakes were filtered. These samples were collected before the initiation of CO_2 . The accuracy of the simulated lakes representing their true compositions from tables 3 and 4 ranged from

approximately 99% to 25% accurate throughout the two rounds of experiments. This range displayed the accuracy of the simulated lakes after the filtration process occurred. Ca seemed to resemble its true value more so than Mg after the filtration process. The accuracy of Ca within the simulated lakes ranged from 99% to 65% of its true value after the lakes were filtered. Filtering the lakes appeared to be harder to accomplish when the simulated lakes contained greater amounts of Mg. This was the case for Dabusun Lake and Donglin Lake, which had the two highest Mg concentrations out of the four experimental lakes. The accuracy of Mg after the filtration process ranged from 75% to 25% of its true value. The initial Ca and Mg sample concentrations for each simulated lake is located in the appendices at the end of the manuscript. Other ions within the simulated lakes chemistry were not analyzed and the effect of change from the filtration process was unknown. Even though the chemistry of each lake was altered after the filtering process, the overall trend and idea behind the study still was able to be determined.

After the lakes were filtered, the remaining solution was then placed back in a clean 2000 mL glass beaker. An atomic 55 mm CO₂ diffuser, purchased from Green Leaf Aquariums LLC, was placed in the bottom of each beaker. Small rubber suction cups on the diffuser were utilized to attach the diffuser to the bottom of the glass beaker. Plastic tubing was used to attach the diffuser to a 50 lb steel CO₂ tank. A pressure of 30 psi was used on each experiment throughout both the first and second rounds.

For the first round of experiments, CO_{2(g)} was bubbled through each of the simulated saline lakes for approximately 2 – 3 weeks. After the 2 – 3 week period, the CO_{2(g)} was then stopped and each lake sat for approximately another 2 weeks at room temperature. Each lake experienced the natural process of evaporation to try and simulate a normal type setting. No barrier was used to interfere with this process. Lake samples were collected daily with the

exclusion of some weekends. Samples were collected through a disposable polyethylene pipette and then transferred to a 5 mL plastic vial. A drop of laboratory grade nitric acid, HNO_3 , was added to each sample to avoid any reactions that may occur within the vial. Parameters of pH, temp °C, date and time were recorded with each sample collected. The effective $p\text{CO}_2$ for each simulated lake experiment was calculated by taking the equivalents of all cations equal to the equivalents of all anions, Henry's law constant (K_H) at 20°C, the first dissociation constant of the carbonate system (K_1) and $p\text{CO}_2$ in solution. The equation is as follows:

$$[\Sigma \text{ cation equivalents}] = (K_1[K_H * p\text{CO}_2]/[\text{H}^+]) + [\Sigma \text{ anion equivalents}]$$

The equation was manipulated to solve for $p\text{CO}_2$.

The second round of experiments started out with replicating everything that was done during the first round of experiments. KOH was not added to Dabusun Lake during the second round. Salts were weighed accordingly and mixed with DI water (room temperature) to equal approximately 1000 mL of solution in a 2000 mL glass beaker. Each lake was then placed on the stir plate for at least 24 hours. Heat was not used this time in hopes that a different outcome may occur than from the first round. This was not the case and each lake had to be filtered again. The filtering process held back a lot of the undissolved solids and once again, the chemical composition of each lake was altered. As from the first round of experiments, the initial sample from each simulated lake represents the actual value of Ca and Mg concentrations. Due to this problem, lake compositions from the second round may vary from that of the first round.

After the filtration process, the remaining solution from each lake was placed back in a clean 2000 mL glass beaker. The CO_2 diffuser was attached back to the bottom of the beaker and a pressure of 30 psi was obtained. $\text{CO}_{2(g)}$ was diffused until full saturation of dissolved CO_2 was reached. This was known from the results of the first round of experiments. Once the full

saturation point was reached, the $\text{CO}_{2(g)}$ was stopped and an ammonium hydroxide solution was immediately added to each of the lakes. The ammonium hydroxide solution was purchased from Fisher Scientific and was made up of 4% ammonium hydroxide and 96% water. The amount of ammonium hydroxide solution added to each lake was determined by following a 2009 study conducted by Mignardi et al (2009). In their experiments, $\text{CO}_{2(g)}$ was bubbled through simulated Mg wastewaters to see the mineralization potential. A stronger ammonium hydroxide solution was used in their experiments to enhance the pH to form carbonates.

The optimum goal was to boost the pH in each lake to approximately 8.5 – 9.5 in order to precipitate carbonates. The addition of the ammonium hydroxide solution ranged between 90 – 100 mL for three out of the four lakes. More specifically, 100 mL was added to the Dead Sea, 100 mL was added to Dabusun Lake and 90 mL was added to the Great Salt Lake. The pH of each of these lakes experienced a rapid increase as planned. Donglin Lake, which originally had 80 mL of ammonium hydroxide solution added, did not react in the same way and a major increase of pH was not observed. Increments of 10 – 25 mL of ammonium hydroxide solution were added until the optimal pH range was reached. Slowly adding small amounts of ammonium hydroxide solution did not have the same effect as a bulk addition. It took approximately 285 mL of ammonium hydroxide solution to elevate the pH of Donglin Lake to the specified range. The samples collected for this round followed the same protocol as the first round.

A Perkin Elmer Atomic Absorption Spectrometer 3110 was used to analyze all samples collected. The software used was Perkin Elmer Atomic Absorption Laboratory Benchtop (1985). Atomic absorption (AA) spectroscopy utilizes the absorption of light to measure the concentrations of gas phase atoms. Liquid samples are extracted through a tiny straw and then

vaporized through a flame in order to release the atoms or ions into a gas phase. The vaporized atoms then pass through a specified wavelength of light which coincides with the ion that is being measured. In this case, Ca and Mg were the two cations that were to be analyzed. Each cation has a specific wavelength that the beam of light is adjusted to. The wavelengths for Ca and Mg are 422.7 nm and 285.2 nm respectively. The ionized atoms absorb the beam of light and the concentration of the analyte is determined by the amount of absorption. Concentration measurements are determined from a calibration curve that is made with a set of standards of known concentrations for the analyte of concern. A graph is then made to compare the linear relationship between absorbance and concentrations. This concept between absorbance and concentration from a light source or absorber is known as Beer's law (the chemistry hypermedia project, <http://www.files.chem.vt.edu/chem-ed/index.html>, 2003).

The results from each lake experiment are displayed in a series of graphs to help decipher the overall process. The Ca and Mg ion concentrations of each lake were too high for the AA to read accurately. To rectify the situation, samples from each lake, with the exception of Donglin Lake, were diluted to 0.5% and then analyzed. The samples collected from Donglin Lake were diluted to 0.25%. Ca and Mg standards were made in order to construct the calibration curve from the AA absorbance results. The standard solutions for each cation included concentrations of 1 part per million (ppm), 10 ppm, 25 ppm, 50 ppm and 75 ppm. If ion concentrations were still too great at their diluted percentages, extrapolation methods were used. The first sample from each lake represents the original composition and was collected before the diffusion of $\text{CO}_{2(g)}$ began. The precision of samples measured using AA analysis showed a standard deviation of 0.01. The calibration curves for each simulated lake throughout both rounds of experiments are listed in the Figures below.

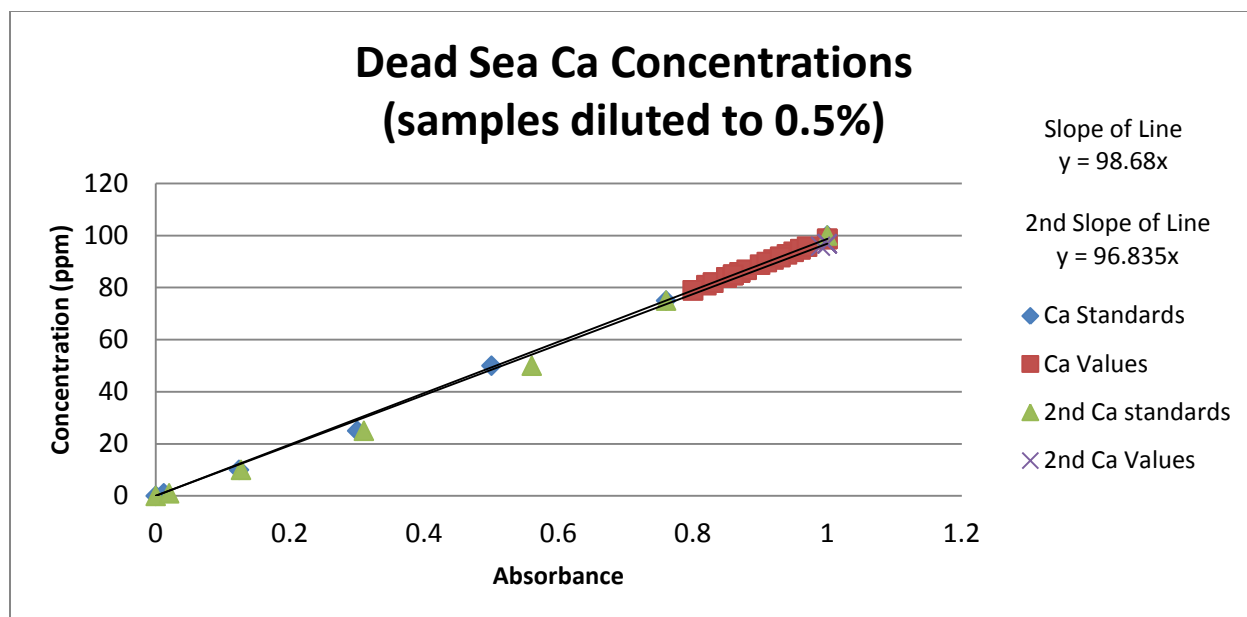


Figure 6 Ca concentrations from the AA calibration curves with samples diluted to 0.5%. Two sets of samples were analyzed which lead to the development of two calibration curves. The slope of each line is shown on the graph.

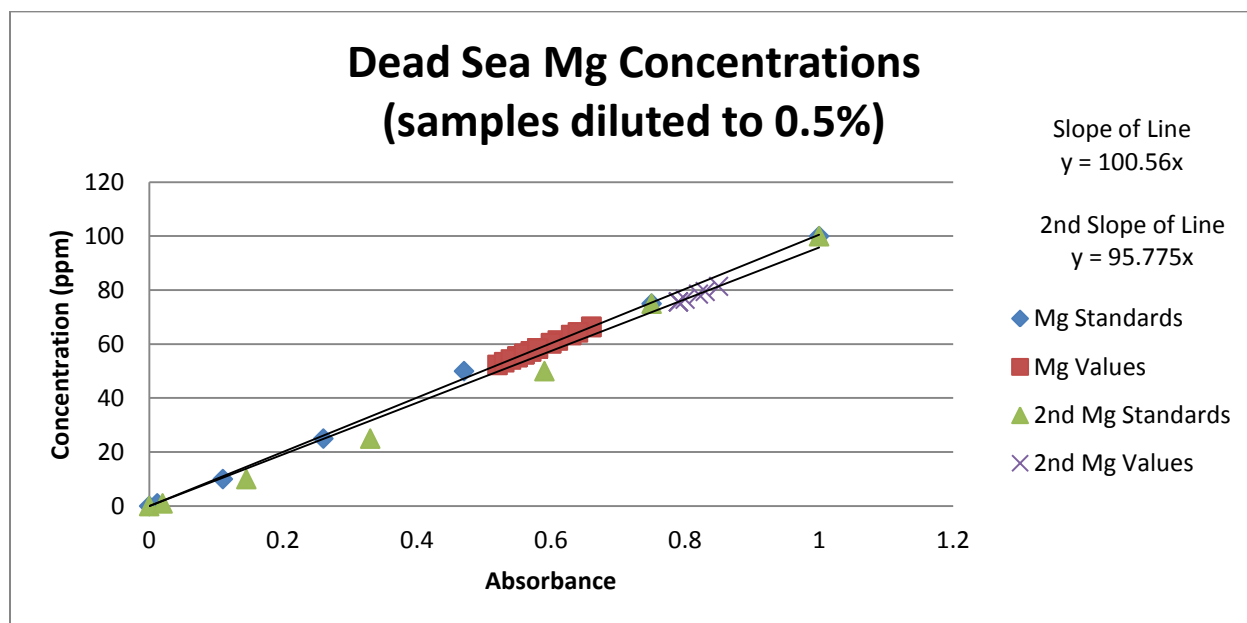


Figure 7 Mg Concentrations from the AA calibration curves with samples diluted to 0.5%. Two sets of samples were analyzed which lead to the development of two calibration curves. The slope of each line is shown on the graph.

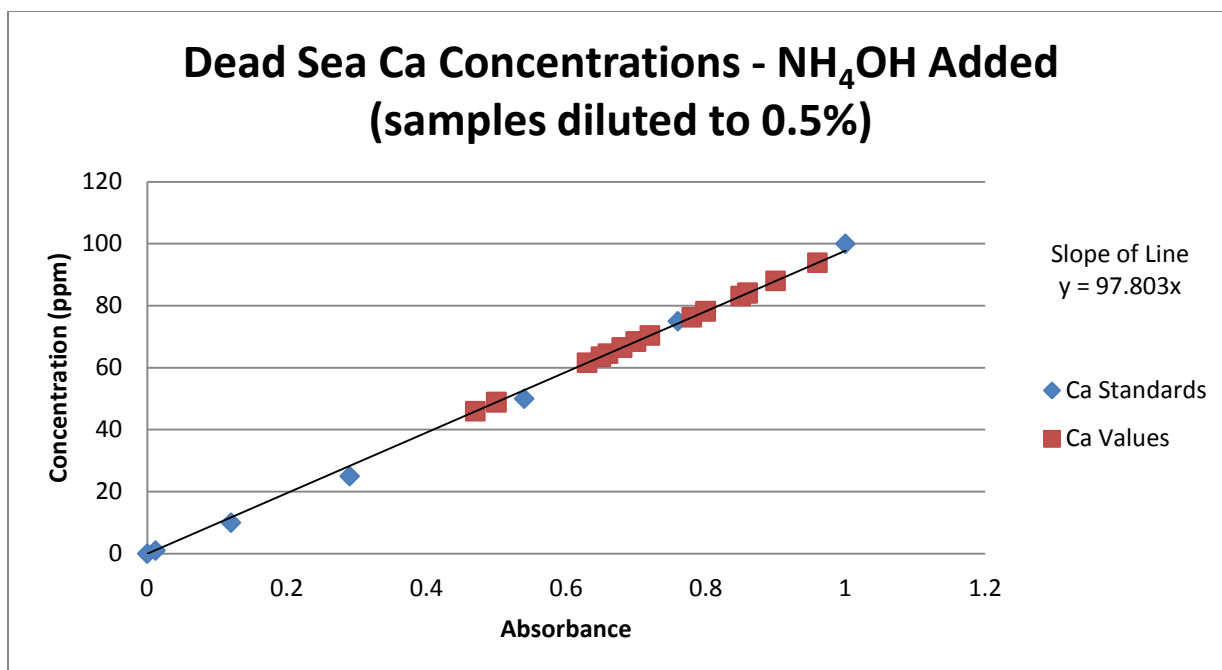


Figure 8 Ca concentrations from the AA calibration curve with samples diluted to 0.5%.

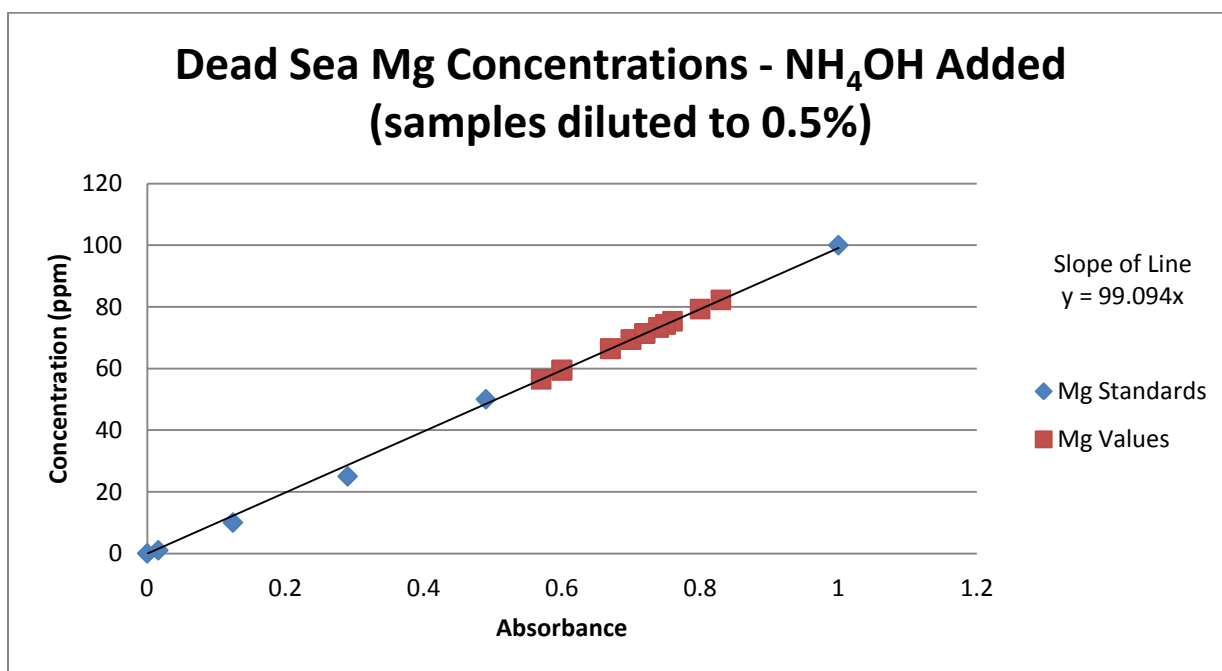


Figure 9 Mg concentrations from the AA calibration curve with samples diluted to 0.5%.

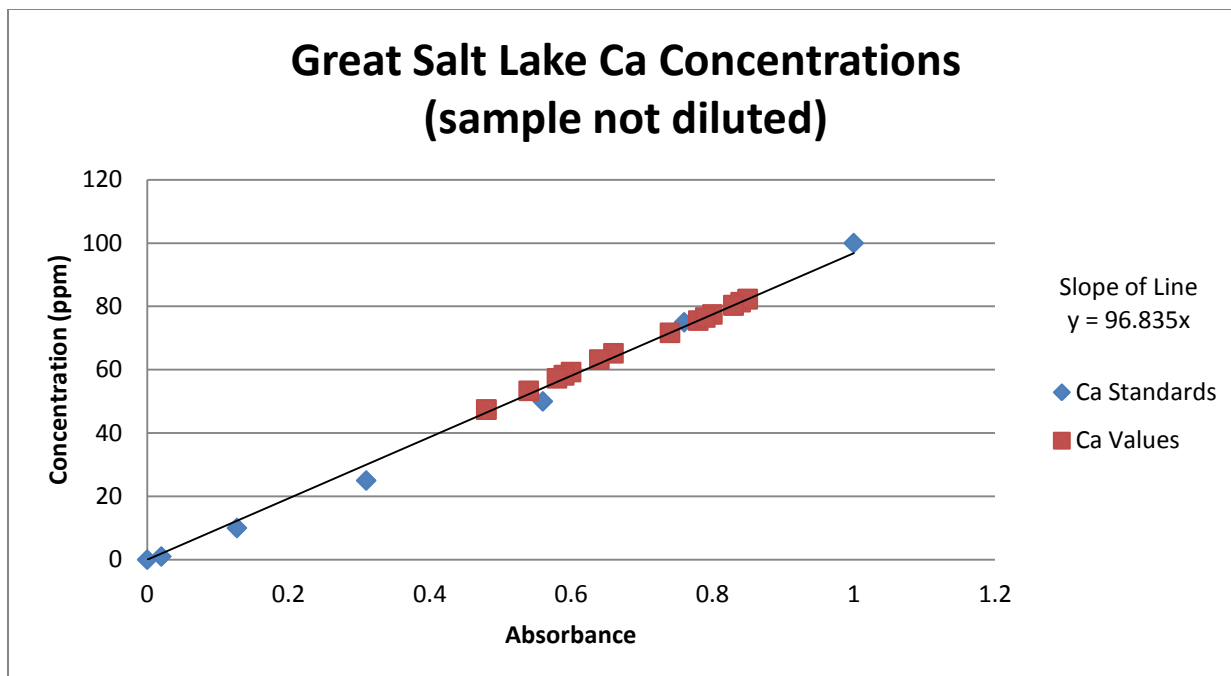


Figure 10 Ca concentrations from the AA calibration curve with samples not diluted.

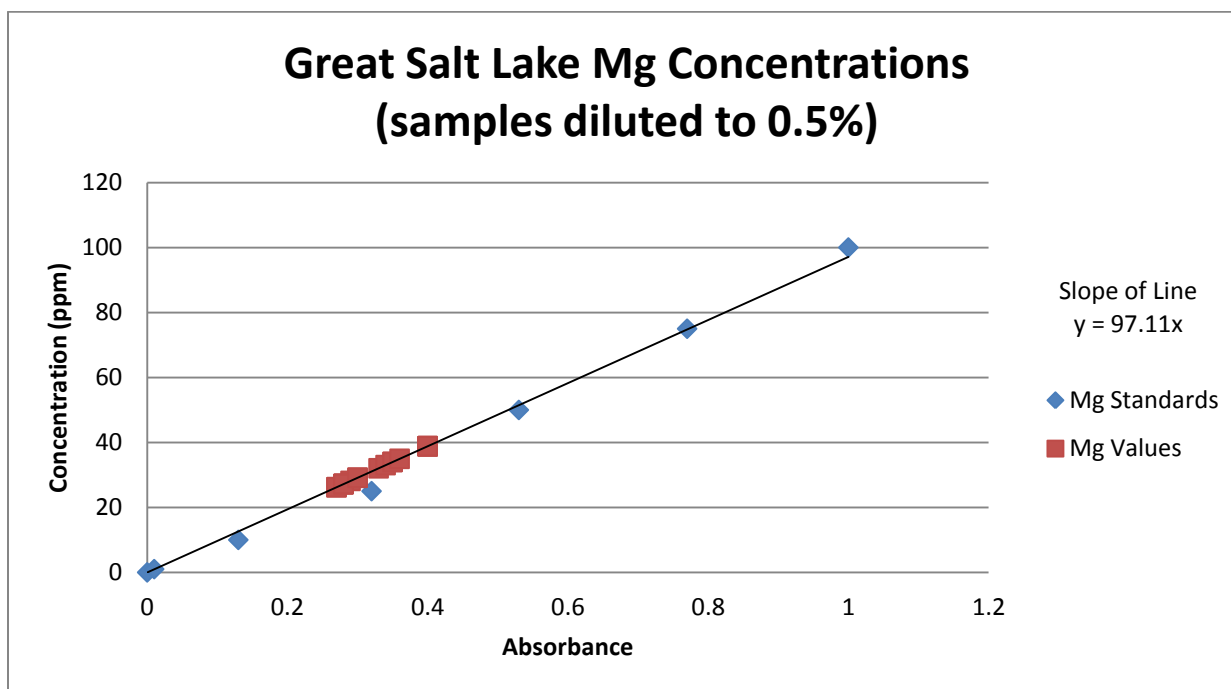


Figure 11 Mg Concentrations from the AA calibration curve with samples diluted to 0.5%.

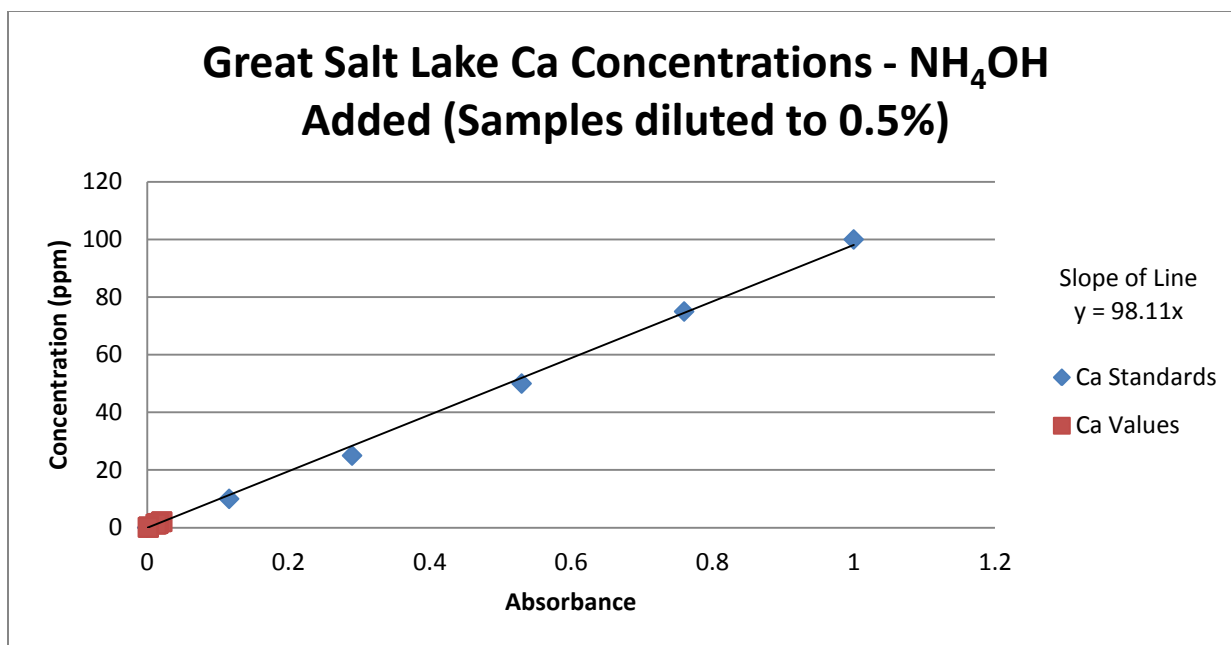


Figure 12 Ca concentrations from the AA calibration curve with samples diluted to 0.5%.

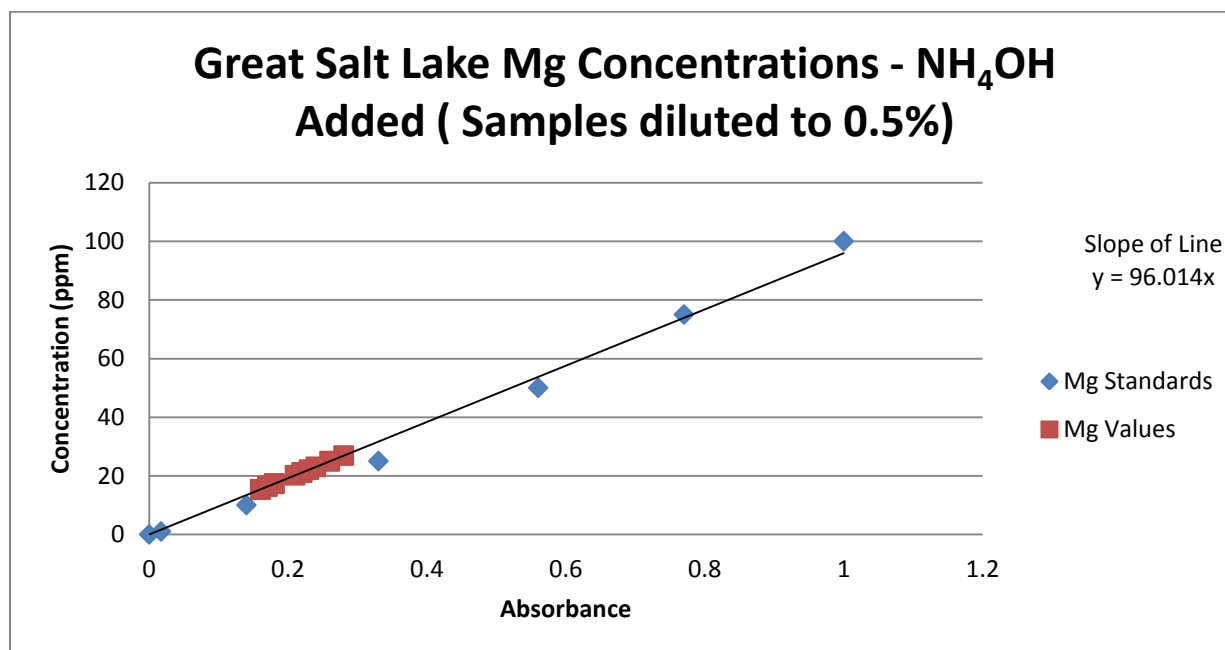


Figure 13 Mg concentrations from the AA calibration curve with samples diluted to 0.5%.

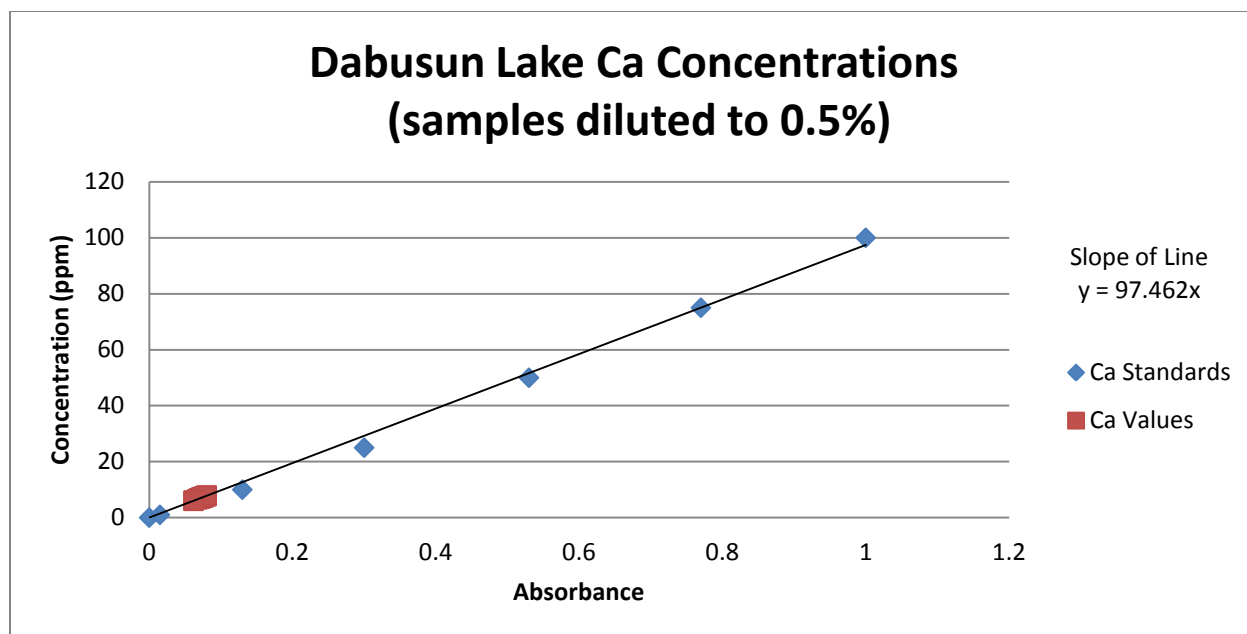


Figure 14 Ca concentrations from the AA calibration curve with samples diluted to 0.5%.

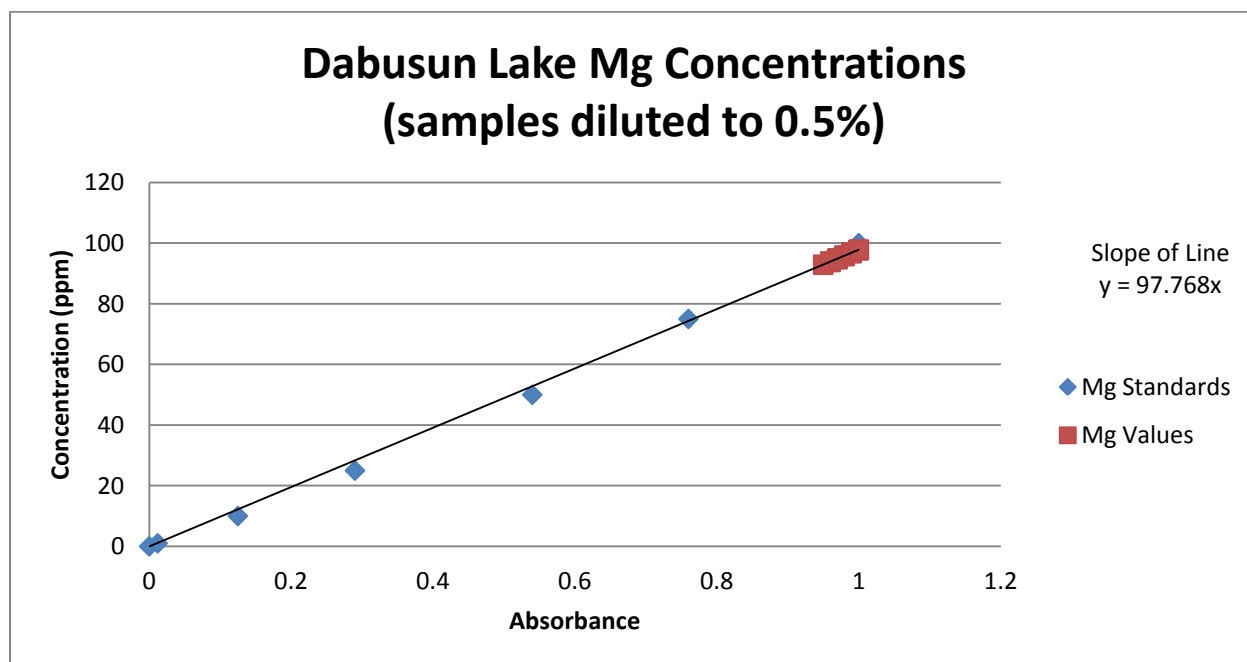


Figure 15 Mg concentrations from the AA calibration curve with samples diluted to 0.5%.

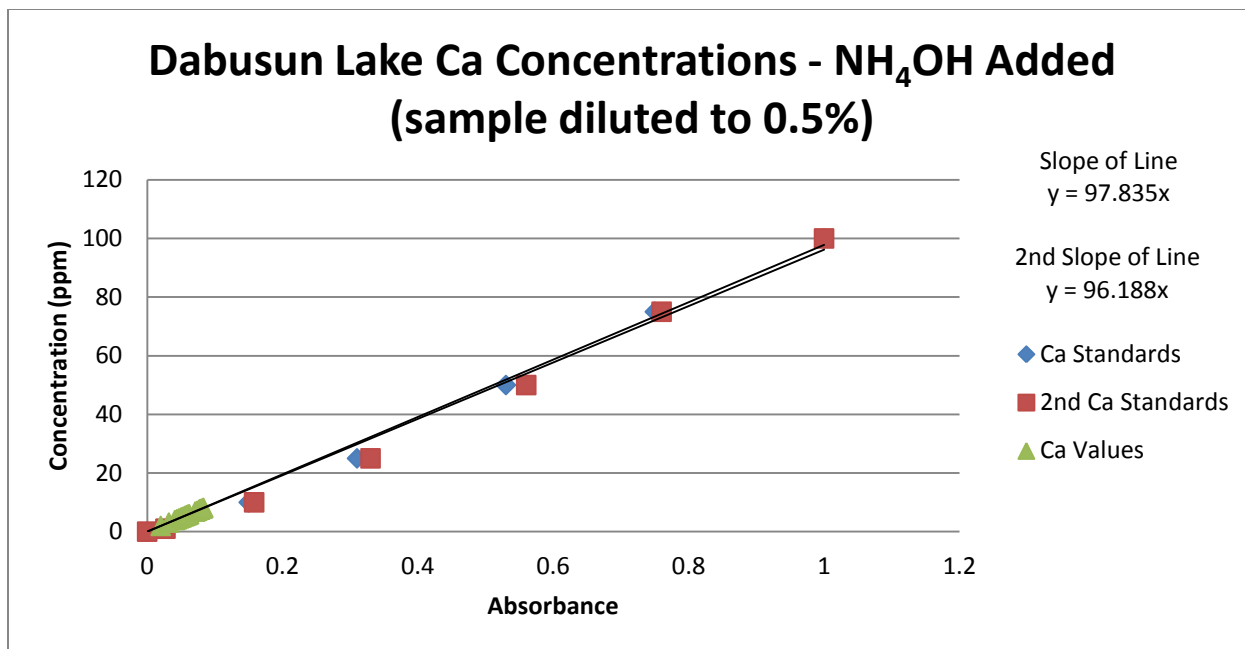


Figure 16 Ca concentrations from the AA with samples diluted to 0.5%. Two sets of samples were analyzed which lead to the development of two calibration curves.

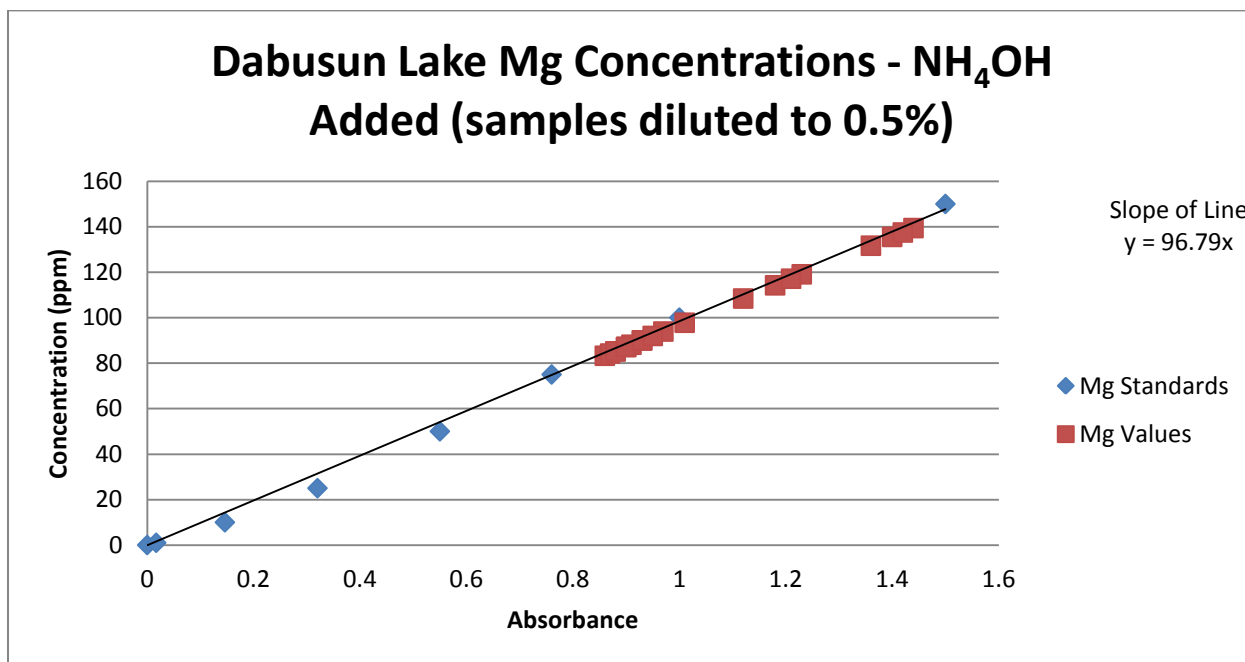


Figure 17 Ca concentrations by day with non-diluted concentrations (scale is different from other Figures).

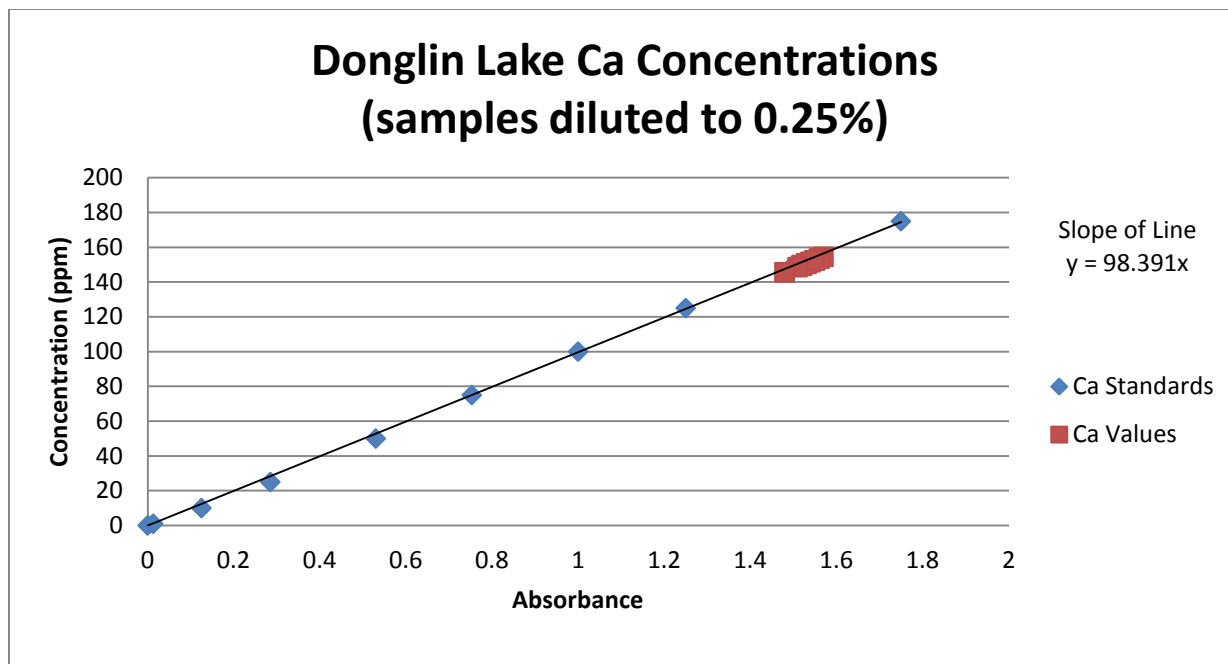


Figure 18 Ca concentrations from the AA calibration curve with samples diluted to 0.25%.

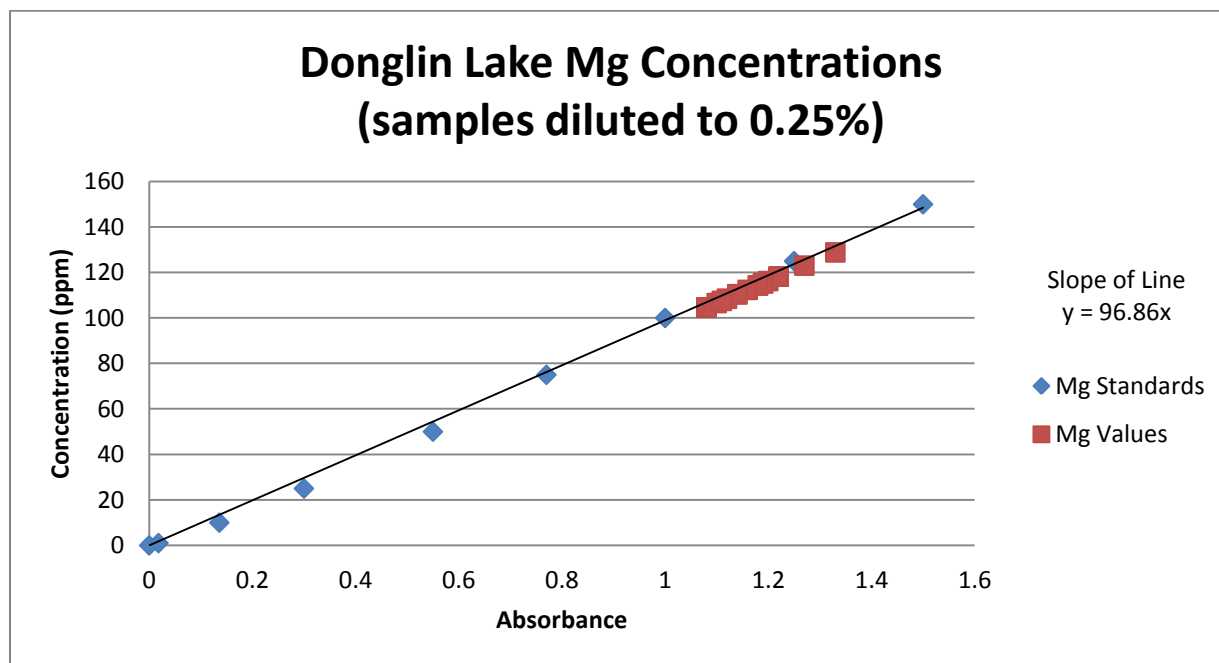


Figure 19 Ca concentrations from the AA calibration curve with samples diluted to 0.25%.

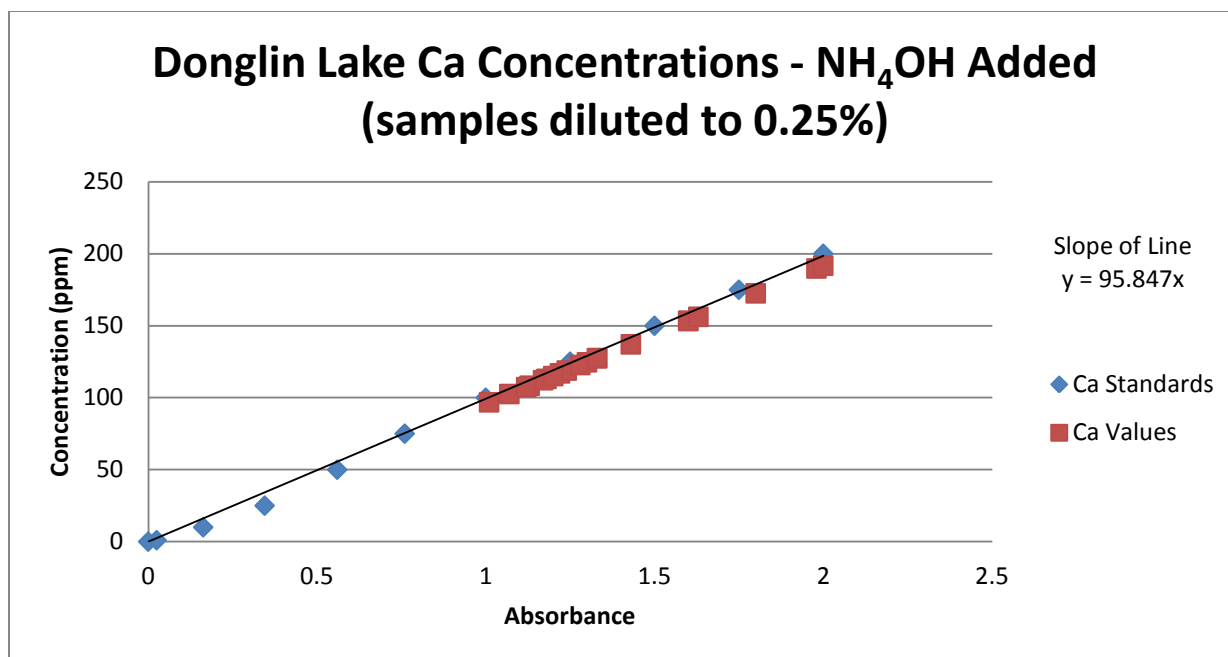


Figure 20 Ca concentrations from the AA calibration curve with samples diluted to 0.25%.

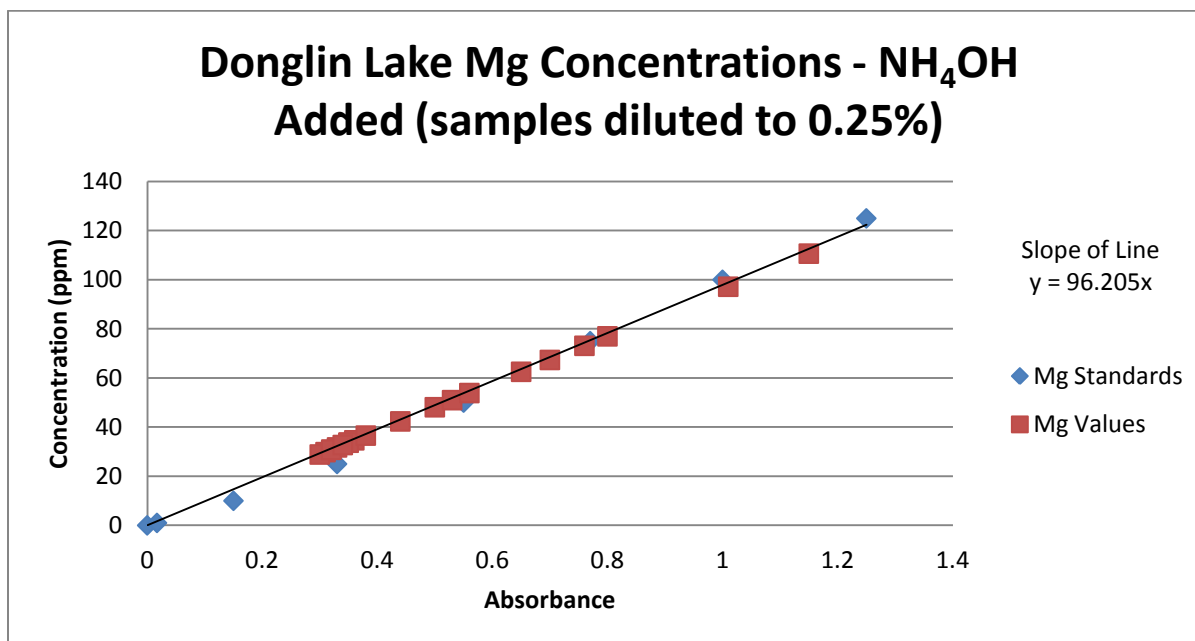


Figure 21 Mg concentrations from the AA calibration curve with samples diluted to 0.25%.

CHAPTER 8 – RESULTS AND DISCUSSION OF SALINE LAKE EXPERIMENTS

The results and discussion from each simulated lake experiment are divided into different sections throughout this chapter.

8.1 – The Dead Sea

The Dead Sea acted as the “guinea pig” for both rounds of experiments. More samples were collected from the Dead Sea and the experiment ran a little longer than the others. The reactions or non-reactions seen within the Dead Sea help lay the guidelines and procedures for future experiments.

The graphical results from the Dead Sea are displayed in the Figures below. Lake temperatures ranged from 23.2 °C to 24.6 °C throughout the first experiment.

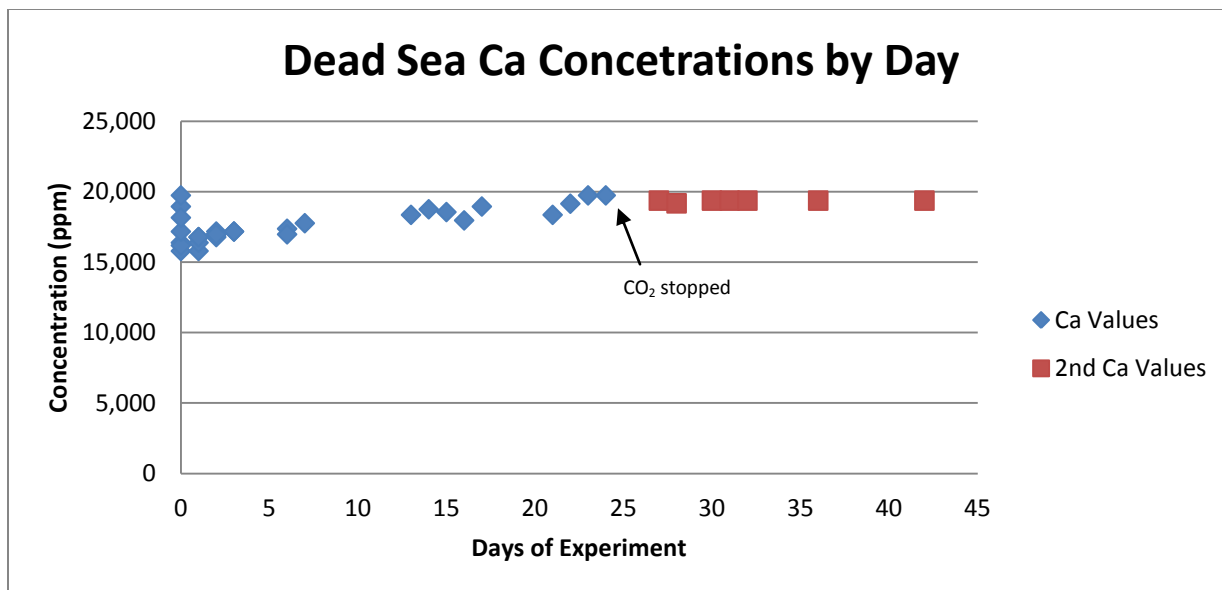


Figure 22 Ca concentrations by day with non-diluted concentrations.

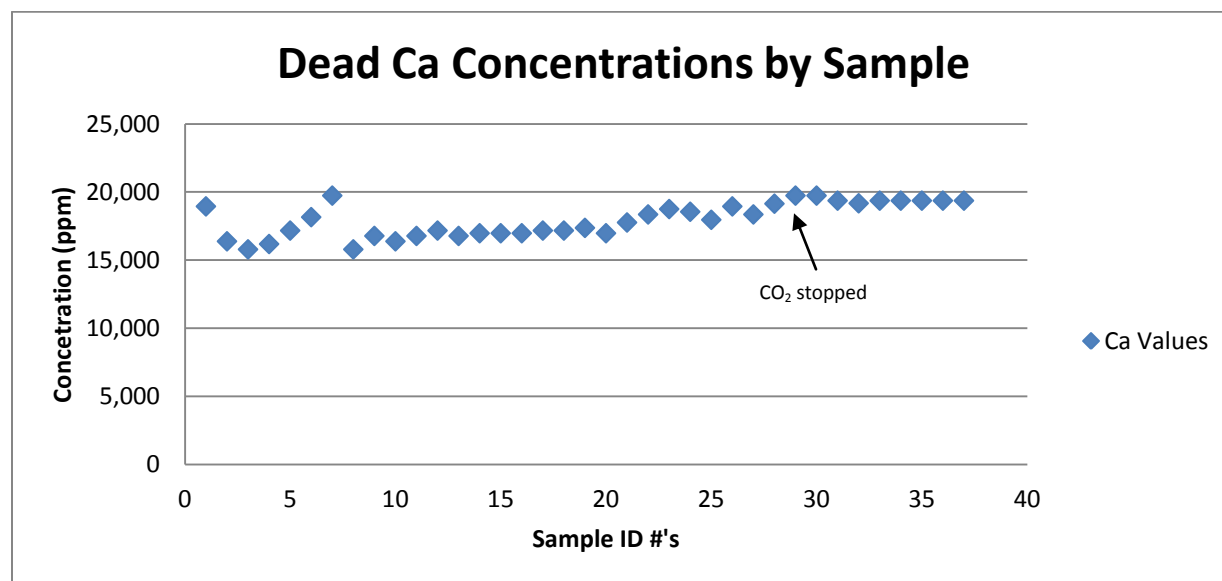


Figure 23 Ca concentrations by sample with non-diluted concentrations.

Ca concentrations ranged from 20,000 ppm (DS-3) to 16,000 ppm (DS-7). For the most part, Ca concentrations remained uniform throughout the experiment. Although a range in Ca values is shown, an overall loss of Ca to precipitation was not observed.

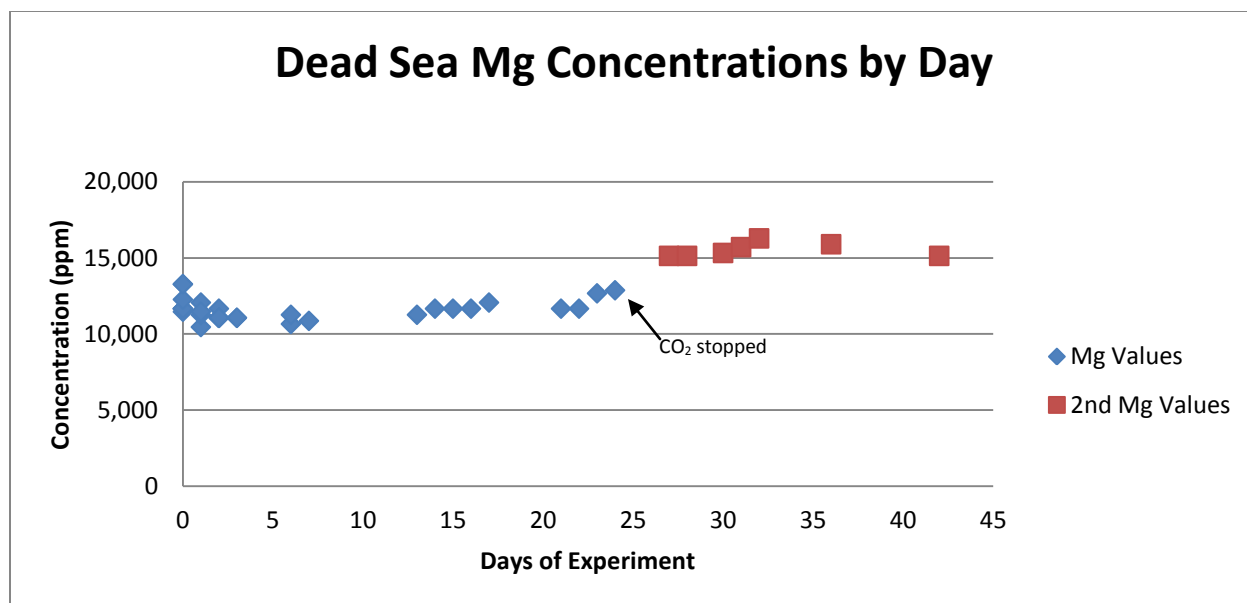


Figure 24 Mg concentrations by day with non-diluted concentrations.

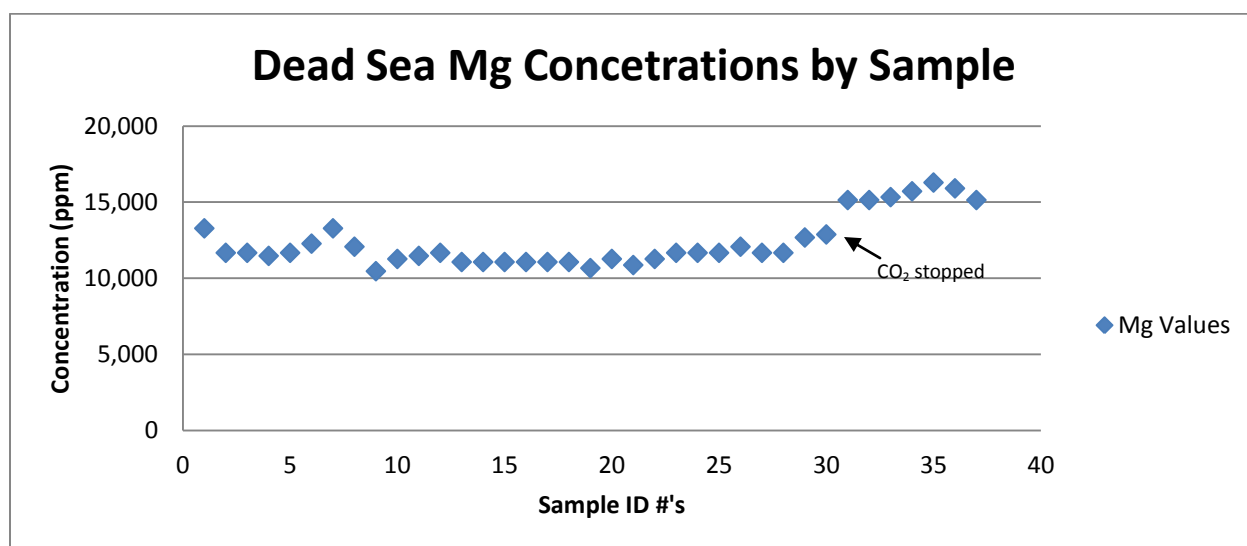


Figure 25 Mg concentrations by sample with non-diluted concentrations

Mg concentrations ranged from 16,000 ppm (DS-35) to 10,000 ppm (DS-9). Although a wider range than Ca concentrations, Mg concentrations also remained moderately consistent with no evidence of flocculation.

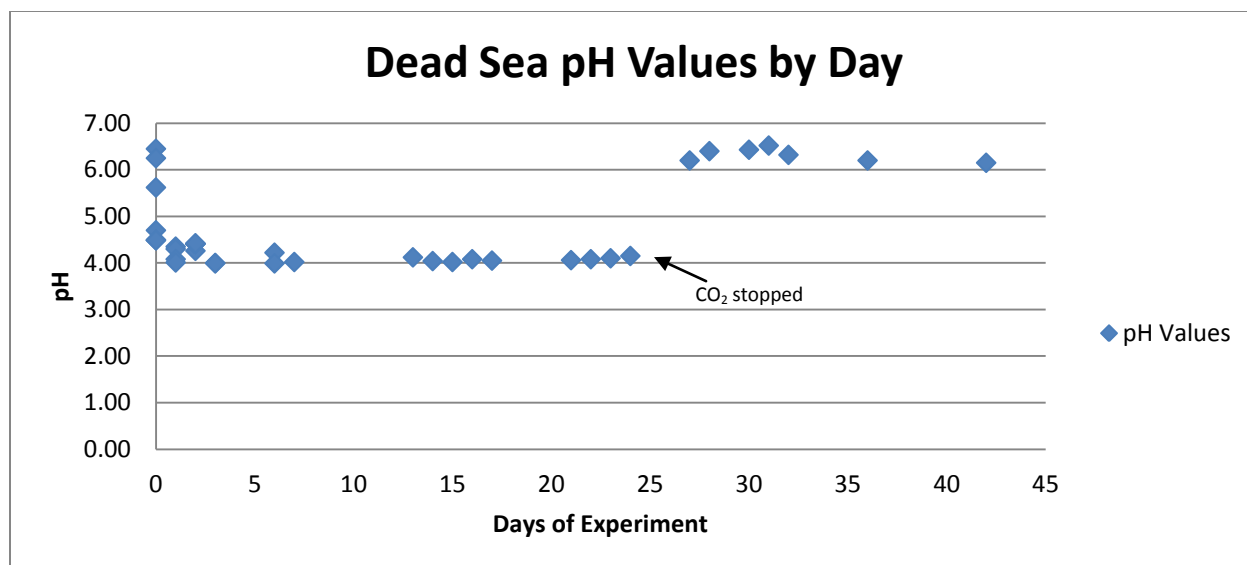


Figure 26 pH values per day.

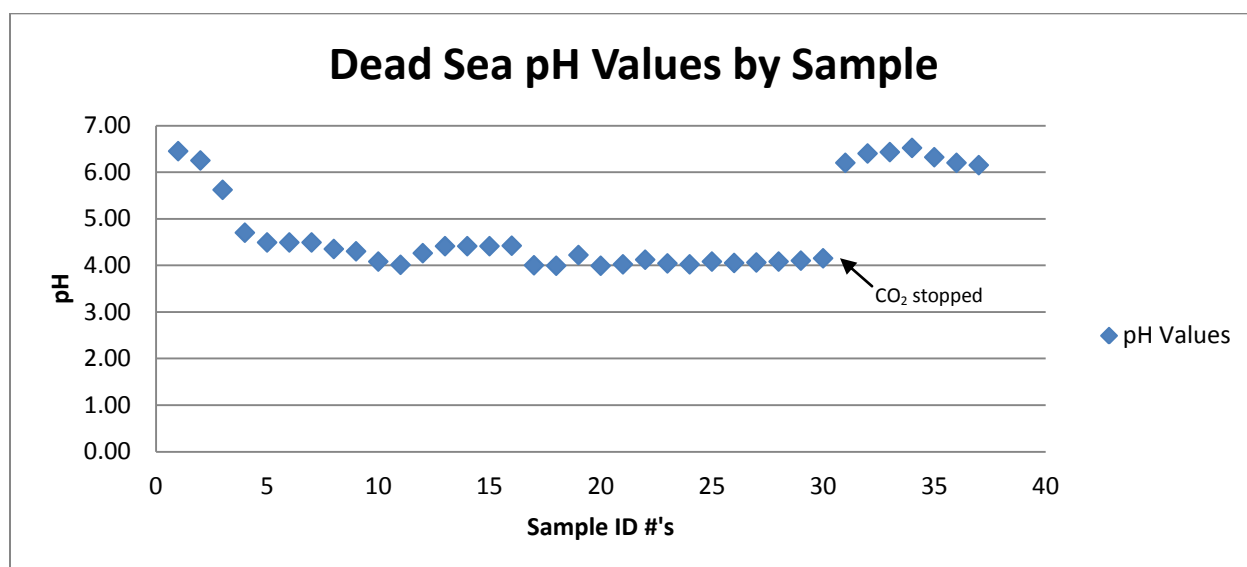


Figure 27 pH values by sample.

pH rapidly decreased once the CO_{2(g)} entered the water. In approximately four hours, pH values dropped from 6.45 to 4.49 and leveled out until the CO_{2(g)} was stopped. A pH range of 6.45 to 3.99 was observed.

8.1.1 – The Dead Sea with NH_4OH Added

Temperatures ranged from 23.5 °C to 24.6°C during this experiment.

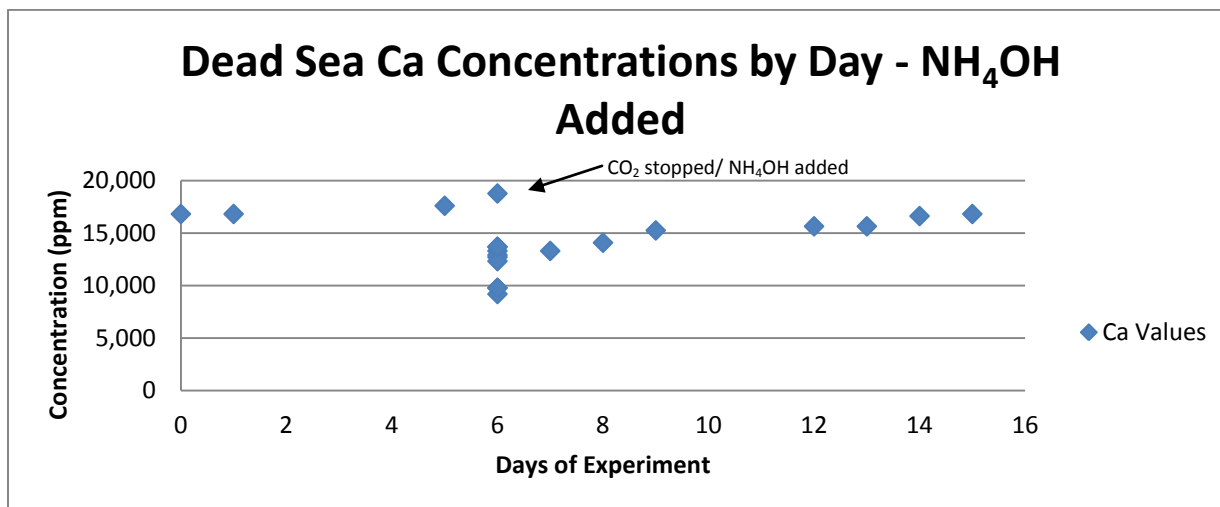


Figure 28 Ca concentrations by day with non-diluted concentrations.

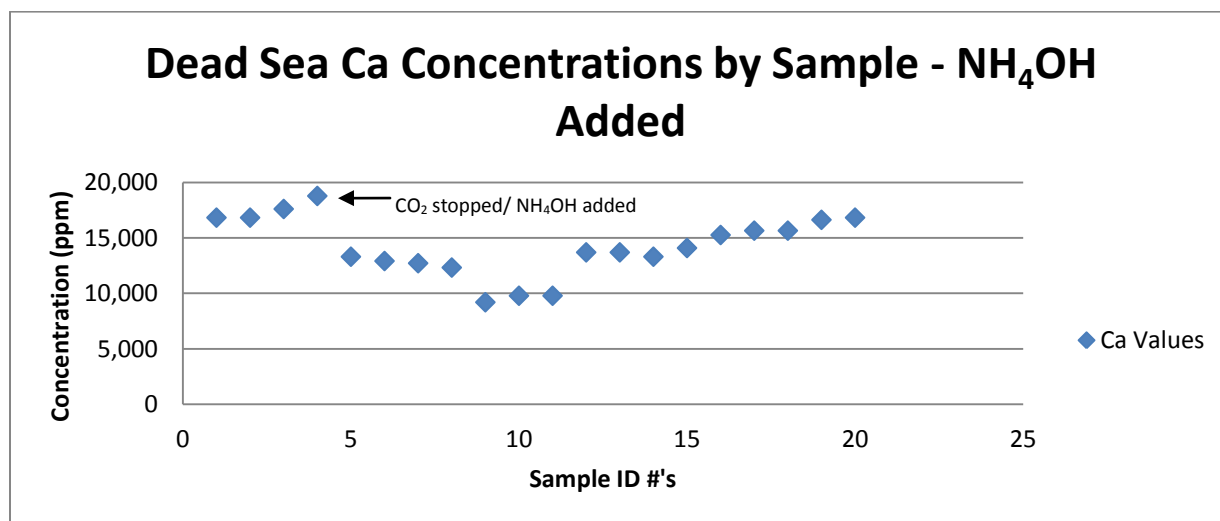


Figure 29 Ca concentrations by sample with non-diluted concentrations.

A wider range of Ca concentrations was observed during this round of experiment with the addition of NH_4OH compared to the first round. Ca concentrations ranged from 17,000 ppm (DS-1) to 9,200 ppm (DS-9) indicating a Ca loss of approximately 7,800 mg to precipitation.

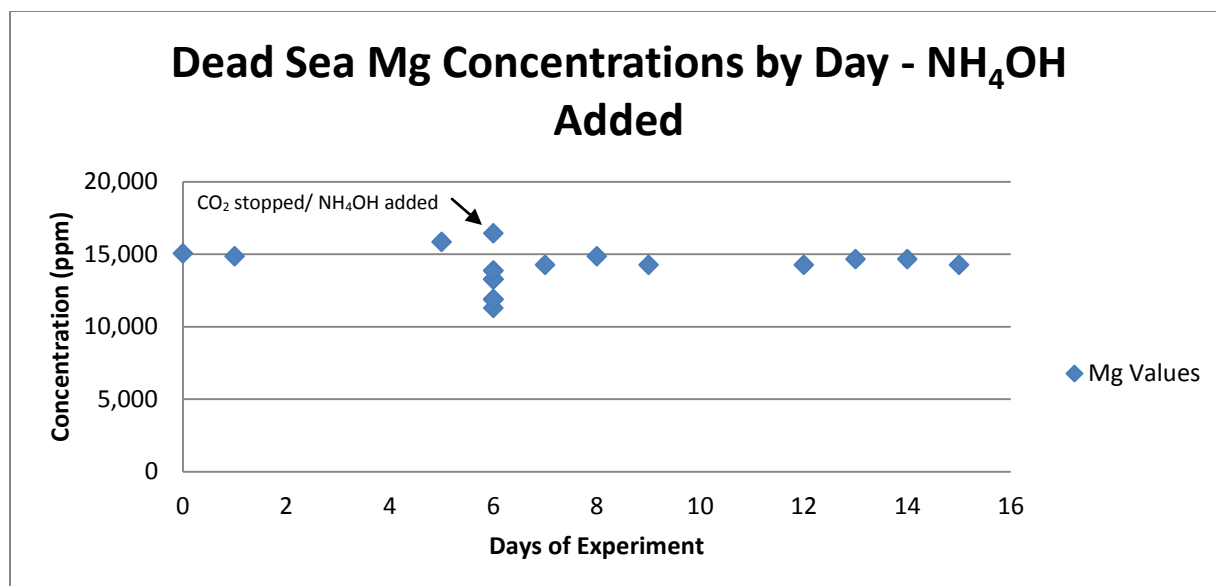


Figure 30 Mg concentrations by day with non-diluted concentrations

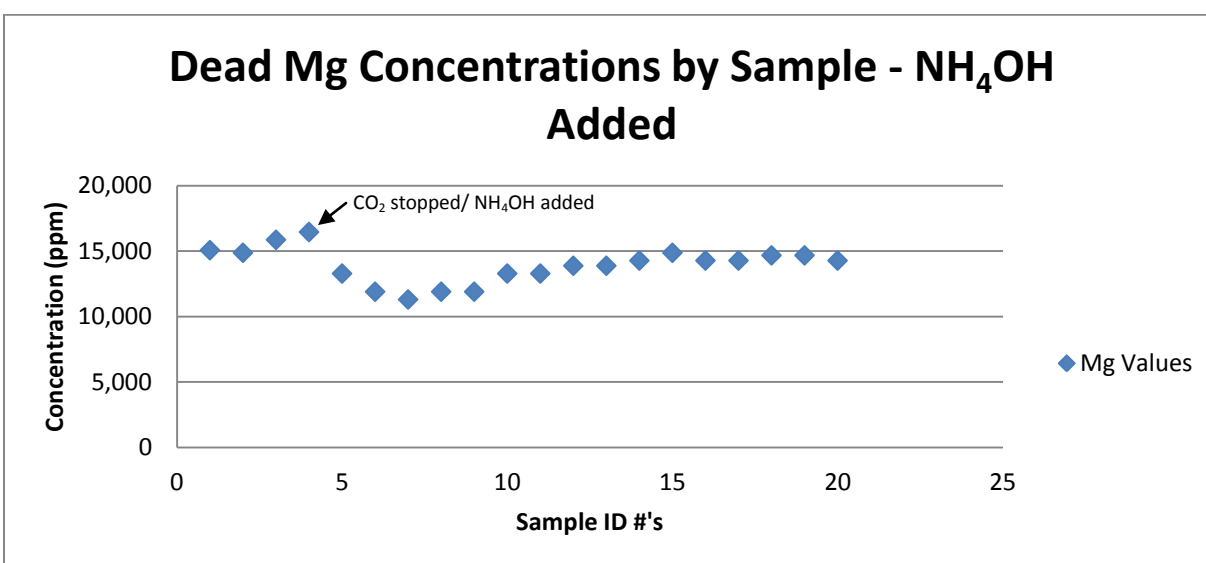


Figure 31 Mg concentrations by sample with non-diluted concentrations.

Mg concentrations dropped with the addition of NH₄OH but concentrations approximately remained within the same range as the first round. Mg concentrations ranged from 16,000 ppm (DS-4) to 11,000 ppm (DS-10 and DS-11) with the addition of NH₄OH indicating a Mg loss of approximately 5,000 mg to precipitation.

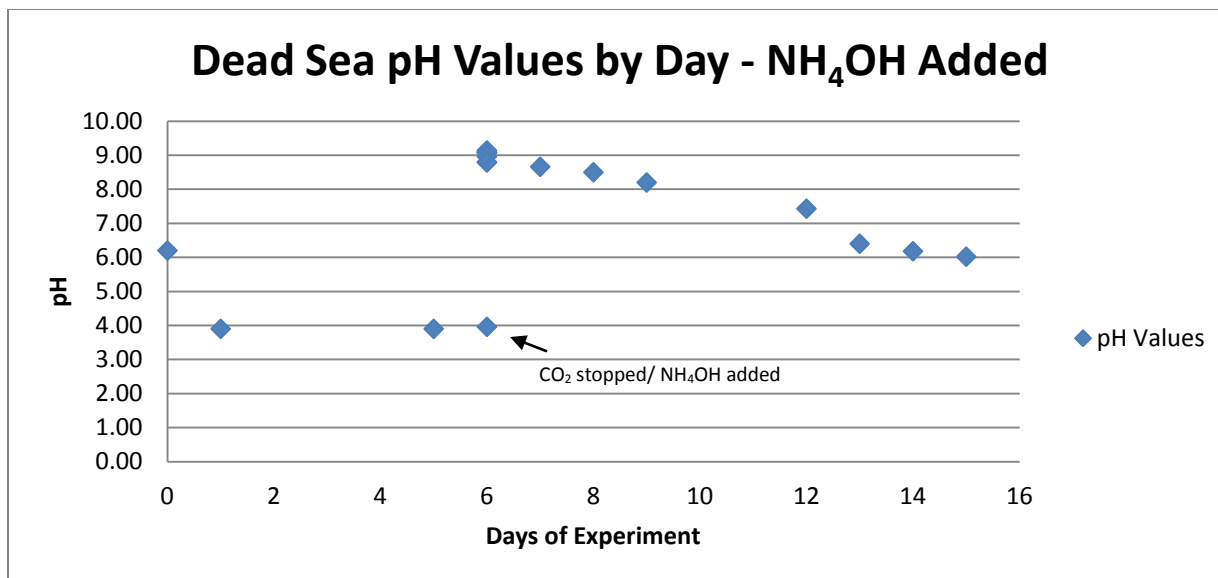


Figure 32 pH values by day.

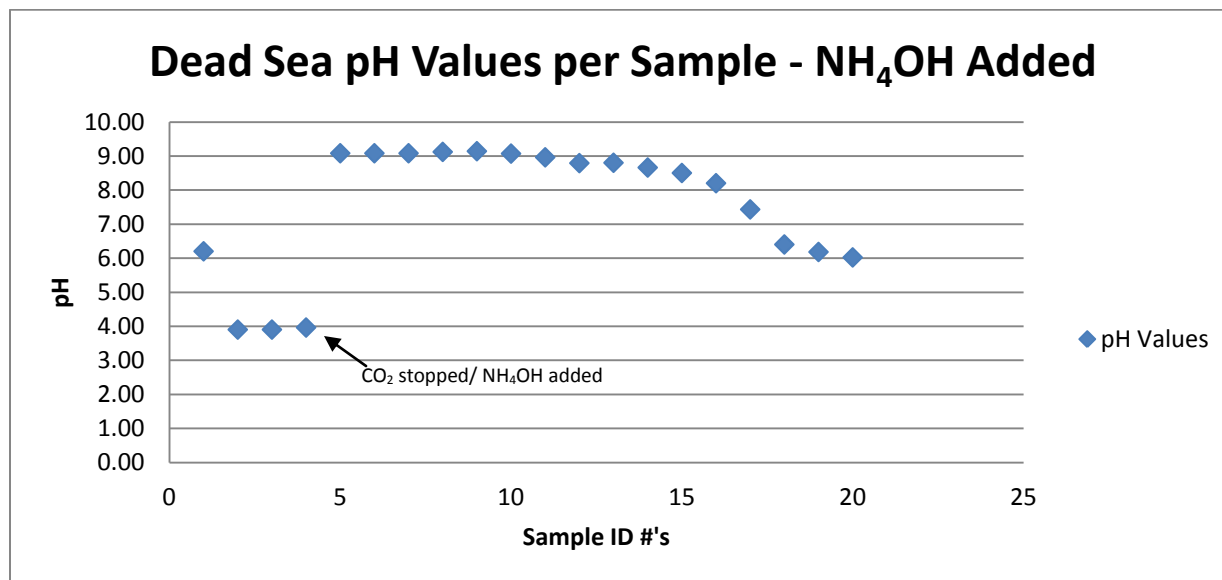


Figure 33 pH values by sample.

pH values ranged from 9.14 (DS-9) to 3.90 (DS-2) with the addition of NH₄OH. An abrupt change in pH from 3.90 (DS-2) to 9.08 (DS-3) occurred within seconds of adding NH₄OH.

8.1.2 – Discussion of Dead Sea Experiments

Not much ion interaction was seen just by bubbling $\text{CO}_{2(g)}$ through the water. The pH of the water did rise after the $\text{CO}_{2(g)}$ was ceased but not high enough to observe any carbonate precipitation. pH values did drop to their lowest levels at around 24 hours after the diffusion process began. Full saturation of dissolved $\text{CO}_{2(g)}$, or the reaction creating H_2CO_3 , was reached at this point. The effective $p\text{CO}_2$ was $10^{4.58}$ atm. Flocculation did occur in about one week after the $\text{CO}_{2(g)}$ was stopped. A chemical test was conducted by dropping a 10% solution of HCl on the crystals but no reaction was seen. Most likely, halite was the precipitant as hopper crystals were evident.

The addition of NH_4OH played more of a role on the depletion of Ca than that of Mg. Both cations revealed a drop in concentration, but Ca showed a greater decrease in concentration than what was seen with Mg. Both concentration curves eventually started to slowly increase approximately three hours after the NH_4OH was added. This may have been due to the depletion of the anion that each of these cations were bonding with. With no anion around to bond with and the evaporation of water taking place, the concentrations of these cations will slowly start to increase. Visual evidence of flocculation was observed at around the 14th day of the experiment. These crystals had a different look than that of the first round. Their appearance was that of a thick white rhombus rectangular shape. A couple days after this, a halite matrix started to precipitate around the bigger crystals. The formation of these minerals followed the order of events that were mentioned in the brine evolution pathways in chapter 5, section 5.4.

Within seconds of adding the NH_4OH , a reaction creating a white milky substance occurred. In approximately 24 hours, the white milky substance separated and sank to the

bottom with a clear solution floating on top. This almost is the resemblance of a stratified lake, even though a white milky substance does not appear in the course of nature.

8.2 – Great Salt Lake

The graphical results from the Great Salt Lake experiments are displayed in the Figures below. A temperature range of 22.9 °C to 23.7 °C was observed during the first experiment.

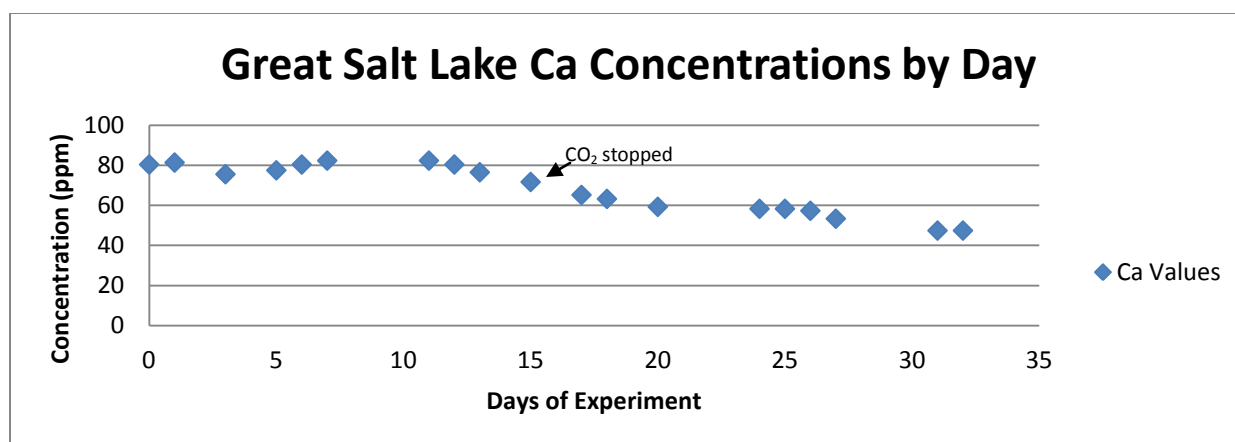


Figure 34 Ca concentrations by day with non-diluted concentrations (scale is different from other Figures).

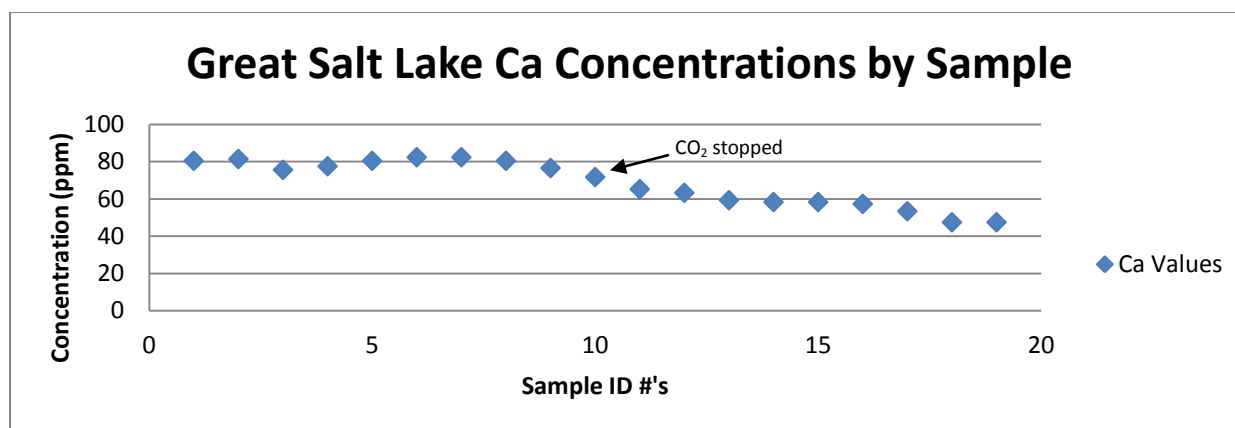


Figure 35 Ca concentrations by sample with non-diluted concentrations (scale is different from other Figures).

Ca concentrations ranged from 82 ppm (G-6) to 47 ppm (G-18 and G-19). Mineral formation occurred within some of the sample vials that were collected towards the end of the experiment. This could account for the slight Ca loss towards the end of the experiment. Approximately 35 mg of Ca was lost to precipitation.

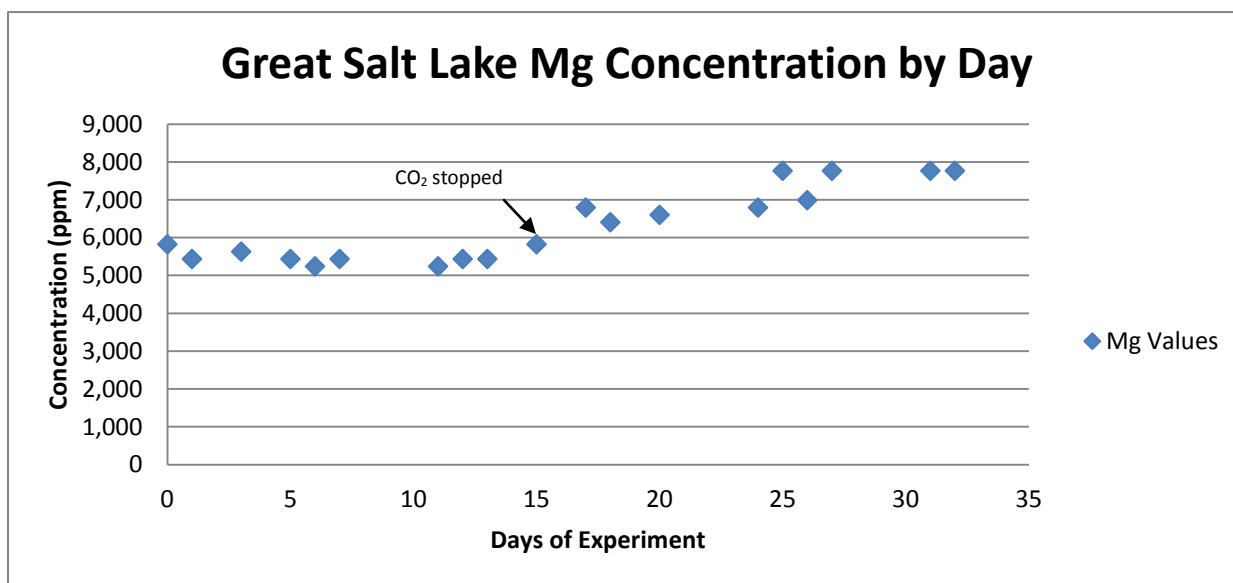


Figure 36 Mg concentrations by day with non-diluted concentrations (scale is different from other Figures).

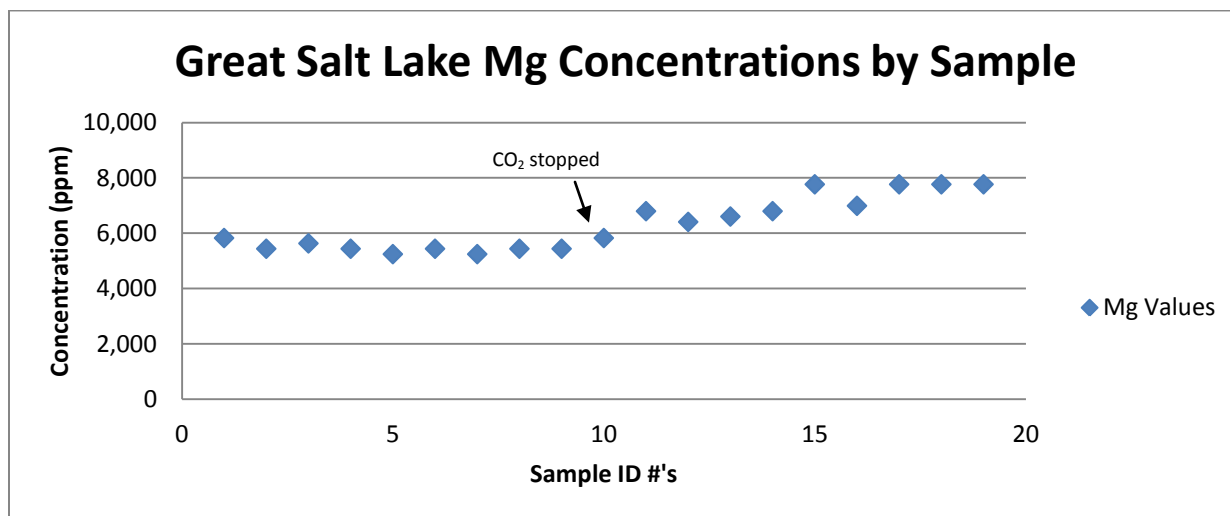


Figure 37 Mg concentrations by sample with non-diluted concentrations (scale is different from other Figures).

Mg concentrations ranged from 7,700 ppm (G-17, G-18 and G-19) to 5,200 ppm (G-5 and G-7). Mg concentrations remained mainly consistent throughout the experiment with no evidence of Mg loss to precipitation.

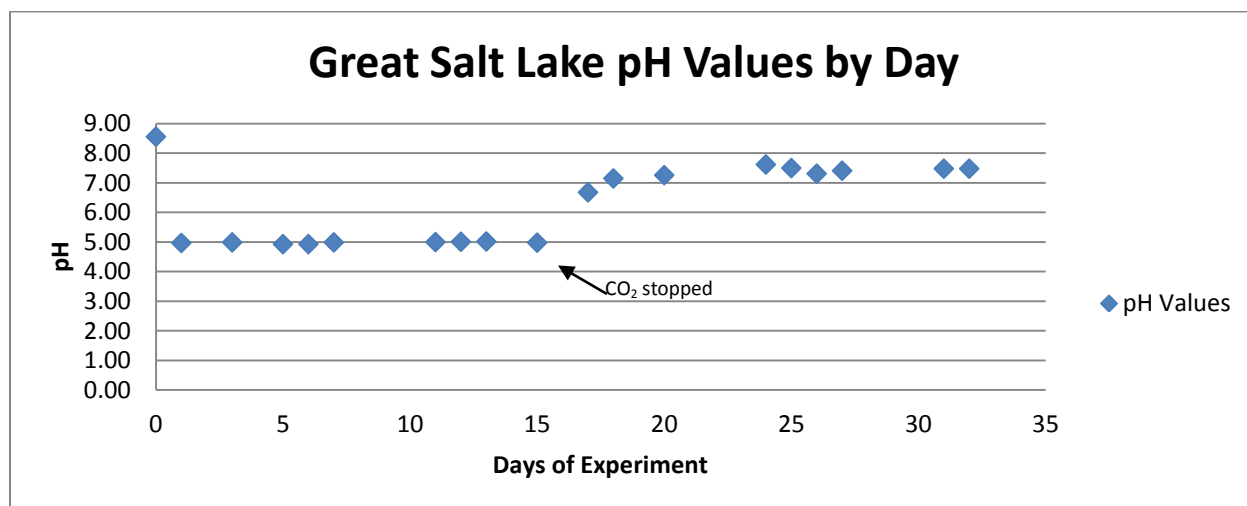


Figure 38 pH values by day.

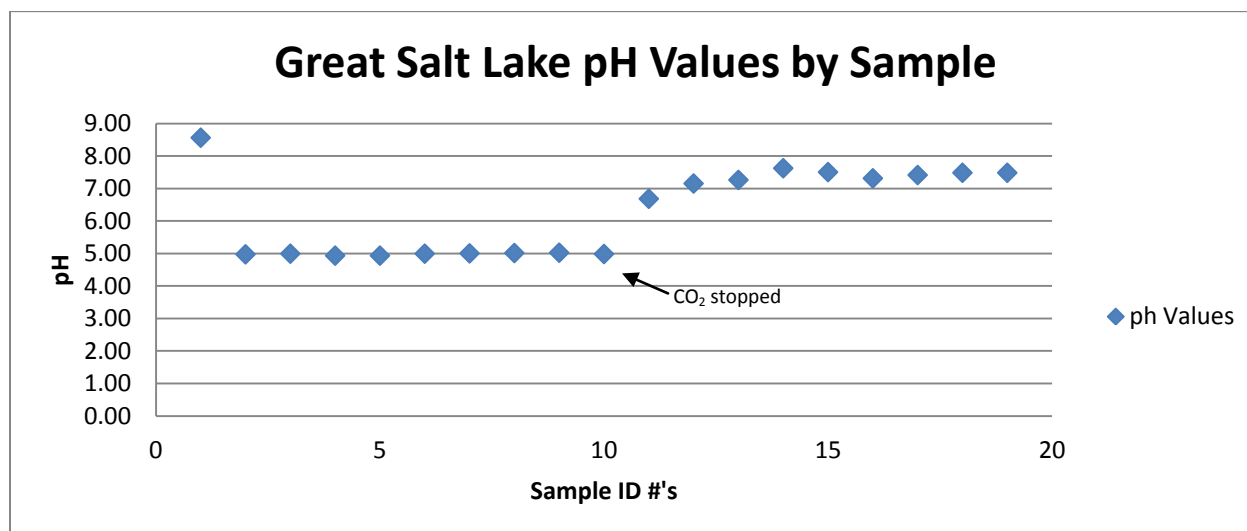


Figure 39 pH values by sample.

The pH of the simulated Great Salt Lake decreased within 24 hours after the $\text{CO}_{2(g)}$ was added from 8.56 to 4.93. This was also the range of the pH values.

8.2.1 – Great Salt Lake with NH_4OH Added

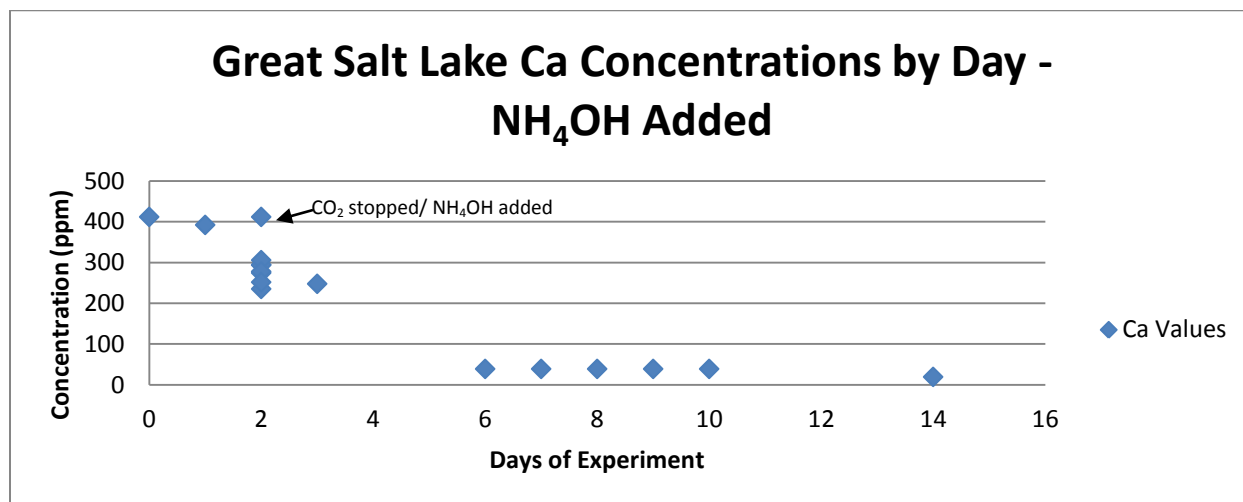


Figure 40 Ca concentrations by day with non-diluted concentrations (scale is different from other Figures).

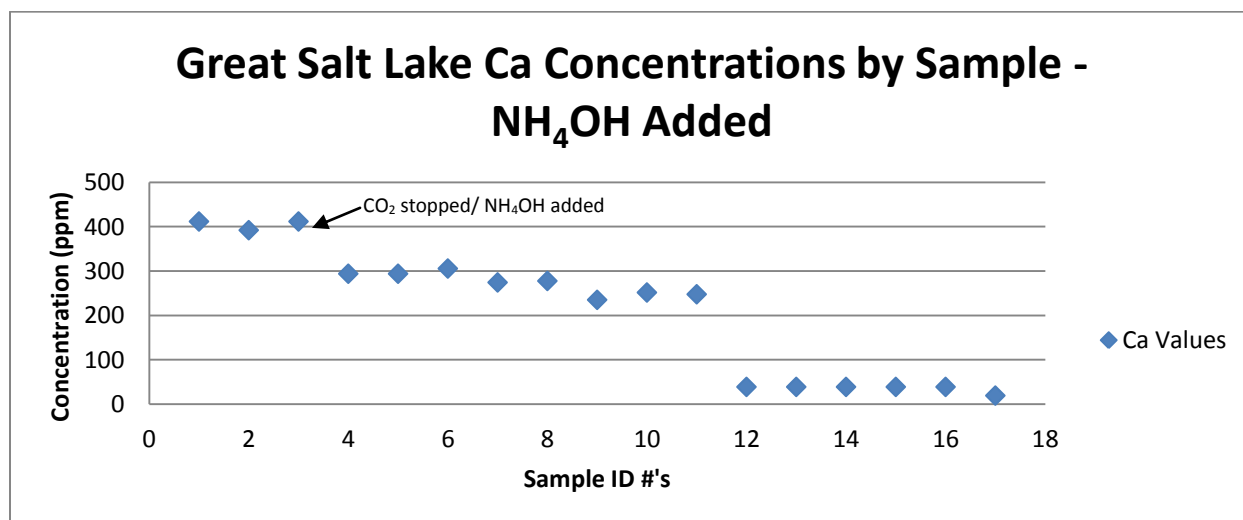


Figure 41 Ca concentrations by sample with non-diluted concentrations (scale is different from other Figures).

A wide range of Ca concentrations was seen with the addition of NH_4OH . Ca concentrations ranged from 400 ppm (G-1) to 20 ppm (G-17) indicating a Ca loss of approximately 380 mg to precipitation. Ca was also most fully depleted by the end of the experiment.

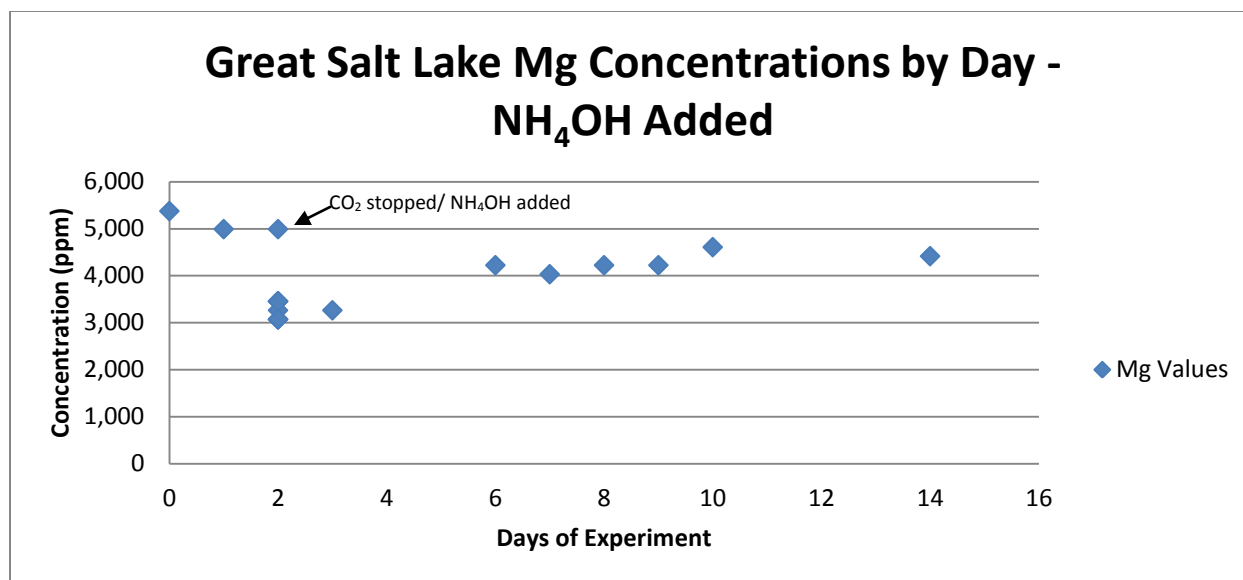


Figure 42 Mg concentrations by day with non-diluted concentrations (scale is different from other Figures).

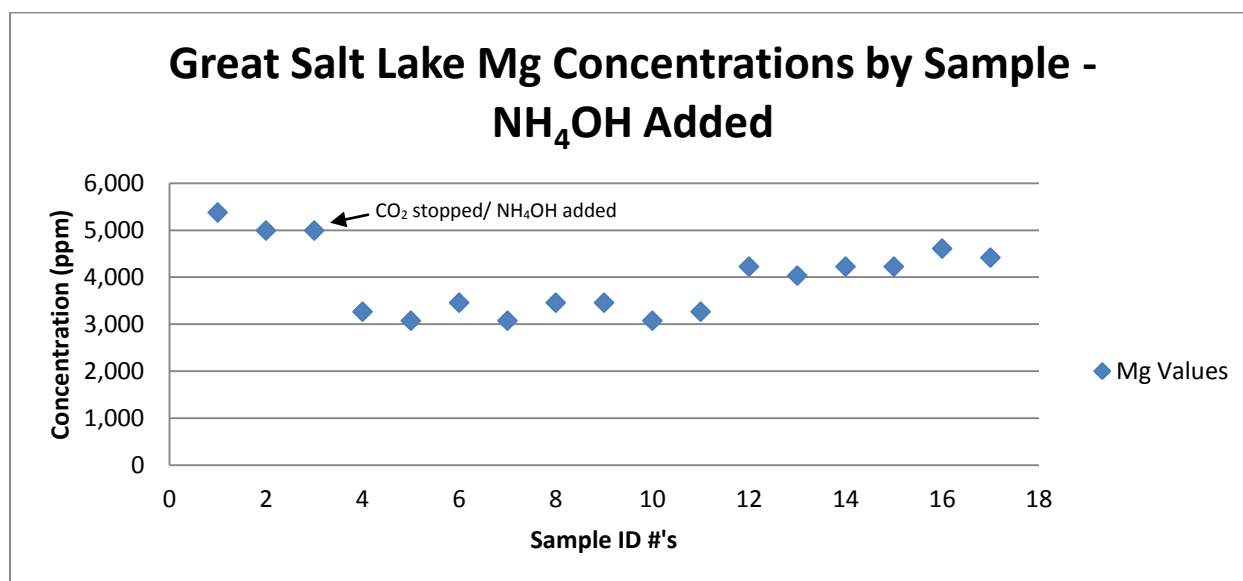


Figure 43 Mg concentrations by sample with non-diluted concentrations (scale is different from other Figures).

Mg concentrations ranged from 5,400 ppm (G-1) to 3,000 ppm (G-7 and G-10) indicating a Mg loss of approximately 2,300 mg to precipitation. A noticeable decrease in Mg was observed as soon as the NH₄OH was added.

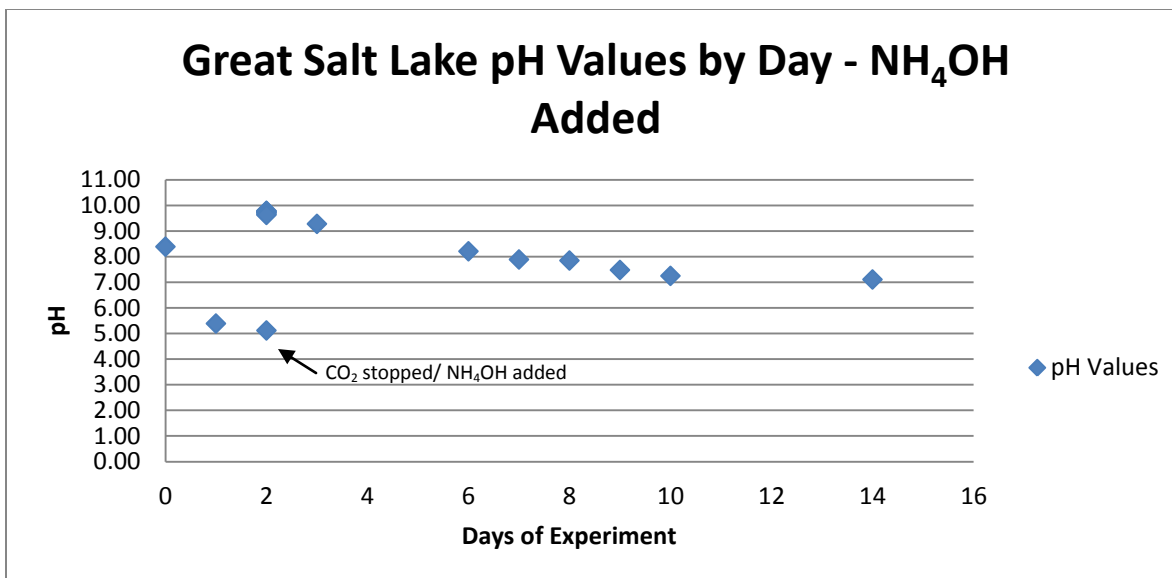


Figure 44 pH values by day.

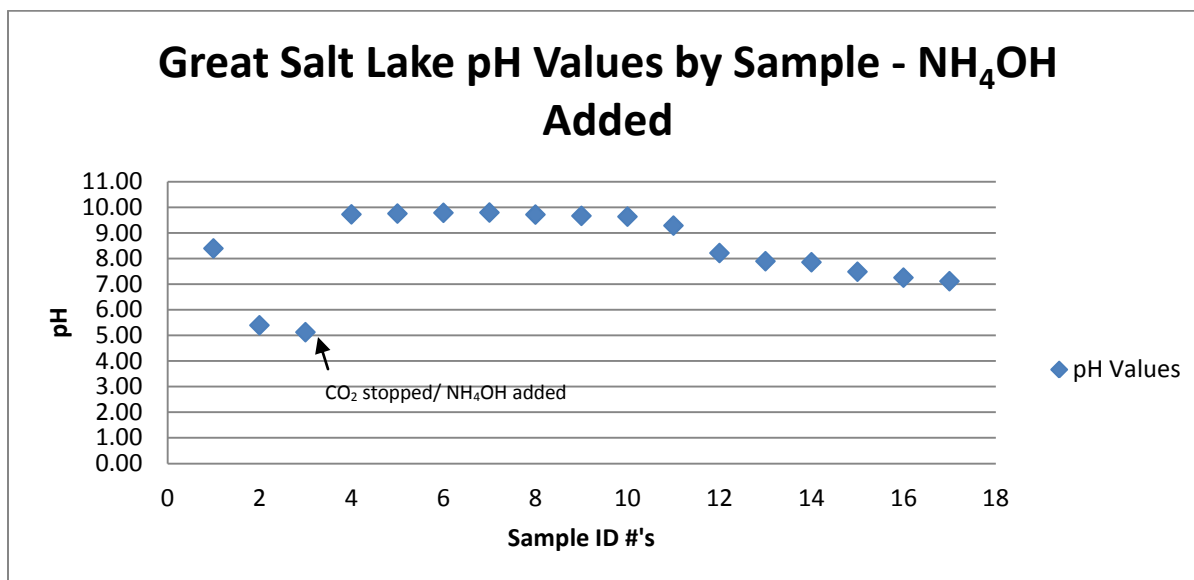


Figure 45 pH values by sample.

A pH range of 9.79 (G-7) to 5.12 (G-3) occurred during this experiment. Within seconds, the pH went from 5.12 (G-3) to 9.72 (G-4) with the addition of NH₄OH. Temperatures ranged from 23.1 °C to 24.3 °C during the course of the second experiment.

8.2.2 – Discussion of Great Salt Lake Experiments

Bubbling CO_{2(g)} through the simulated Great Salt Lake did not prove to result in any carbonate interaction, but a loss of Ca was observed. Precipitants were evident in the later sample vials which showed a drop in Ca concentration on the graphs. A drop of 10% HCl solution was placed on these crystals but no reaction occurred. Halite was evident around the 18th day into the experiment, but would not explain the decrease in Ca concentration. Due to the fact that the Great Salt Lake has a high amount of Cl and SO₄, the Ca cation may have bonded with one of these anions. Possibly, the formation of a CaCl₂ type salt or gypsum may have occurred. Polymorphs of those structures may have also developed. The effective $p\text{CO}_2$ was 10^{3.45} atm.

The addition of NH₄OH had a great affect on the Ca cation. A decrease from 400 ppm in the first sample to 20 ppm in the last sample was observed. Ca was almost fully exhausted with enhancing the pH of the water. The Ca cation bonded with a more abundant anion until it was close to being fully consumed. The anion most likely saw an increase once the Ca cation was gone. Mg concentrations also exhibited a decrease during this time. Since Ca was almost gone, Mg was the next cation in the brine evolution pathway to bond with. Towards the end of the experiment, the Mg concentrations slowly started to increase as the anion it was bonding with may have become sparse.

Evidence of flocculation occurred around the 13th day of the experiment. This time, as seen with the Dead Sea, the precipitants displayed a somewhat large thick white rhomb to rectangular shape crystal. These crystals were much larger than the crystals observed in the Dead Sea with the addition of NH₄OH. A halite matrix was then formed around the bigger crystals a couple days later. Again following the brine evolution pathway stated in section 5.4.

A white milky substance again was the reaction product from adding the NH_4OH . Stratification between this white milky substance and the clear solution was observed within a 24 hour period. As time went on, this substance crystallized into the materials mentioned above.

8.3 – Dabusun Lake

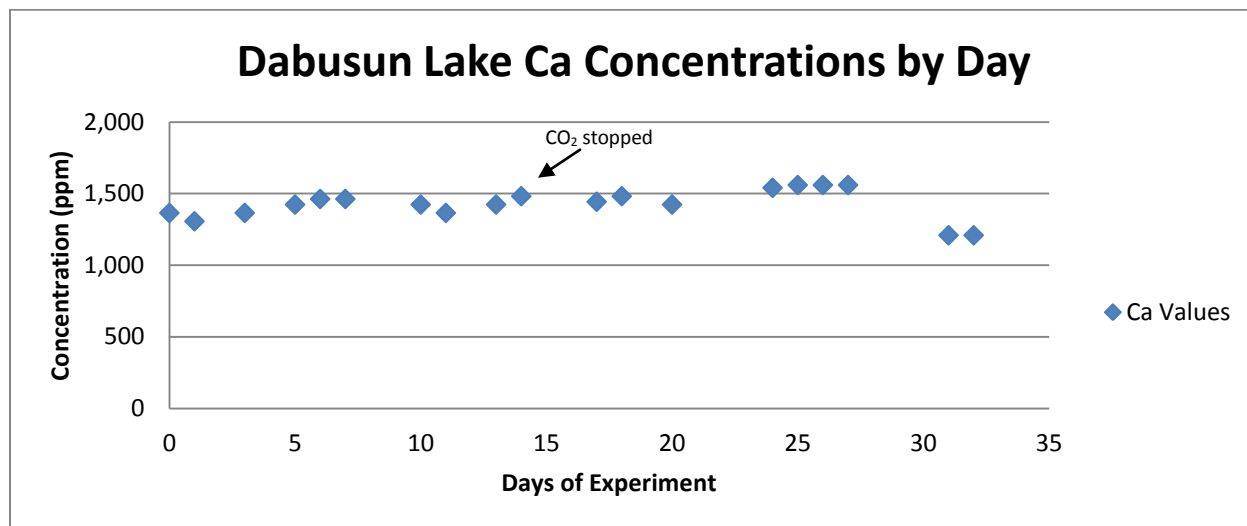


Figure 46 Ca concentrations by day with non-diluted concentrations (scale is different from other Figures).

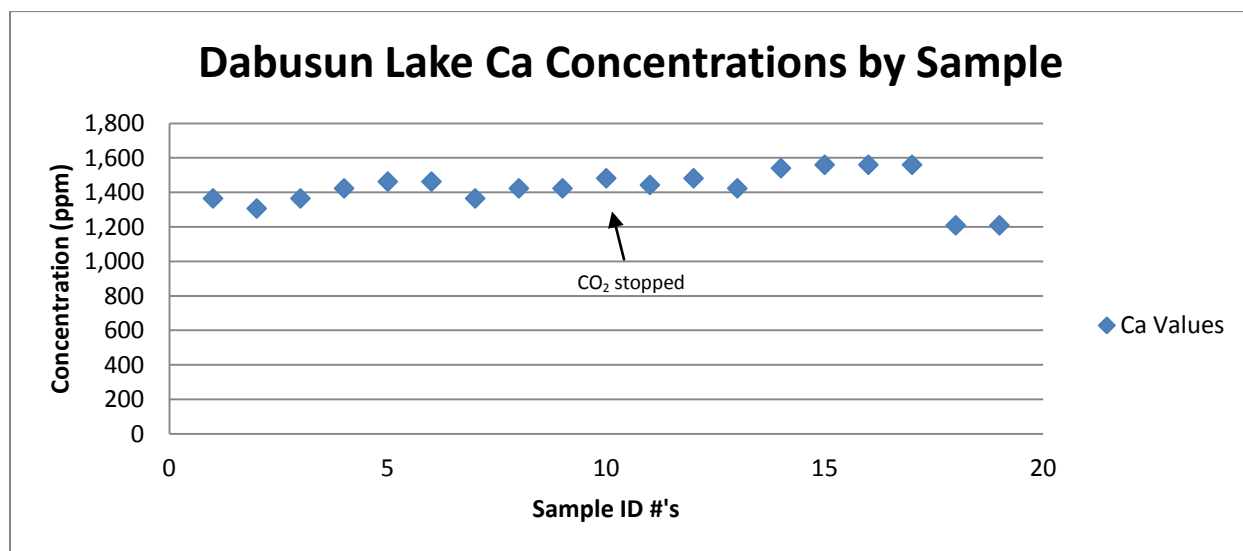


Figure 47 Ca concentrations by sample with non-diluted concentrations (scale is different from other Figures).

Ca concentrations ranged from 1,500 ppm (D-15, D-16 and D-17) to 1,200 ppm (D-19). The original concentration of the first sample, D-1, was 1,300 ppm. Results show that Ca concentrations remain uniform throughout the first experiment. A slight loss of Ca was observed towards the end of the experiment. No evidence of flocculation was seen.

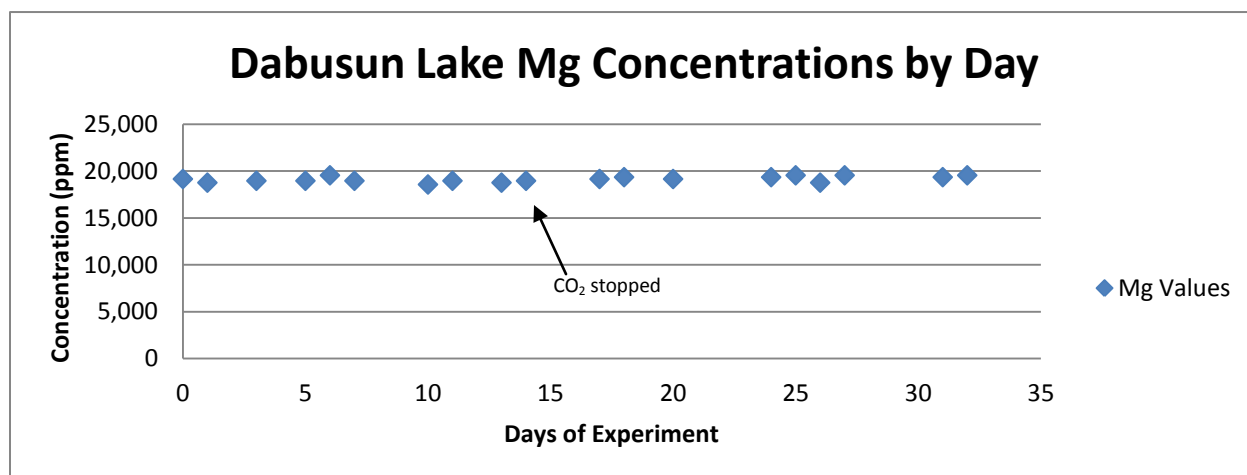


Figure 48 Mg concentrations by day with non-diluted concentrations (scale is different from other Figures).

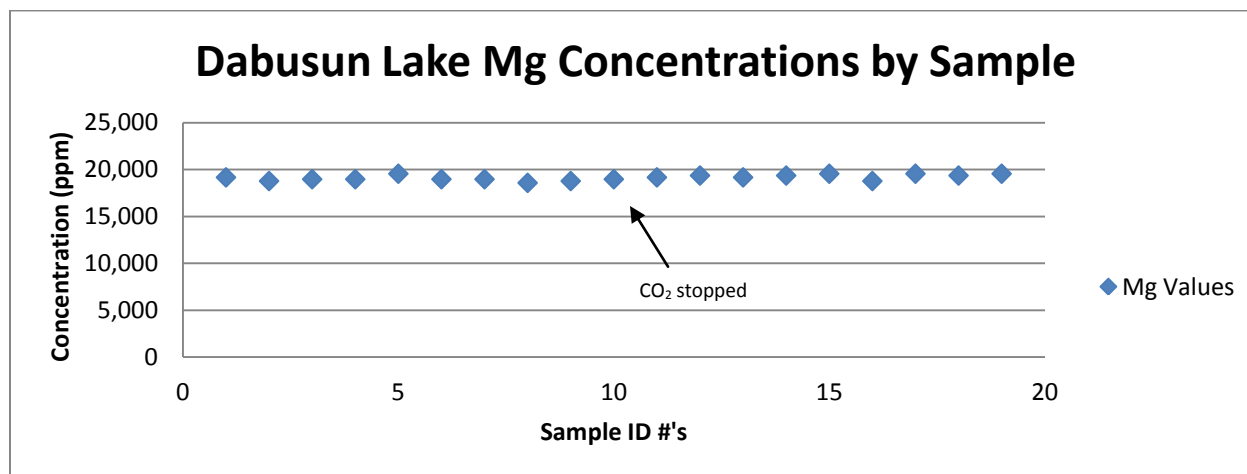


Figure 49 Mg concentrations by sample with non-diluted concentrations (scale is different from other Figures).

Mg concentrations ranged from 20,000 ppm (D-17 and D-19) to 19,000 ppm (D-1). Mg concentrations remained very consistent during the course of this experiment.

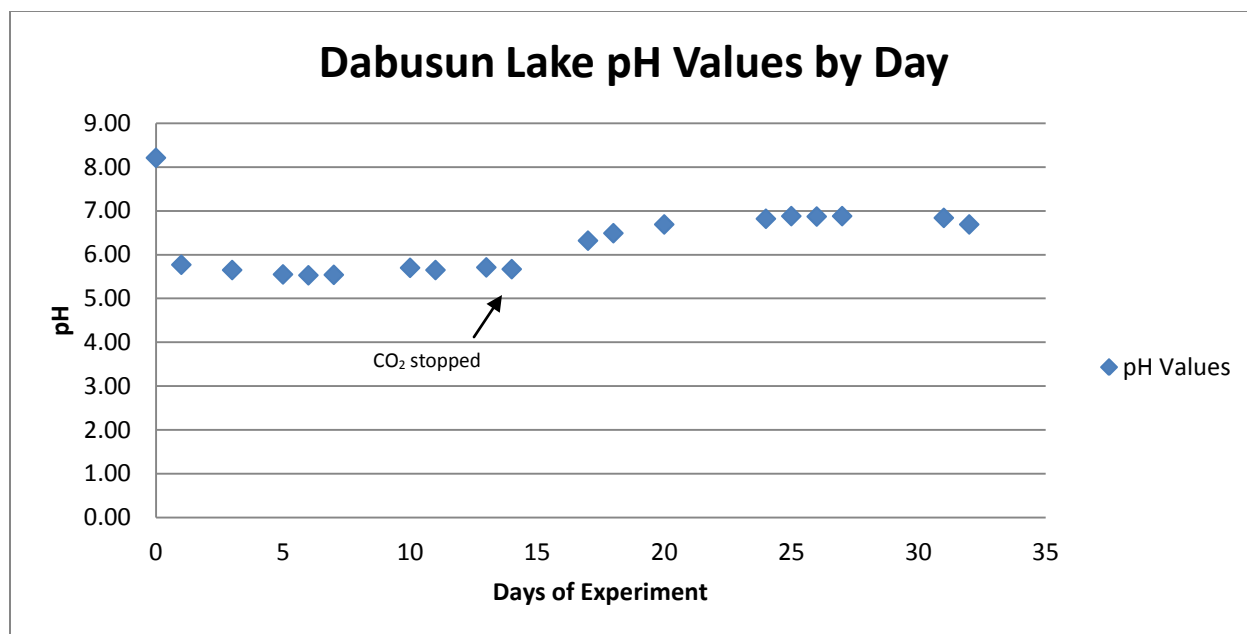


Figure 50 pH values by day.

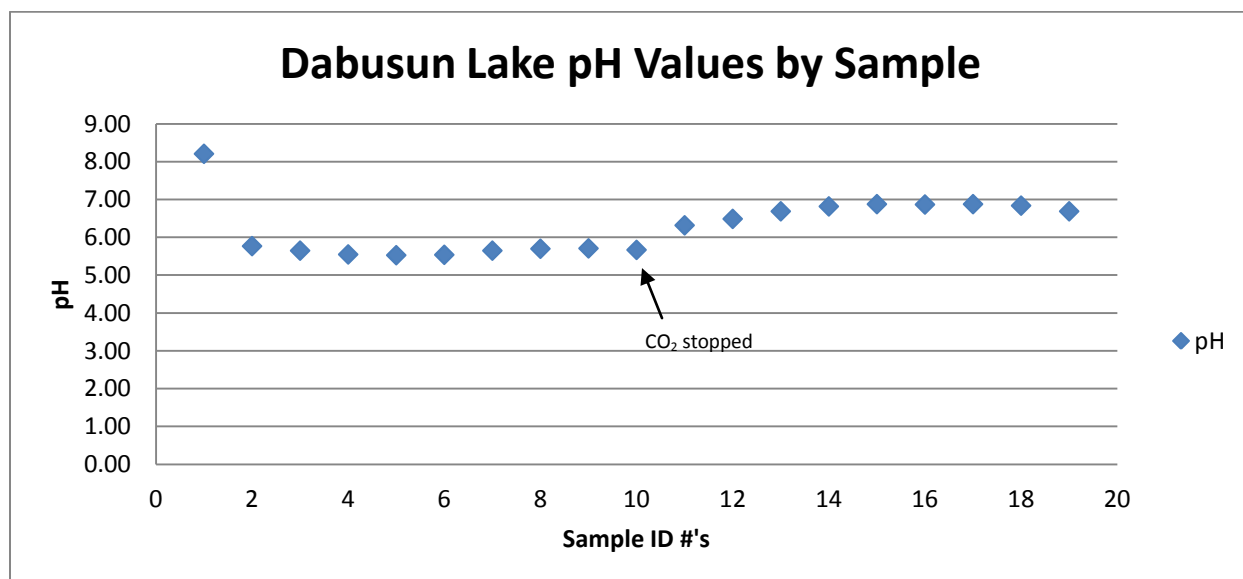


Figure 51 pH values by sample.

A pH range of 8.21 (D-1) to 5.53 (D-4) was recorded during this experiment. Within 24 hours of the addition of CO_{2(g)}, the pH of the water dropped from 8.21 (D-1) to 5.77 (D-2).

8.3.1 – Dabusun Lake with NH_4OH Added

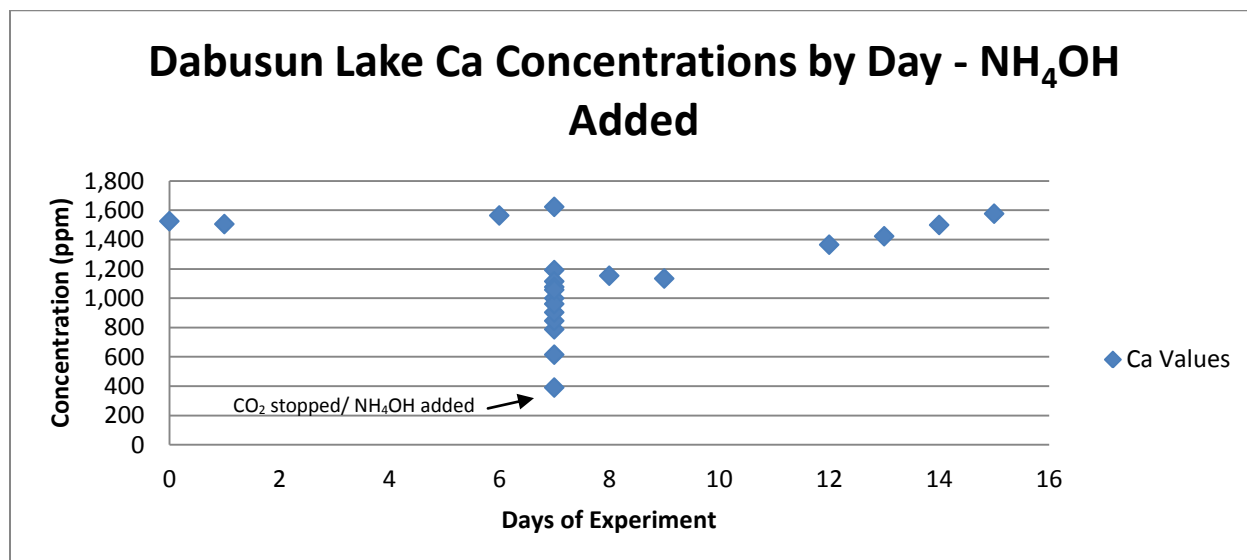


Figure 52 Ca concentrations by day with non-diluted concentrations (scale is different from other Figures).

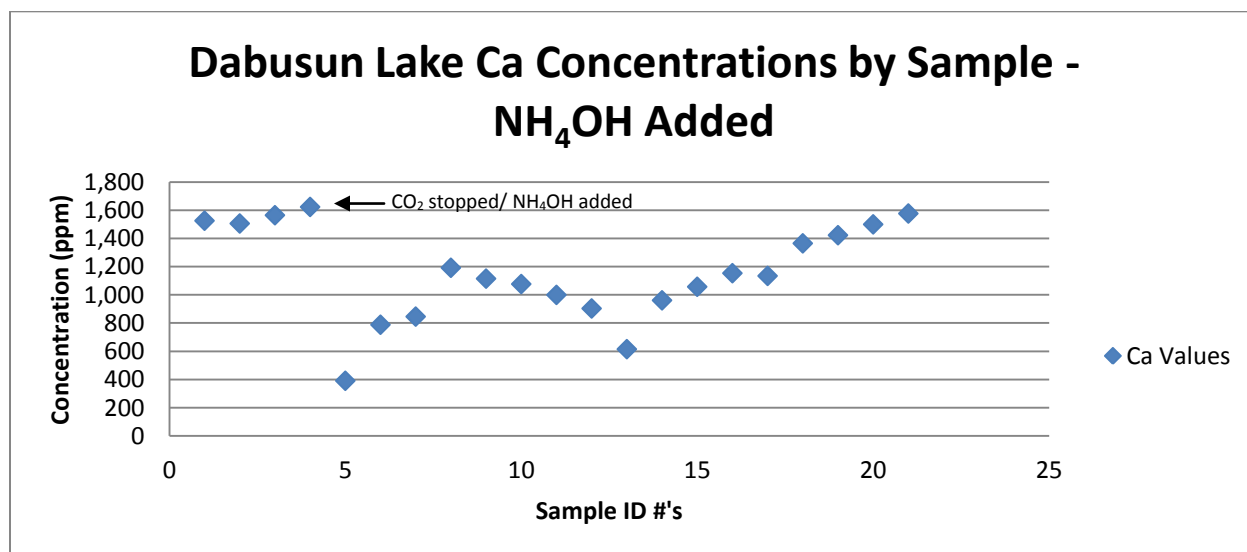


Figure 53 Ca concentrations by sample with non-diluted concentrations (scale is different from other Figures).

Ca concentrations ranged from 1,600 ppm (D-4) to 400 ppm (D-5) indicating a Ca loss approximately of 1,200 mg to precipitation. A very big decrease in Ca was observed once the $\text{CO}_{2(g)}$ was stopped and NH_4OH was added.

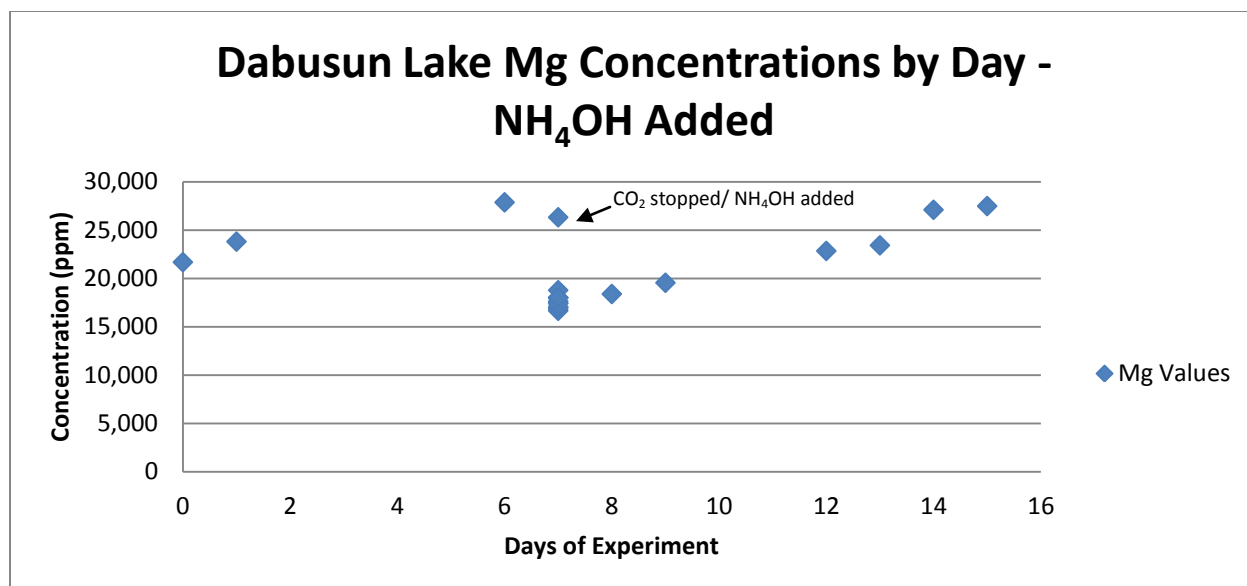


Figure 54 Mg concentrations by day with non-diluted concentrations (scale is different from other Figures).

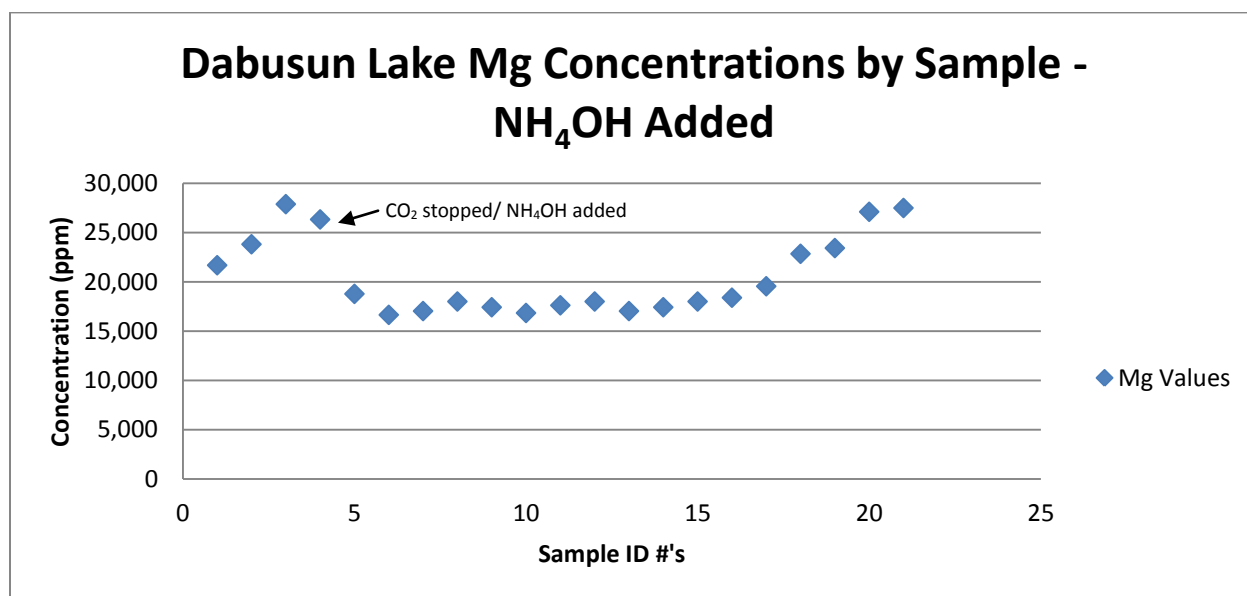


Figure 55 Mg concentrations by sample with non-diluted concentrations (scale is different from other Figures).

Mg concentrations ranged from 28,000 ppm (D-3) to 17,000 ppm (D-5) indicating a Mg loss of approximately 11,000 mg to precipitation. As with Ca concentrations, Mg also displayed a rapid decline once the addition of NH₄OH was initiated.

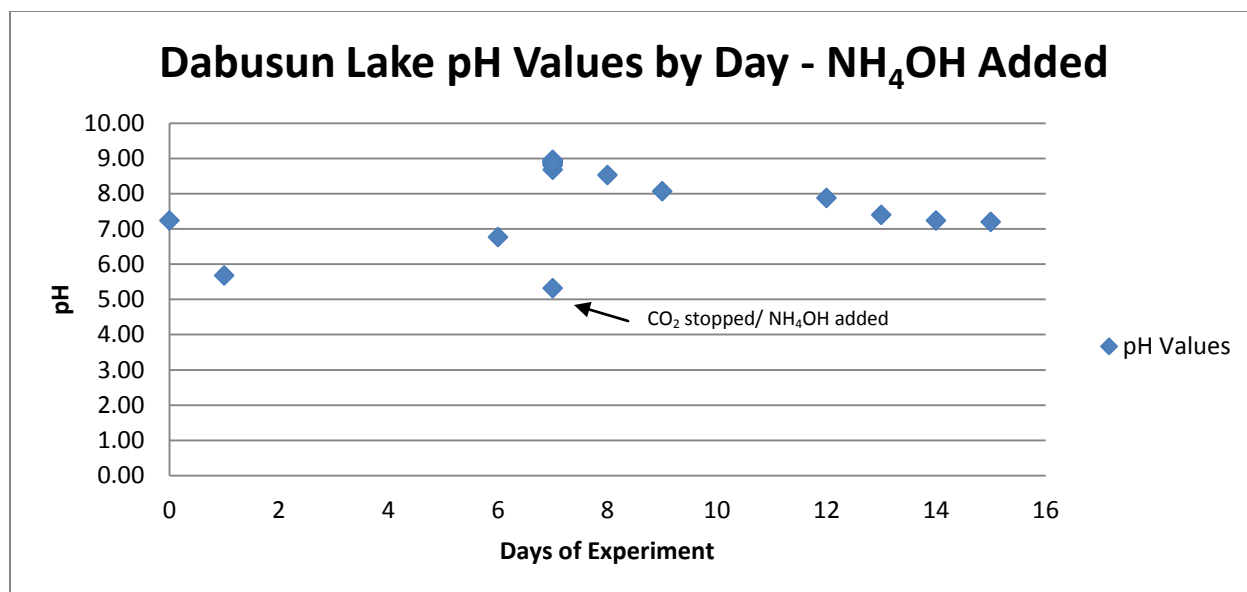


Figure 56 pH values by day.

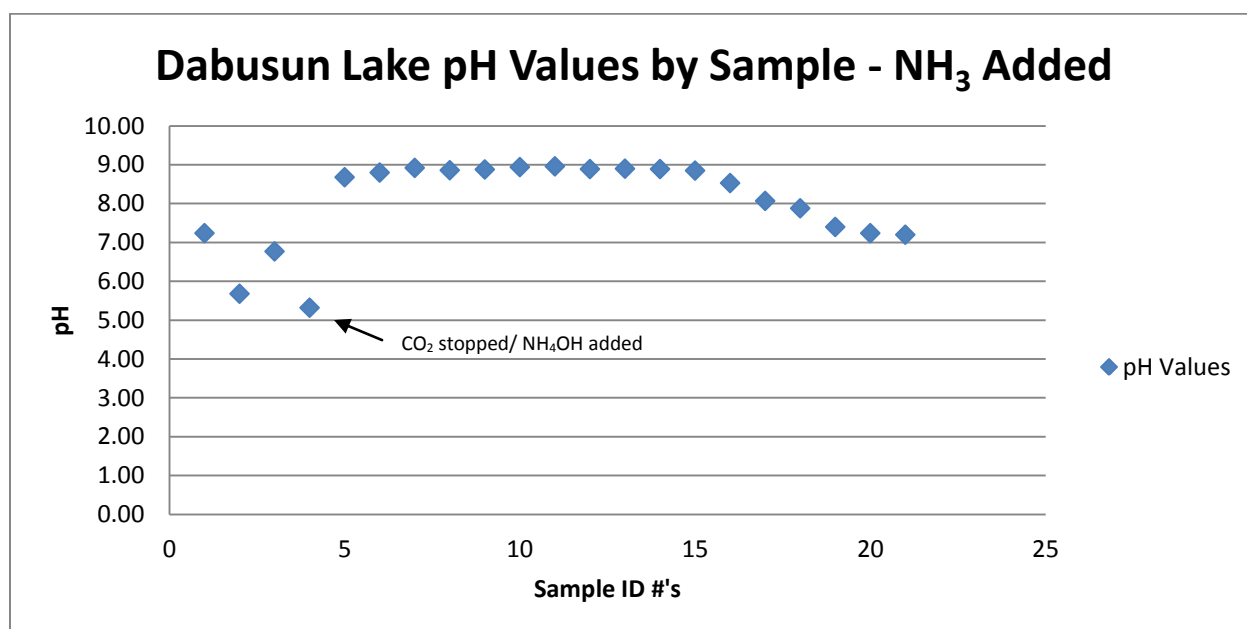


Figure 57 pH values by sample.

The pH of the simulated Dabusun Lake ranged from 8.96 (D-11) to 5.32 (D-4) during this experiment. The pH increased within seconds from 5.32 (D-4) to 8.68 (D-5) with the addition of NH₄OH. Temperatures ranged from 22.6 °C to 24.1 °C throughout this experiment.

8.3.2 – Discussion of Dabusun Lake Experiments

The diffusion of CO₂(g) within the simulated Dabusun Lake did not show any affect on ion interaction. Evidence of flocculation did not appear until around the 32nd day of the experiment which proved to be a lot longer than the previous two lakes in this study. Once precipitation did occur, the mineral that formed had the characteristics and physical appearance of halite. Chemical testing was done with 10% HCl and no reaction occurred. A higher amount of Mg and HCO₃+CO₃ ions compared to the first two lakes may have played a role with late precipitation. Although it was strange that Ca concentrations exceeded the amount that was created in the recipe via AA analysis, the overall concentration did not see that much of a change. This was also the case with Mg. The effective pCO₂ was 10^{-3.19} atm.

The addition of NH₄OH had a great effect on the decrease of both Ca and Mg concentrations. Within five minutes of the addition of NH₄OH, Ca concentrations plummeted from 1,600 ppm to 400 ppm. Mg also decreased within this time dropping in concentration from 28,000 ppm to 17,000 ppm. Both cations slowly started to increase after the original depletion was seen. This was most likely due from the depletion of the anion they were reacting with. With a depleting anion and the natural evaporation of water, abundant ion concentrations will begin to increase.

A milky white substance was again observed as soon as the NH₄OH was added. This substance separated from the rest of the solution and represented the same stratification as seen with the two previous lakes. Precipitation was very slow with this experiment as seen in the first experiment of Dabusun Lake. Small white thick rhomb to rectangular shape minerals started to appear after the 20th day of the experiment. The minerals resemble that of what was seen in the Dead Sea.

8.4 – Donglin Lake

Temperatures ranged from 23.6 °C to 24.7 °C during this experiment.

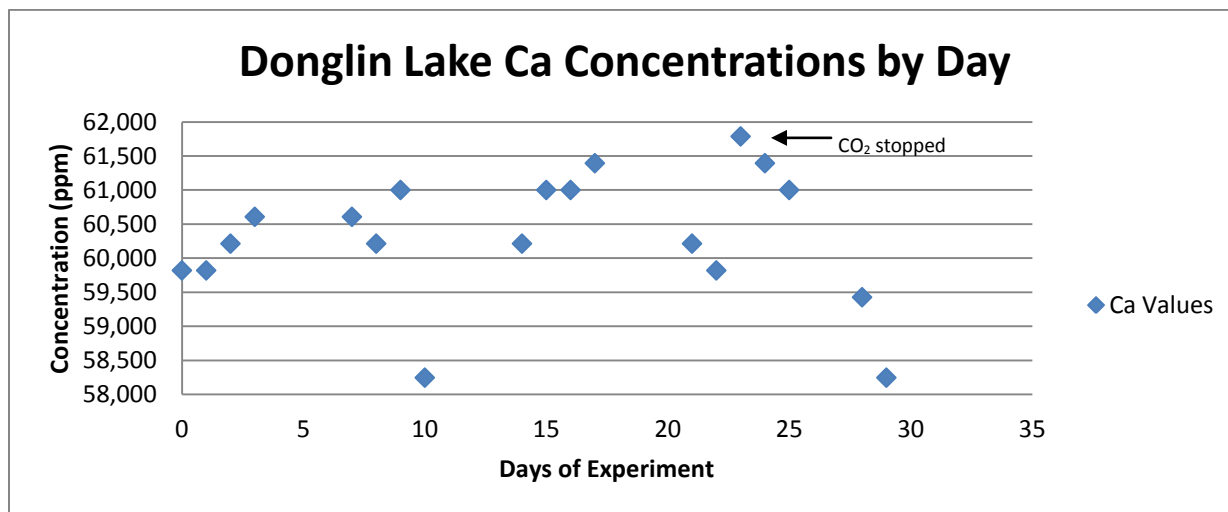


Figure 58 Ca concentrations by day with non-diluted concentrations (scale is different from other Figures).

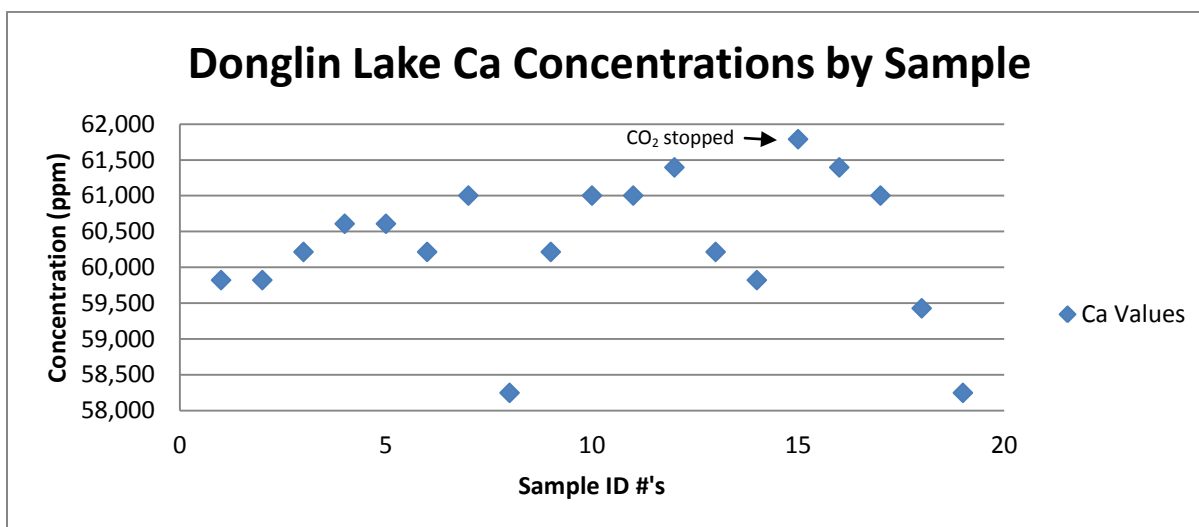


Figure 59 Ca concentrations by sample with non-diluted concentrations (scale is different from other Figures).

Ca Concentrations ranged from 62,000 ppm (DG-15) to 58,000 ppm (DG-8 and DG-19).

The original concentration of DG-1 was 60,000 ppm. Not much of a change was observed and Ca concentrations remained consistent.

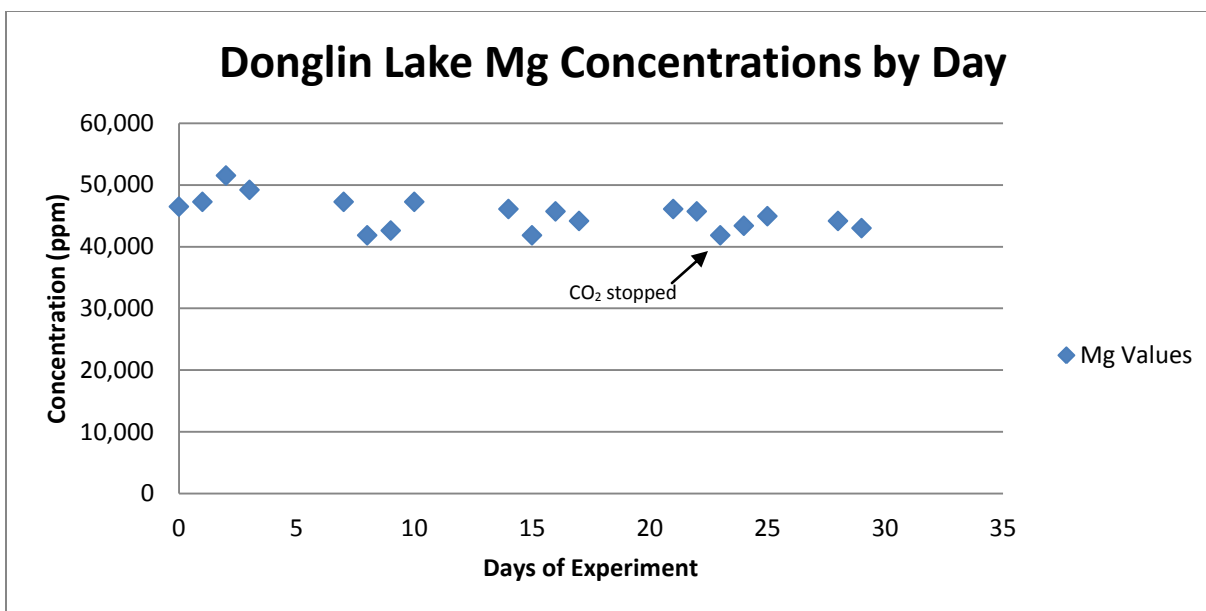


Figure 60 Mg concentrations by sample with non-diluted concentrations (scale is different from other Figures).

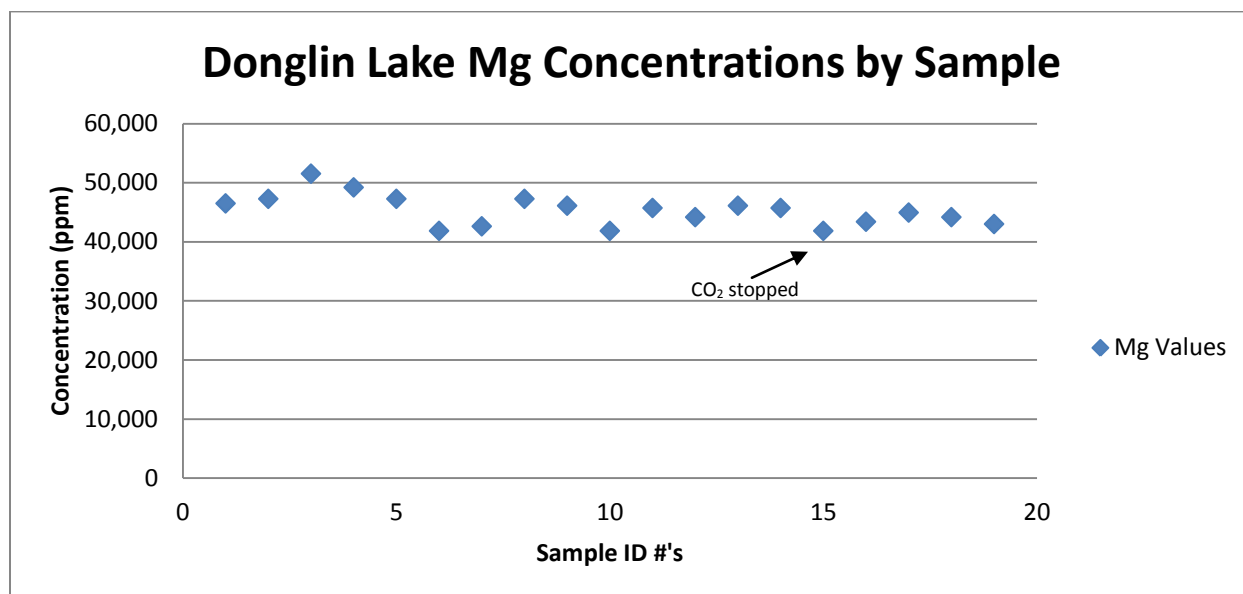


Figure 61 Mg concentrations by sample with non-diluted concentrations (scale is different from other Figures).

Mg concentrations ranged from 52,000 ppm (DG-3) to 42,000 ppm (DG-6). The original sample, DG-1, Mg concentration registered at 46,000 ppm. Although a wide range in Mg concentrations was seen, no evidence of any reaction involving the $\text{CO}_{2(g)}$ occurred.

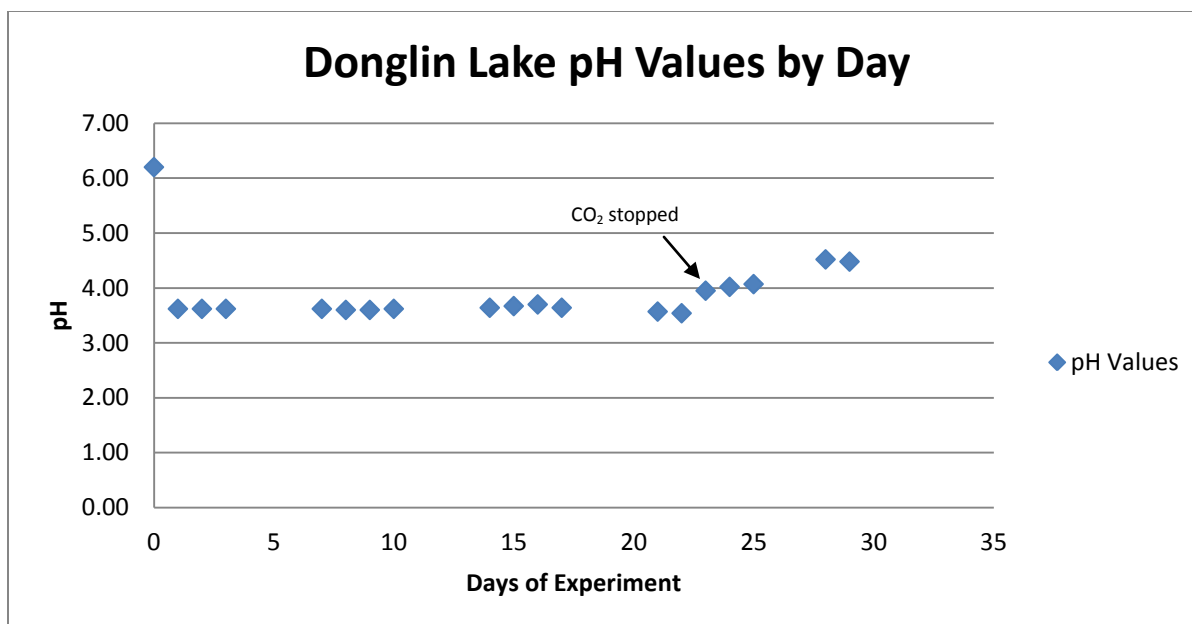


Figure 62 pH values by day.

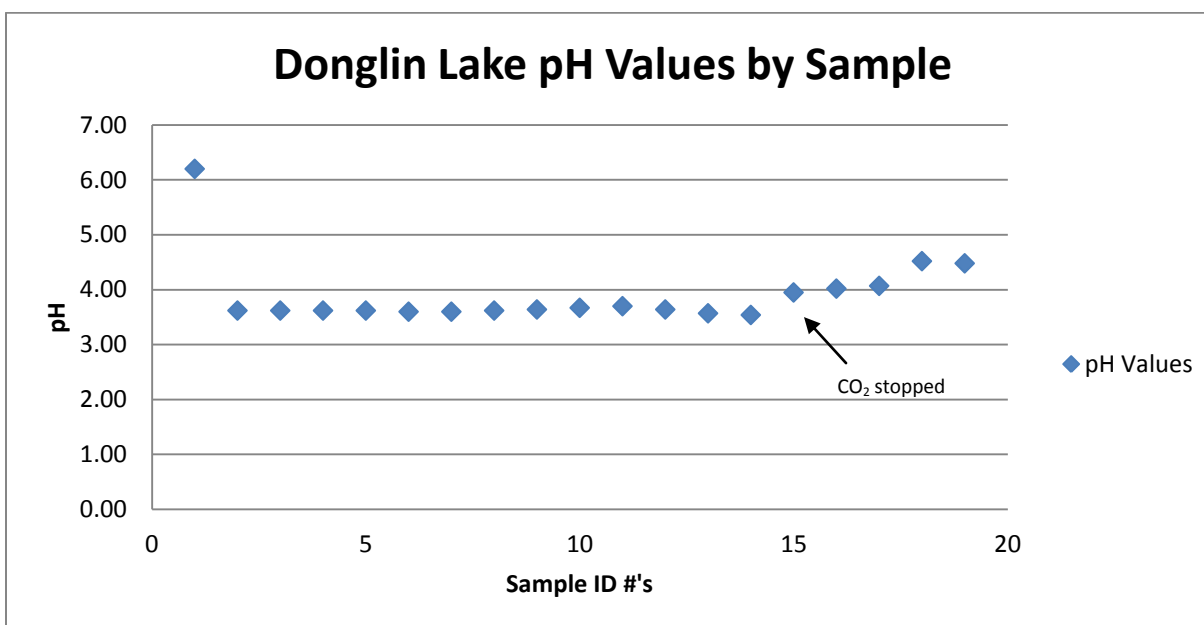


Figure 63 pH values by day.

pH values ranged from 6.20 (DG-1) to 3.60 (DG-2). Within 24 hours of activating the CO_{2(g)}, the pH dropped to its lowest value of 3.60.

8.4.1 – Donglin Lake with NH_4OH Added

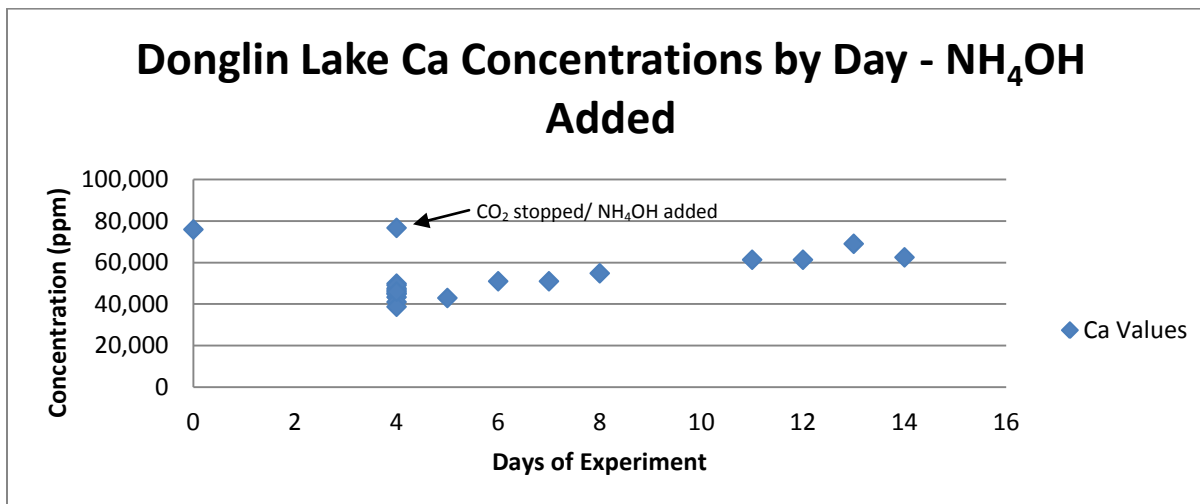


Figure 64 Ca concentrations by day with non-diluted concentrations (scale is different from other Figures).

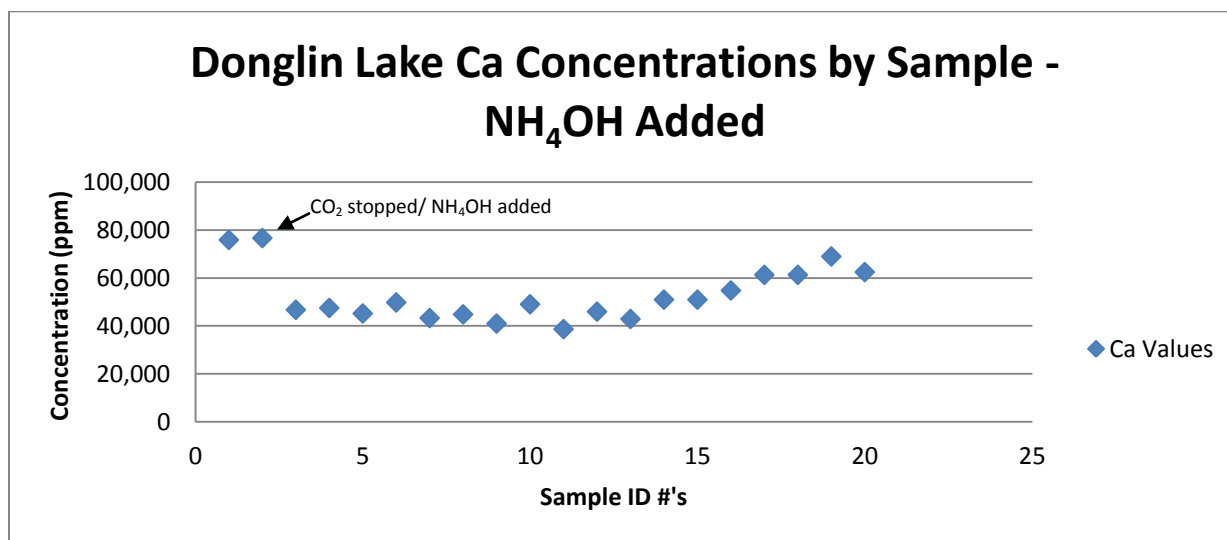


Figure 65 Ca concentrations by sample with non-diluted concentrations (scale is different from other Figures).

Ca concentrations ranged from 77,000 ppm (DG-2) to 39,000 ppm (DG-11) indicating a Ca loss of approximately 38,000 mg to precipitation. A major decrease in Ca concentration was observed once the NH_4OH was added. Within 5 minutes, Ca concentrations fell from 77,000 ppm (DG-2) to 47,000 ppm (DG-3) and kept declining until a later increase was seen.

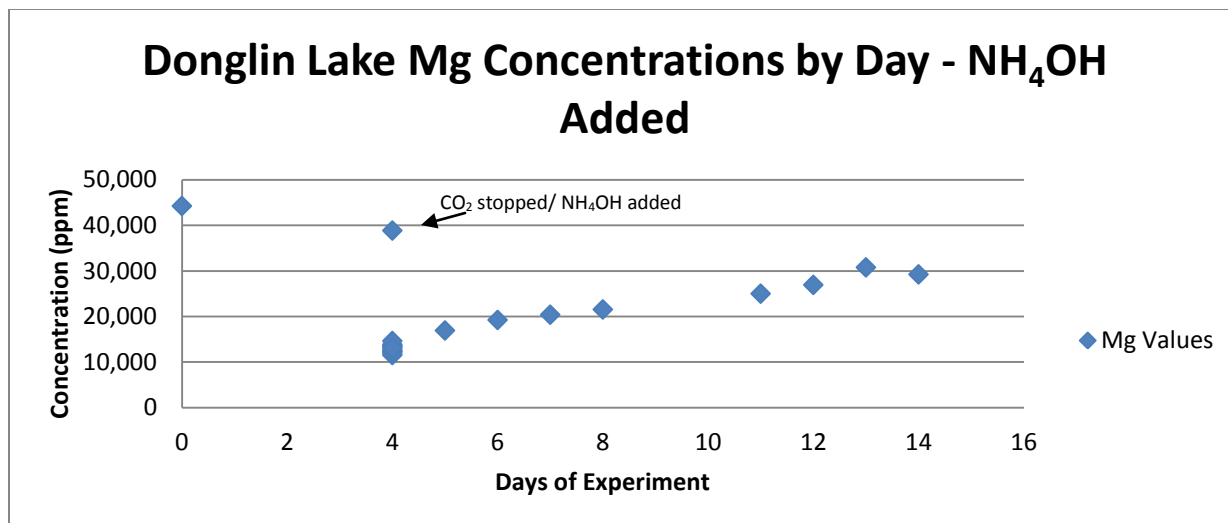


Figure 66 Mg concentrations by day with non-diluted concentrations (scale is different from other Figures).

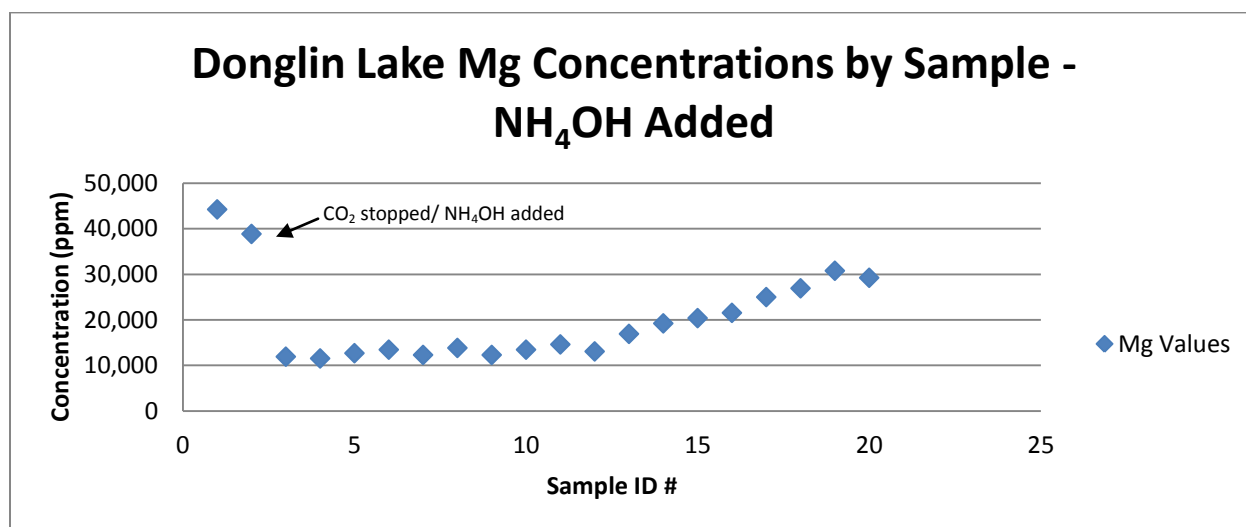


Figure 67 Mg concentrations by sample with non-diluted concentrations (scale is different from other Figures).

Mg concentrations ranged from 44,000 ppm (DG-1) to 12,000 ppm (DG-4) indicating a Mg loss of approximately 32,000 mg to precipitation. This marks another major decrease in concentration as seen with Ca in the simulated Donglin Lake once NH₄OH has been added. Mg concentrations dropped from 39,000 (DG-2) to 12,000 ppm (DG-3) within 5 minutes of adding NH₄OH.

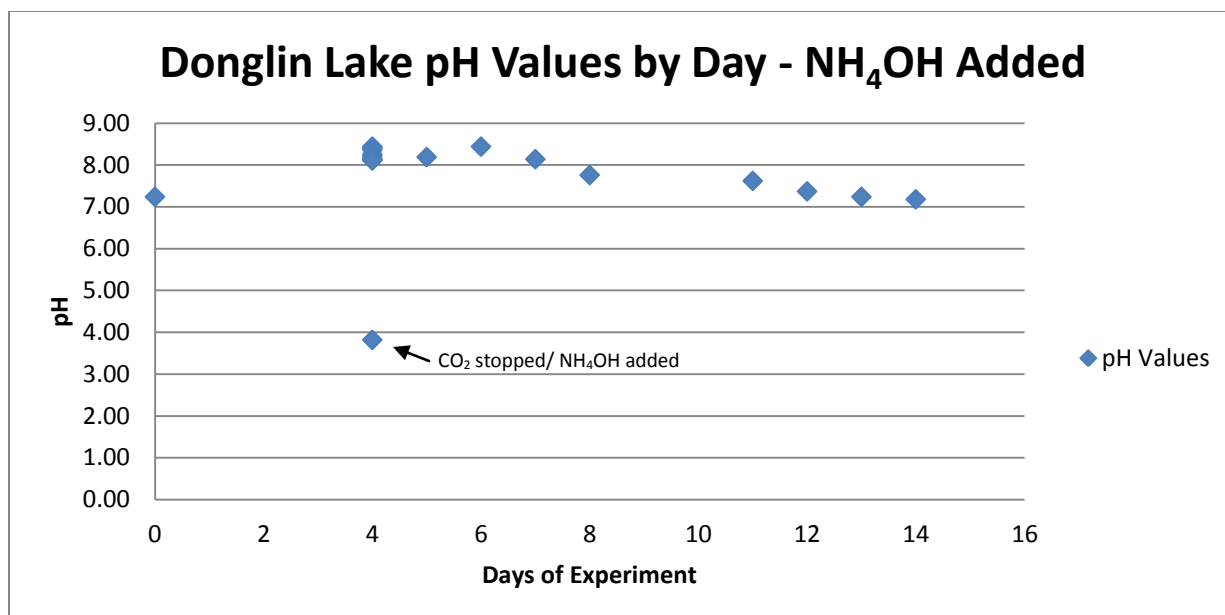


Figure 68 pH values by day.

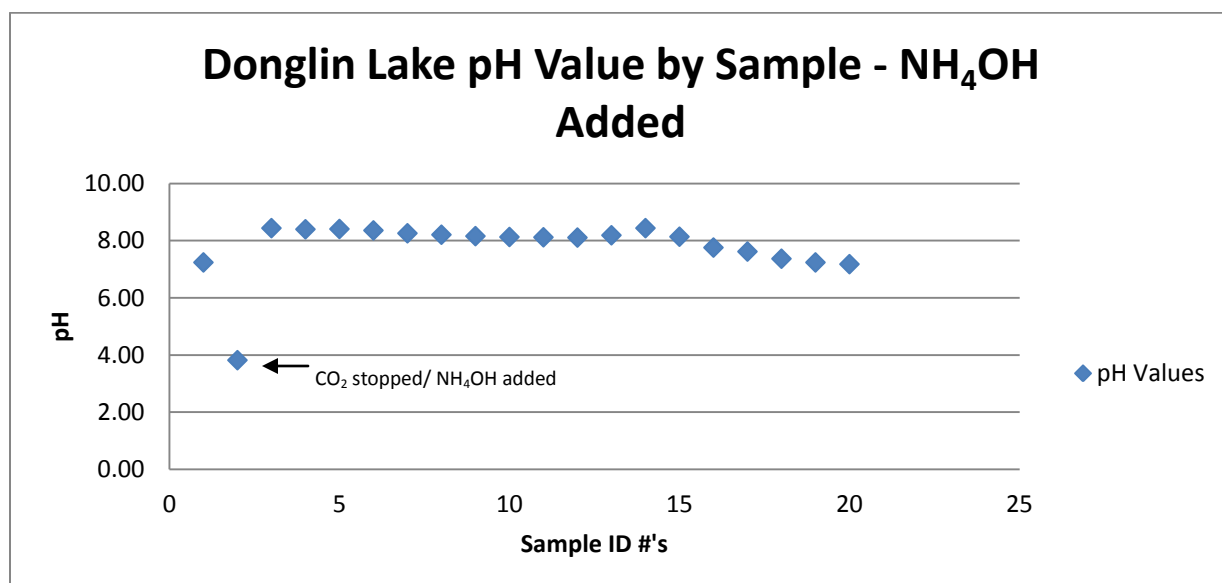


Figure 69 pH values by sample.

pH values ranged from 8.44 (DG-3) to 3.82 (DG-2). The pH increased within seconds after the NH₄OH solution was added. Temperatures ranged from 23.1 °C to 25.8 °C during this experiment.

8.4.2 – Discussion of Donglin Lake Experiments

The diffusion of CO_{2(g)} alone did not prove to result in any ion interaction in the simulated Donglin Lake. As seen with Dabusun Lake, evidence of precipitation did not appear in Donglin Lake until approximately the 35th day. Crystals of halite looked to be the first minerals to form after conducting chemical and physical tests. Donglin Lake had the highest concentrations of Ca and Mg compared to any other lake in this study. The second highest amounts of these cation concentrations, especially Mg, were observed in Dabusun Lake. There is a possibility that high amounts of Mg prevents or slows down reactions between cations and anions in a simulated evaporative lake setting. The effective $p\text{CO}_2$ was $10^{5.28}$ atm.

The addition of NH₄OH had a major effect on both Ca and Mg concentrations. The concentration of Ca dropped from 77,000 ppm (DG-2) to 47,000 ppm (DG-3) within 5 minutes of adding the NH₄OH solution. Ca levels remained to follow this trend until approximately 7 hours later when Ca concentrations slowly started to climb. Mg concentrations followed the same path. Mg values dropped from 39,000 ppm (DG-2) to 12,000 ppm (DG-3) within 5 minutes of the added NH₄OH. Mg concentrations slowly began to increase approximately 4 hours after the addition of NH₄OH.

A noticeable difference observed with the second experiment conducted on Donglin Lake was the range in temperature from 23.1 °C to 25.8 °C. The one dissimilarity between Donglin Lake and all the other lakes was the amount of NH₄OH that was added. Originally, 80 mL of the NH₄OH solution was added to enhance the pH. As the pH did not respond as planned, small increments of NH₄OH were added until the pH reached its optimal range. This took a total of 285 mL of NH₄OH to achieve this goal. During this time, a noticeable increase in heat was felt on the outside of the glass beaker. Temperatures cooled down quickly, within one hour after the

added NH_4OH , but the massive amount of NH_4OH must have created a reaction to cause an increase of heat.

As seen with the other lakes, a milky white substance took form once the NH_4OH was added. After 24 hours, the milky white substance separated from the rest of the solution and resulted in a stratified appearance within the beaker. Evidence of flocculation occurred approximately 24 days after the experiment began. The precipitants present took on the same appearance of the thick white rhomb to rectangular shape formation as seen in the Dead Sea and Dabusun Lake.

CHAPTER 9 – OVERALL DISCUSSION OF SALINE LAKE EXPERIMENTS

Four simulated saline lakes were created during this study to test the possibilities of capturing CO_2 within a saline lake environment. $\text{CO}_{2(g)}$ was bubbled through a diffuser at a constant rate of 30 psi in each of the simulated lakes to test if mineralization, mainly in the form of carbonates, would occur. The first set of experiments examined the potential of diffusing $\text{CO}_{2(g)}$ through a simulated lake created in a lab. The setting was kept as natural as possible to see if any ion interaction would arise. Natural evaporation rates, as best within a laboratory facility, were permitted with no barriers in place to obstruct the process. Artificial enhancers were also kept out of the picture during the first set of experiments.

The result of just diffusing $\text{CO}_{2(g)}$ throughout each of the saline lakes did not show any evidence of ion interaction with the exception of Great Salt Lake. For the most part, all four simulated lakes displayed very little change in Ca and Mg concentrations as the $\text{CO}_{2(g)}$ was being diffused. Great Salt Lake did show a loss of Ca, approximately 35 mg, but not in the form of carbonate precipitation. High amounts of Cl and SO_4 anions in the Great Salt Lake may have bonded with the Ca cation leading to the precipitation of CaCl_2 or gypsum. The $\text{CO}_{2(g)}$ was ceased after a couple weeks into each of the experiments to see if the pH would rise high enough to perform carbonate mineralization. For this to occur, the pH of the water or any waters in that matter needs to rise to a value of at least 8 to 8.5. This was not achieved in the first set of experiments. With the introduction of $\text{CO}_{2(g)}$, pH levels did drop dramatically. All four lakes possessed a level of full saturation of dissolved CO_2 within a 24 hour period. pH levels dropped to as low as 3 to 4 and seem to level out as long as the diffusing of $\text{CO}_{2(g)}$ continued. Once the $\text{CO}_{2(g)}$ was stopped, the pH of each simulated lake did increase but not enough for any reactions

to occur. The effective $p\text{CO}_2$ for the simulated Dead Sea, Great Salt Lake, Dabusun Lake and Donglin Lake registered at $10^{4.58}$ atm, $10^{3.45}$ atm, $10^{3.19}$ atm and $10^{5.28}$ atm respectively.

The second set of experiments consisted of saturating each lake with dissolved $\text{CO}_{2(g)}$ and then enhancing the pH with an NH_4OH solution. In about 24 hours, full saturation of dissolved $\text{CO}_{2(g)}$ was achieved. These results were known from conducting the first set of experiments. Immediately after this point was reached, the NH_4OH solution was added to each of the lakes. Within seconds, the pH of each of the lakes rose to a level to where carbonate production would be possible. Also, Ca and Mg concentrations began to decrease drastically. Dabusun Lake and Donglin Lake showed the biggest decrease in Ca and Mg concentrations but also had the highest amount of each cation to begin with. The Great Salt Lake, which had a low Ca concentration of 400 ppm, saw a decrease in Ca to where it was almost fully depleted. All the other lakes, having higher concentrations, demonstrated a decrease in both cations after the NH_4OH was added and then, after approximately 5 - 7 hours, the concentrations of Ca and Mg began to slowly increase. This was seen with the Mg concentrations in the Great Salt Lake.

The total mass of CO_2 sequestered in each simulated lake during the second set of experiments can be seen in Figure 70 below.

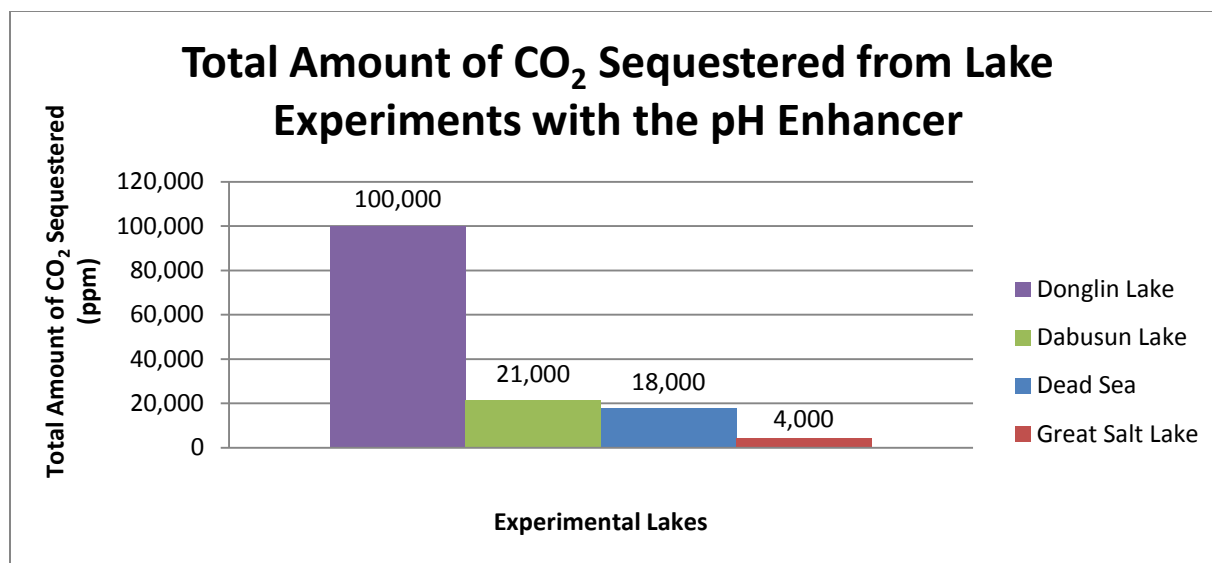


Figure 70 Total amount of CO₂ sequestered from lake experiments with the pH enhancer.

The total amount of CO₂ sequestered was determined by the loss of Ca and Mg from each simulated lake, as these cations bonded with CO₃ to form Ca and Mg-carbonates. The results from Figure 70 show that the experimental lakes with higher concentrations of Ca and Mg proved to sequester more CO₂ than lakes with lower concentrations. The simulated Donglin Lake, which had the highest amounts of Ca and Mg, displayed the greatest amount of CO₂ sequestered from any of the experimental lakes. Each simulated lake after this followed the same trend and showed that the higher the concentration of Ca and Mg, the greater the amount of CO₂ sequestered. The experimental Donglin Lake, Dabusun Lake, Dead Sea and Great Salt Lake sequestered approximately 100 g L⁻¹, 21 g L⁻¹, 18 g L⁻¹ and 4 g L⁻¹ of CO₂ respectively.

The concentration pathway that each lake followed portrayed the resemblance of what different cations and anions go through in real saline lake environments. For a reaction to occur and a mineral to precipitate, a cation and anion will come together and form a bond. Out of these two ions, the ion that is lacking in concentration will precipitate with the other ion until the lacking ion becomes exhausted. At this point, the more abundant ion will begin to increase as it

has nothing to bond with at that moment. The effects of evaporation come into play as the liquid solution surrounding the ion converts to a vapor. With less of a solution, the remaining ion's concentration will increase per volume of solution.

An example of the scenario mentioned above can be explained by using a scarce Ca cation and an abundant CO_3 anion, a resemblance of what was seen in the Great Salt Lake experiment with the addition of NH_4OH . Once the pH is enhanced to where carbonate production can occur, the Ca^{+2} cation will begin to bond with the CO_3^{-2} anion. The concentrations of each of these ions will level out as long as they keep forming a carbonate mineral, or in this case, calcite. Eventually, the Ca cation will become depleted and the CO_3 anion will begin to increase as the solution begins to evaporate. In nature, various inflow sources bringing in more of the CO_3 anion will also lead to its increased concentration. In a matter of time, the CO_3 anion will begin to bond with the Mg cation in this situation. This scenario can happen to either cations or anions. Whichever one is less in concentration will be depleted first. This was seen throughout the second set of experiments with the addition of NH_4OH . A decrease in Ca and Mg occurred once the pH was enhanced by the addition of NH_4OH . Once mineralization took place and the anion between the cation-anion interaction became exhausted, an increase in the two cations, Ca and Mg, began. The increase of these cations may have also resulted from the drop in pH towards the end of each simulated lake experiment. With a drop in pH, the newly formed carbonate minerals may begin to dissociate. At this point, the ions would go back into solution resulting in an increase of Ca and Mg. This curve is evident on the experimental graphs created with the addition of NH_4OH in chapter 8.

The precipitation of minerals in each of the saline lakes during the second set of experiments appeared to follow the brine evolution pathways discussed in section 5.4. With the

addition of NH_4OH , larger crystals were formed than what was seen from the first set of experiments. These crystals had characteristics that took on a thick white rhomb to rectangular shape appearance and were confirmed by microscopic analysis as possible carbonate minerals. These were also the first to precipitate out of solution. A couple days after these minerals formed, a halite matrix was seen surrounding the bigger crystals. A series of chemical and physical tests, as well as X-ray diffraction (XRD) analysis was completed to determine that this mineral was in fact halite. Overall, halite was the most abundant mineral to precipitate as is the case with the majority of saline lakes around the world.

The minerals that formed in each lake were removed and dried in an oven until majority of the water was evaporated. A small drop of 10% HCl solution was placed on each of the crystals to observe effervescence. This is a quick way to test carbonate minerals. The minerals collected from the Dead Sea, Donglin Lake and Dabusun Lake all demonstrated a clear indication of effervescence once the HCl solution was added. Table 7 below describes which minerals showed a clear indication of effervescence from each simulated lake experiment.

Table 7 Minerals precipitated from each simulated lake that showed a clear indication of effervescence.

<u>Experimental Lake</u>	<u>Indication of Effervescence (10% HCl solution)</u>
Dead Sea	YES
Great Salt Lake	NO
Dabusun Lake	YES
Donglin Lake	YES

Donglin Lake was also the only lake that did not have any $\text{HCO}_3 + \text{CO}_3$ in its original composition. The crystals from the Great Salt Lake did not exhibit the same effect with the

addition of HCl. Although AA analysis resulted in an almost fully depleted Ca cation once the NH_4OH solution was added, the chemical test of adding HCl to the produced mineral showed no response. Ca was depleted but maybe not in the form of a carbonate mineral. If at all, the carbonate mineral that formed may have been so inadequate to where a reaction with HCl was nonexistent. A hand lens was also used to determine the physical characteristics of the different minerals that precipitated. White rhombus and needle-like shaped crystals were found within the halite matrix.

Future work will be conducted using XRD analysis to better identify the minerals that precipitated. Smaller amounts of carbonates formed, as possibly seen with the Great Salt Lake experiment in Figure 70, may be harder to detect through XRD analysis as the halite mineral dominates in each of the experimental lakes. Multiple runs using XRD analysis will be conducted on the minerals produced from each experimental lake to ensure that the insufficient carbonate minerals present get detected within the abundance halite. The small amounts of carbonate minerals formed may be insufficient when dealing with XRD analysis as the halite mineral dominates.

CHAPTER 10 – CONCLUSIONS

The objective of this research was to determine if saline lake environments have the capabilities to sequester anthropogenic CO₂. The results from the experimental approach indicate that significant carbonate mineralization does not occur via simple diffusion of CO_{2(g)} within a saline lake. No significant evidence of cation loss was observed through the initiation or termination of CO_{2(g)} with the exception of Great Salt Lake. A loss of Ca was noticed in the Great Salt Lake but most likely due to the precipitation of CaCl₂ or gypsum. Carbonate mineralization was not evident during the first round of the Great Salt Lake experiment. pH levels did rise once the CO_{2(g)} was stopped, but not high enough for carbonate production to occur.

The second set of experiments introduced an ammonium hydroxide solution to enhance the pH of the lakes after full saturation of dissolved CO₂ was achieved. This was done in an attempt to control the pH to levels where carbonate mineralization can occur. Within seconds of adding the NH₄OH, the pH of each lake, with the exception of Donglin Lake, increased to an optimal range for carbonates to form. Through AA analysis, cation loss in Ca and Mg was observed within minutes. The concentration of these cations continued to decline for approximately 5 to 7 hours after the addition of NH₄OH. Once this time passed, Ca and Mg concentrations began to increase as indicated on the graphs in chapter 8. Saline lakes with higher concentrations of Ca and Mg appeared to have a greater result in cation loss than the lakes with lower concentrations. These lakes with higher concentrations of Ca and Mg also showed their ability to sequester more CO₂ than the lakes with lower concentrations. As seen with the Great Salt Lake experiment, insufficient levels of Ca were exhausted fairly quickly after the NH₄OH was introduced. This experimental portion concludes that ion interaction can take place

within a saline lake environment as long as the pH is manually enhanced to a range for carbonate mineralization to occur. These results indicate that saline lake environments can serve a purpose as a sequestering agent for anthropogenic CO₂.

The first component of this study exploited the carbon sequestration capacity of an actual geologic formation in the Wilkins Peak Member of the Green River Formation. The Na-carbonate mineral trona was used to determine the natural carbonate flux rates within the lower half of the Wilkins Peak Member throughout its 0.7 million year existence during the Eocene epoch. A comparison was then made to the 2009 global CO₂ emission rates to determine how many of these formations would be required to sequester this entire amount of anthropogenic CO₂. Through calculations declared in chapters 3 and 4, the Wilkins Peak Member would be able to sequester the 2009 globally produced CO₂ emissions 0.47 times. This is roughly half the amount of CO₂ produced throughout the entire year. Relatively, the size and area of two Wilkins Peak Member formations would be needed to sequester one year's worth of globally produced CO₂ if an analogous modern sedimentary environment were to be constructed.

REFERENCES

- Andrews, J.E., Brimblecombe, P., Jickels, T.D., Liss, P.S., Reid, B.J., *An Introduction to Environmental Chemistry, 2nd Edition*. Blackwell Science Ltd., UK., 2004.
- Bohacs, K.M., Carroll, A.R., Pietras, J., Rhodes, M., Smith, M., *Evolution of the great lakes system of the green river formation: tectonically and topographically conditioned records of climate change*. Geological Society of America Bulletin, 2002.
- Bradley, W.H. and H.P. Eugster, *Geochemistry and paleolimnology of the trona deposits and associated authigenic minerals of the Green River Formation of Wyoming*. U. S. Geological Survey Professional Paper, 1969: p. B1-b71.
- Brown, T.L., J. H. Eugene Lemay, and B.E. Bursten, *Chemistry, The Central Science, Eighth Edition*. Prentice-Hall, Inc., New Jersey, 2000.
- Brownlow, A.H., *Geochemistry, second edition*. Prentice-Hall, Inc., New Jersey, 1996.
- Carroll, A.R. and K.M. Bohacs, *Stratigraphic classification of ancient lakes: Balancing tectonic and climatic controls*. *Geology*, 1999. 27(2): p. 99-102.
- Carroll, A.R., Smith, E.M., Pietras, J.T., Rhodes, M.K., Singer, B., *Accumulation Rates in Ancient Lakes: Relationship to Lake Type Evolution of the Green River Formation, Wyoming*. Geological Society of America, 2002. Denver Annual Meeting.
- DeCelles, P.G., *Late Jurassic to Eocene evolution of the Cordilleran thrust belt and foreland basin system, western U.S.A.* *Am J Sci*, 2004. 304(2): p. 105-168.
- Deocampo, D.M., *Chapter 1 The Geochemistry of Continental Carbonates*, in *Developments in Sedimentology*, A.M. Alonso-Zarza and L.H. Tanner, Editors. 2010, Elsevier. p. 1-59.
- DeCelles, P.G., *Late Jurassic to Eocene evolution of the Cordilleran thrust belt and foreland basin system, western U.S.A.* *Am J Sci*, 2004. 304(2): p. 105-168.
- Deocampo, D.M., *Chapter 1 The Geochemistry of Continental Carbonates*, in *Developments in Sedimentology*, A.M. Alonso-Zarza and L.H. Tanner, Editors. 2010, Elsevier. p. 1-59.

- Deocampo, D.M. and G.M. Ashley, *Siliceous islands in a carbonate sea: Modern and Pleistocene records of spring-fed wetlands in Ngorongoro Crater and Olduvai Gorge, Tanzania*. *Journal of Sedimentary Research*, 1999. 69(5): p. 974 - 979.
- Drever, J.I., *The Geochemistry of Natural Waters: Surface and Groundwater Environments*. 3rd Edition. Prentice-Hall, Inc., New Jersey, 1996.
- Eugster, H.P., and L A Hardie., *Sedimentation in an ancient playa-lake complex: the Wilkins Peak Member of the Green River Formation of Wyoming*. *Geological Society of America Bulletin*, 1975: p. 319 - 334.
- Eugster, H.P., *Geochemistry of Evaporitic Lacustrine Deposits*. *Annual Review of Earth and Planetary Sciences*, 1980. 8(1): p. 35-63.
- John K, W., *Evaporites through time: Tectonic, climatic and eustatic controls in marine and nonmarine deposits*. *Earth-Science Reviews*, 2010. 98(3-4): p. 217-268.
- Jones, B.F. and D.M. Deocampo, *Geochemistry of Saline Lakes*. *Treatise on Geochemistry*. Drever, Ed., 2003. 5: p. 393 - 424.
- Kaldi, J.G., C.M. Gibson-Poole, and T.H.D. Payenberg, *Geological input to selection and evaluation of CO₂ geosequestration sites*. 2010, The American Association of Petroleum Geologists.
- Lee, J. and J.W. Morse, *Influences of alkalinity and pCO₂ on CaCO₃ nucleation from estimated Cretaceous composition seawater representative of "calcite seas"*. *Geology*, 2010. 38(2): p. 115-118.
- Lowenstein, T.K. and R.V. Demicco, *Elevated Eocene Atmospheric CO₂ and Its Subsequent Decline*. *Science*, 2006. 313(5795): p. 1928.
- Metz, B., et al., *Carbon Dioxide Capture and Storage*. IPCC, 2005. Cambridge University Press, UK: p. 431.

- Mignardi, S., et al., *The efficiency of CO₂ sequestration via carbonate mineralization with simulated wastewaters of high salinity*. Journal of Hazardous Materials, 2011. 191(1–3): p. 49-55.
- Pellant, C., *Rocks and Minerals*. Dorling Kindersley Limited, London, 1992.
- Pietras, J.T. and A.R. Carroll, *High-Resolution Stratigraphy of an Underfilled Lake Basin: Wilkins Peak Member, Eocene Green River Formation, Wyoming, U.S.A.* Journal of Sedimentary Research, 2006. 76(11): p. 1197-1214.
- Sass, E. and S. Ben-Yaakov, *The carbonate system in hypersaline solutions: dead sea brines*. Marine Chemistry, 1977. 5(2): p. 183-199.
- Smith, E.M., *Weathering, Springs, and the Origin of Na-Evaporites in the Early Eocene Green River Formation, Wyoming*. Geological Society of America 2009. 41(7): p. 512.
- Smith, E.M., A.R. Carroll, and E.R. Mueller, *Elevated weathering rates in the Rocky Mountains during the Early Eocene Climatic Optimum*. Nature Geosci, 2008. 1(6): p. 370-374.
- Smith, M.E., A.R. Carroll, and B.S. Singer, *Synoptic reconstruction of a major lake system: Eocene Green River Formation, western United States*. Geological Society of America Bulletin, 2008. 120: p. 54-84.
- Smith, E.M., B.S. Singer, and A.R. Carroll, *⁴⁰Ar/³⁹Ar geochronology of the Eocene Green River Formation, Wyoming*. Geological Society of America Bulletin, 2003. 115(5): p. 549 - 565.
- Spencer, R.J., et al., *Origin of potash salts and brines in the Qaidam Basin, China*. The Geochemical Society 1990.
- Zeppenfeld, Z., *Calcite precipitation from aqueous solutions with different calcium and hydrogen carbonate concentrations*. Journal of water supply : research and technology. AQUA, 2010. 59: p. 482 - 491.

APPENDIX A – ANALYTICAL DATA FROM THE DEAD SEA EXPERIMENTS

Table 8 Analytical data from the Dead Sea experiment.

Sample ID	Days	Time	pH	Temp °C	Ca Absorbance	Ca Conc. (diluted 0.5%)	Ca ppm - not diluted	Mg Absorbance	Mg Conc (diluted 0.5%)	Mg ppm - not diluted
DS-1	0	15:30	6.45	24.4	0.96	94.73	18,947	0.66	66.37	13,274
DS-2	0	15:40	6.25	24.4	0.83	81.90	16,381	0.58	58.32	11,665
DS-3	0	16:00	5.62	24.3	0.80	78.94	15,789	0.58	58.32	11,665
DS-4	0	16:30	4.70	24.4	0.82	80.92	16,184	0.57	57.32	11,464
DS-5	0	17:00	4.49	24.3	0.87	85.85	17,170	0.58	58.32	11,665
DS-6	0	17:30	4.49	24.3	0.92	90.79	18,157	0.61	61.34	12,268
DS-7	0	19:25	4.49	24.2	1.00	98.68	19,736	0.66	66.37	13,274
DS-8	1	10:20	4.35	24.2	0.80	78.94	15,789	0.60	60.34	12,067
DS-9	1	11:50	4.30	24.2	0.85	83.88	16,776	0.52	52.29	10,458
DS-10	1	13:35	4.08	24.2	0.83	81.90	16,381	0.56	56.31	11,263
DS-11	1	15:15	4.01	24.4	0.85	83.88	16,776	0.57	57.32	11,464
DS-12	2	10:05	4.26	24.1	0.87	85.85	17,170	0.58	58.32	11,665
DS-13	2	12:55	4.41	24.4	0.85	83.88	16,776	0.55	55.31	11,062
DS-14	2	16:00	4.41	24.6	0.86	84.86	16,973	0.55	55.31	11,062
DS-15	2	17:00	4.41	24.6	0.86	84.86	16,973	0.55	55.31	11,062
DS-16	2	19:00	4.42	24.4	0.86	84.86	16,973	0.55	55.31	11,062
DS-17	3	11:15	4.00	23.9	0.87	85.85	17,170	0.55	55.31	11,062
DS-18	3	13:00	3.99	24.2	0.87	85.85	17,170	0.55	55.31	11,062
DS-19	6	9:25	4.22	24.0	0.88	86.84	17,368	0.53	53.30	10,659
DS-20	6	16:30	3.99	24.5	0.86	84.86	16,973	0.56	56.31	11,263

DS-21	7	10:45	4.02	24.4	0.90	88.81	17,762	0.54	54.30	10,860
DS-22	13	15:45	4.12	24.2	0.93	91.77	18,354	0.56	56.31	11,263
DS-23	14	14:55	4.04	23.5	0.95	93.75	18,749	0.58	58.32	11,665
DS-24	15	11:00	4.02	23.3	0.94	92.76	18,552	0.58	58.32	11,665
DS-25	16	15:50	4.08	23.7	0.91	89.80	17,960	0.58	58.32	11,665
DS-26	17	10:35	4.05	23.5	0.96	94.73	18,947	0.60	60.34	12,067
DS-27	21	11:30	4.06	23.8	0.93	91.77	18,354	0.58	58.32	11,665
DS-28	22	16:30	4.08	23.5	0.97	95.72	19,144	0.58	58.32	11,665
DS-29	23	12:30	4.10	23.5	1.00	98.68	19,736	0.63	63.35	12,671
DS-30	24	13:20	4.15	23.2	1.00	98.68	19,736	0.64	64.36	12,872
DS-31	27	10:30	6.20	24.1	1.00	96.84	19,367	0.79	75.66	15,132
DS-32	28	12:00	6.40	24.1	0.99	95.87	19,173	0.79	75.66	15,132
DS-33	30	16:00	6.43	24.3	1.00	96.84	19,367	0.8	76.62	15,324
DS-34	31	19:00	6.52	24.2	1.00	96.84	19,367	0.82	78.54	15,707
DS-35	32	13:05	6.32	23.6	1.00	96.84	19,367	0.85	81.41	16,282
DS-36	36	10:30	6.20	24.0	1.00	96.84	19,367	0.83	79.49	15,899
DS-37	42	11:10	6.15	23.6	1.00	96.84	19,367	0.79	75.66	15,132

Table 9 Analytical data from the Dead Sea experiment with the addition of NH₄OH.

Sample ID	Days	Time	pH	Temp °C	Ca Absorbance	Ca Conc. (diluted 0.5%)	Ca ppm (not diluted)	Mg Absorbance	Mg Conc (diluted 0.5%)	Mg ppm - not diluted
DS-1	0	17:45	6.20	23.6	0.86	84.11	16,822	0.76	75.31	15,062
DS-2	1	13:50	3.90	24.4	0.86	84.11	16,822	0.75	74.32	14,864
DS-3	5	12:15	3.90	23.9	0.90	88.02	17,605	0.80	79.28	15,855
DS-4	6	8:10	3.96	24.1	0.96	93.89	18,778	0.83	82.25	16,450
DS-5	6	9:09	9.08	23.7	0.68	66.51	13,301	0.67	66.39	13,279
DS-6	6	9:11	9.08	23.8	0.66	64.55	12,910	0.60	59.46	11,891
DS-7	6	9:16	9.08	23.8	0.65	63.57	12,714	0.57	56.48	11,297
DS-8	6	9:32	9.12	23.7	0.63	61.62	12,323	0.60	59.46	11,891
DS-9	6	10:15	9.14	23.8	0.47	45.97	9,193	0.60	59.46	11,891
DS-10	6	10:45	9.07	23.5	0.50	48.90	9,780	0.67	66.39	13,279
DS-11	6	11:45	8.96	23.5	0.50	48.90	9,780	0.67	66.39	13,279
DS-12	6	13:05	8.79	23.6	0.70	68.46	13,692	0.70	69.37	13,873
DS-13	6	14:05	8.80	23.7	0.70	68.46	13,692	0.70	69.37	13,873
DS-14	7	10:45	8.66	23.5	0.68	66.51	13,301	0.72	71.35	14,270
DS-15	8	11:00	8.50	24.4	0.72	70.42	14,084	0.75	74.32	14,864
DS-16	9	9:30	8.20	23.5	0.78	76.29	15,257	0.72	71.35	14,270
DS-17	12	8:30	7.43	24.6	0.80	78.24	15,648	0.72	71.35	14,270
DS-18	13	10:45	6.40	24.2	0.80	78.24	15,648	0.74	73.33	14,666
DS-19	14	11:20	6.18	24.2	0.85	83.13	16,627	0.74	73.33	14,666
DS-20	15	10:30	6.02	24.0	0.86	84.11	16,822	0.72	71.35	14,270

APPENDIX B – ANALYTICAL DATA FROM THE GREAT SALT LAKE EXPERIMENTS

Table 10 Analytical data from the Great Salt Lake experiment.

Sample ID	Days	Time	pH	Temp °C	Ca Absorbance	Ca ppm - not diluted	Mg Absorbance	Mg Conc (diluted 0.5%)	Mg ppm - not diluted
G-1	0	16:30	8.56	23.2	0.83	80.37	0.30	29.13	5,827
G-2	1	13:00	4.97	23.5	0.84	81.34	0.28	27.19	5,438
G-3	3	10:30	4.99	22.9	0.78	75.53	0.29	28.16	5,632
G-4	5	10:00	4.93	23.6	0.80	77.47	0.28	27.19	5,438
G-5	6	10:30	4.93	23.7	0.83	80.37	0.27	26.22	5,244
G-6	7	12:30	4.99	23.4	0.85	82.31	0.28	27.19	5,438
G-7	11	11:00	5.00	23.1	0.85	82.31	0.27	26.22	5,244
G-8	12	16:40	5.01	22.9	0.83	80.37	0.28	27.19	5,438
G-9	13	15:15	5.02	23.9	0.79	76.50	0.28	27.19	5,438
G-10	15	13:50	4.98	23.3	0.74	71.66	0.30	29.13	5,827
G-11	17	13:10	6.68	23.1	0.66	65.19	0.35	33.99	6,798
G-12	18	15:30	7.15	22.9	0.64	63.21	0.33	32.05	6,409
G-13	20	9:40	7.26	22.9	0.60	59.26	0.34	33.02	6,603
G-14	24	12:30	7.62	24.0	0.59	58.27	0.35	33.99	6,798
G-15	25	10:10	7.50	23.9	0.59	58.27	0.40	38.84	7,769
G-16	26	17:35	7.31	23.9	0.58	57.29	0.36	34.96	6,992
G-17	27	14:25	7.41	23.5	0.54	53.34	0.40	38.84	7,769
G-18	31	11:25	7.48	23.0	0.48	47.41	0.40	38.84	7,769
G-19	32	10:30	7.48	23.4	0.48	47.41	0.40	38.84	7,769

Table 11 Analytical data from the Great Salt Lake experiment with the addition of NH₄OH.

Sample ID	Days	Time	pH	Temp °C	Ca Absorbance	Ca Conc. (diluted 0.5%)	Ca ppm - not diluted	Mg Absorbance	Mg Conc (diluted 0.5%)	Mg ppm - not diluted
G-1	0	9:00	8.39	23.1	0.021	2.06	412	0.28	26.88	5,377
G-2	1	10:50	5.39	23.5	0.02	1.96	392	0.26	24.96	4,993
G-3	2	8:30	5.12	23.9	0.021	2.06	412	0.26	24.96	4,993
G-4	2	10:23	9.72	24.0	0.015	1.47	294	0.17	16.32	3,264
G-5	2	10:30	9.75	24.0	0.015	1.47	294	0.16	15.36	3,072
G-6	2	10:40	9.78	24.1	0.016	1.53	306	0.18	17.28	3,457
G-7	2	10:57	9.79	24.3	0.014	1.37	275	0.16	15.36	3,072
G-8	2	11:25	9.71	24.2	0.015	1.39	278	0.18	17.28	3,457
G-9	2	12:25	9.66	24.2	0.012	1.18	235	0.18	17.28	3,457
G-10	2	15:00	9.63	24.2	0.014	1.26	252	0.16	15.36	3,072
G-11	3	8:30	9.28	23.4	0.013	1.24	248	0.17	16.32	3,264
G-12	6	16:35	8.21	24.1	0.002	0.20	39	0.22	21.12	4,225
G-13	7	13:30	7.89	23.8	0.002	0.20	39	0.21	20.16	4,033
G-14	8	15:40	7.85	23.8	0.002	0.20	39	0.22	21.12	4,225
G-15	9	12:10	7.48	23.9	0.002	0.20	39	0.22	21.12	4,225
G-16	10	17:30	7.25	23.5	0.002	0.20	39	0.24	23.04	4,609
G-17	14	16:00	7.11	23.3	0.001	0.10	20	0.23	22.08	4,417

APPENDIX C – ANALYTICAL DATA FROM THE DABUSUN LAKE EXPERIMENTS

Table 12 Analytical data from the Dabusun Lake experiment.

Sample ID	Days	Time	pH	Temp °C	Ca Absorbance	Ca Conc. (diluted 0.5%)	Ca ppm - not diluted)	Mg Absorbance	Mg Conc (diluted 0.5%)	Mg ppm - not diluted
D-1	0	18:30	8.21	23.1	0.070	6.82	1,364	0.98	95.81	19,163
D-2	1	13:00	5.77	23.4	0.067	6.53	1,306	0.96	93.86	18,771
D-3	3	10:25	5.65	23.5	0.070	6.82	1,364	0.97	94.83	18,967
D-4	5	10:00	5.55	23.8	0.073	7.11	1,423	0.97	94.83	18,967
D-5	6	10:30	5.53	23.9	0.075	7.31	1,462	1.0	97.77	19,554
D-6	7	12:30	5.54	23.6	0.075	7.31	1,462	0.97	94.83	18,967
D-7	11	11:00	5.65	23.4	0.070	6.82	1,364	0.97	94.83	18,967
D-8	10	16:40	5.7	23.4	0.073	7.11	1,423	0.95	92.88	18,576
D-9	13	15:15	5.71	23.7	0.073	7.11	1,423	0.96	93.86	18,771
D-10	14	13:50	5.67	23.7	0.076	7.41	1,481	0.97	94.83	18,967
D-11	17	13:10	6.32	23.2	0.074	7.21	1,442	0.98	95.81	19,163
D-12	18	15:30	6.49	22.9	0.076	7.41	1,481	0.99	96.79	19,358
D-13	20	9:40	6.69	22.9	0.073	7.11	1,423	0.98	95.81	19,163
D-14	24	12:30	6.82	24.1	0.079	7.70	1,540	0.99	96.79	19,358
D-15	25	10:10	6.88	23.9	0.080	7.80	1,559	1.0	97.77	19,554
D-16	26	17:35	6.87	24.0	0.080	7.80	1,559	0.96	93.86	18,771
D-17	27	14:30	6.88	23.6	0.080	7.80	1,559	1.0	97.77	19,554
D-18	31	11:25	6.84	23.0	0.062	6.04	1,209	0.99	96.79	19,358
D-19	32	10:30	6.69	23.6	0.062	6.04	1,209	1.0	97.77	19,554

Table 13 Analytical data from the Dabusun Lake experiment with the addition of NH₄OH.

Sample ID	Days	Time	pH	Temp °C	Ca Absorbance	Ca Conc. (diluted 0.5%)	Ca ppm (not diluted)	Mg Absorbance	Mg Conc (diluted 0.5%)	Mg ppm - not diluted
D-1	0	12:00	7.24	22.6	0.078	7.63	1,526	1.12	108.40	21,681
D-2	1	9:00	5.68	24.0	0.077	7.53	1,507	1.23	119.05	23,810
D-3	6	10:30	6.77	24.1	0.08	7.83	1,565	1.44	139.38	27,876
D-4	7	8:30	5.32	23.2	0.083	8.12	1,624	1.36	131.63	26,327
D-5	7	8:48	8.68	24.1	0.02	1.96	391	0.97	93.89	18,777
D-6	7	8:53	8.80	24.1	0.041	3.94	789	0.86	83.24	16,648
D-7	7	9:00	8.92	24.1	0.044	4.23	846	0.88	85.18	17,035
D-8	7	9:05	8.86	24.0	0.062	5.96	1,193	0.93	90.01	18,003
D-9	7	9:30	8.88	23.9	0.058	5.58	1,116	0.9	87.11	17,422
D-10	7	9:50	8.94	23.6	0.056	5.39	1,077	0.87	84.21	16,841
D-11	7	10:50	8.96	23.6	0.052	5.00	1,000	0.91	88.08	17,616
D-12	7	11:50	8.89	23.6	0.047	4.52	904	0.93	90.01	18,003
D-13	7	12:50	8.90	23.7	0.032	3.08	616	0.88	85.18	17,035
D-14	7	13:50	8.89	23.6	0.05	4.81	962	0.9	87.11	17,422
D-15	7	15:00	8.85	23.8	0.055	5.29	1,058	0.93	90.01	18,003
D-16	8	12:30	8.53	23.5	0.06	5.77	1,154	0.95	91.95	18,390
D-17	9	17:15	8.07	23.1	0.059	5.68	1,135	1.01	97.76	19,552
D-18	12	9:30	7.88	23.1	0.071	6.83	1,366	1.18	114.21	22,842
D-19	13	16:20	7.40	23.6	0.074	7.12	1,424	1.21	117.12	23,423
D-20	14	16:05	7.24	23.7	0.078	7.50	1,501	1.4	135.51	27,101
D-21	15	11:05	7.20	23.6	0.082	7.89	1,577	1.42	137.44	27,488

APPENDIX D – ANALYTICAL DATA FROM THE DONGLIN LAKE EXPERIMENTS

Table 14 Analytical data from the Donglin Lake experiment.

Sample ID	Days	Time	pH	Temp °C	Ca Absorbance	Ca Conc. (diluted 0.25%)	Ca ppm (not diluted)	Mg Absorbance	Mg Conc (diluted 0.25%)	Mg ppm - not diluted
DG-1	0	17:00	6.20	23.6	1.52	149.55	59,822	1.20	116.23	46,493
DG-2	1	10:05	3.62	24.0	1.52	149.55	59,822	1.22	118.17	47,268
DG-3	2	17:30	3.62	24.2	1.53	150.54	60,215	1.33	128.82	51,530
DG-4	3	14:25	3.62	24.0	1.54	151.52	60,609	1.27	123.01	49,205
DG-5	7	11:25	3.62	23.8	1.54	151.52	60,609	1.22	118.17	47,268
DG-6	8	10:30	3.60	24.0	1.53	150.54	60,215	1.08	104.61	41,844
DG-7	9	17:00	3.60	24.0	1.55	152.51	61,002	1.10	106.55	42,618
DG-8	10	13:40	3.62	24.4	1.48	145.62	58,247	1.22	118.17	47,268
DG-9	14	11:30	3.64	24.2	1.53	150.54	60,215	1.19	115.26	46,105
DG-10	15	18:20	3.67	24.4	1.55	152.51	61,002	1.08	104.61	41,844
DG-11	16	17:00	3.70	24.6	1.55	152.51	61,002	1.18	114.29	45,718
DG-12	17	13:50	3.64	24.7	1.56	153.49	61,396	1.14	110.42	44,168
DG-13	21	12:15	3.57	23.9	1.53	150.54	60,215	1.19	115.26	46,105
DG-14	22	8:15	3.54	23.7	1.52	149.55	59,822	1.18	114.29	45,718
DG-15	23	11:00	3.95	24.1	1.57	154.47	61,790	1.08	104.61	41,844
DG-16	24	10:00	4.02	24.6	1.56	153.49	61,396	1.12	108.48	43,393
DG-17	25	8:45	4.07	23.8	1.55	152.51	61,002	1.16	112.36	44,943
DG-18	28	16:30	4.52	24.7	1.51	148.57	59,428	1.14	110.42	44,168
DG-19	29	14:00	4.48	24.5	1.48	145.62	58,247	1.11	107.51	43,006

Table 15 Analytical data from the Donglin Lake experiment with the addition of NH₄OH.

Sample ID	Days	Time	pH	Temp °C	Ca Absorbance	Ca Conc. (diluted 0.25%)	Ca ppm (not diluted)	Mg Absorbance	Mg Conc (diluted 0.25%)	Mg ppm - not diluted
DG-1	0	17:00	7.24	23.9	1.98	189.78	75,911	1.15	110.64	44,254
DG-2	4	8:20	3.82	24.1	2.0	191.69	76,678	1.01	97.17	38,867
DG-3	4	9:06	8.44	23.9	1.22	116.93	46,773	0.31	29.82	11,929
DG-4	4	9:11	8.40	25.8	1.24	118.85	47,540	0.30	28.86	11,545
DG-5	4	9:21	8.41	25.8	1.18	113.10	45,240	0.33	31.75	12,699
DG-6	4	9:36	8.36	25.4	1.3	124.60	49,840	0.35	33.67	13,469
DG-7	4	10:06	8.26	24.9	1.13	108.31	43,323	0.32	30.79	12,314
DG-8	4	10:40	8.21	24.6	1.17	112.14	44,856	0.36	34.63	13,854
DG-9	4	11:06	8.16	24.4	1.07	102.56	41,023	0.32	30.79	12,314
DG-10	4	12:08	8.13	24.2	1.28	122.68	49,074	0.35	33.67	13,469
DG-11	4	13:10	8.12	24.1	1.01	96.81	38,722	0.38	36.56	14,623
DG-12	4	15:43	8.11	23.9	1.2	115.02	46,007	0.34	32.71	13,084
DG-13	5	13:14	8.19	23.7	1.12	107.35	42,939	0.44	42.33	16,932
DG-14	6	15:30	8.44	23.7	1.33	127.48	50,991	0.50	48.10	19,241
DG-15	7	12:45	8.14	23.6	1.33	127.48	50,991	0.53	50.99	20,395
DG-16	8	17:40	7.76	23.2	1.43	137.06	54,824	0.56	53.87	21,550
DG-17	11	9:35	7.62	23.1	1.6	153.36	61,342	0.65	62.53	25,013
DG-18	12	14:30	7.37	23.7	1.6	153.36	61,342	0.70	67.34	26,937
DG-19	13	14:00	7.24	23.6	1.8	172.52	69,010	0.80	76.96	30,786
DG-20	14	13:30	7.18	23.6	1.63	156.23	62,492	0.76	73.12	29,246